The Investigation and Development of Gas Sensors with Carbon Nanomaterials

by

Nicolaas Jacobus de Jager

Thesis presented in partial fulfilment of the requirements for the degree of Master of Science in Engineering at the University of Stellenbosch

Department of Electrical and Electronic Engineering
University of Stellenbosch
Private Bag X1, 7602 Matieland, South Africa

Supervisor: Prof. W.J. Perold

December 2011

Declaration

By submitting this thesis electronically, I declare that the work contained therein is my own, original work, that I am the sole author thereof (save to the extent explicitly otherwise stated), that reproduction and publication thereof by Stellenbosch University will not infringe any third party rights and that I have not previously in its entirety or in part submitted it for any qualification.

Date: December 2011

Abstract

The Investigation and Development of Gas Sensors with Carbon Nanomaterials

N.J. de Jager

Department of Electrical and Electronic Engineering
University of Stellenbosch
Private Bag X1, 7602 Matieland, South Africa

Thesis: MScEng (Electrical and Electronic Engineering)

December 2011

In this research the possible utilization of carbon nanomaterials in gas sensing applications are investigated. These materials include the 2-dimensional honeycomb-lattice carbon structure called graphene, and the 1-dimensional structures referred to as carbon nanotubes (CNTs). The extraordinary properties and unique morphology of these nanomaterials, make them excellent candidates for sensory applications. This research thus entails the investigation and development of gas sensors with these carbon nanomaterials. This includes the synthesis of CNTs via a chemical vapour deposition (CVD) technique and the fabrication of resistive thin film sensors with the various materials. The functionalization of carbon nanomaterials is also explored, which delivers promising results for sensing gases at room temperature, especially acetylene (C_2H_2). Furthermore, a unique method is developed to fabricate ultra thin aluminium microstructures. These metallic electrodes are found to be ideal for nanomaterial integration. An experiment is performed to manufacture an integrated sensor with MWCNTs and following the results, a refinement of the procedure and the investigation of FET-based devices are recommended. The results obtained during this work, indicate that engineered carbon nanostructures, such as CNTs and graphene, can potentially be applied in future sensing technologies.

Opsomming

Die Ondersoek en Ontwikkeling van Gas-Sensors met Koolstof Nanomateriale

N.J. de Jager

Department of Electrical and Electronic Engineering
University of Stellenbosch
Private Bag X1, 7602 Matieland, South Africa

Tesis: MScEng (Electrical and Electronic Engineering)
Desember 2011

Hierdie navorsing ondersoek die moontlike toepassing van koolstof nano-materiale as gas-sensor tegnologie. Hierdie materiale sluit die 2-dimensionele koolstof struktuur, grafeen, asook die sogenaamde 1-dimensionele koolstof nano-buise in. Die buitengewone eienskappe en unieke morfologie van hierdie nano-materiale, maak hul uitstekende kandidate vir sensor toepassings. Hierdie navorsing ondersoek dus die ontwikkeling van gas-sensors met koolstof nano-materiale, insluitend die sintese van koolstof nano-buise deur middel van 'n chemiese damp-neerslag proses, asook die fabrikasie van resistiewe dun film sensors. Die funksionalisering van koolstof nano-materiale is ook ondersoek en belowende resultate is opgelewer met betrekking tot die deteksie van gasse by kamertemperatuur, veral vir asetileen (C_2H_2) gas. Verder is 'n unieke metode ontwikkel om ultra dun aluminium mikrostrukture te vervaardig en hierdie metaal elektrodes word as ideaal beskou vir die integrasie van nano-materiale. 'n Eksperiment is uitgevoer om 'n geïntegreerde sensor te vervaardig met multi-wand koolstof nano-buise, waarvan die resultate aandui dat die proses verfyn moet word en dat die moontlike toepassing van veld-effek-transistor toestelle ondersoek moet word. Die resultate wat opgelewer is gedurende hierdie navorsing dui daarop dat ontwikkelde nanostrukture, soos koolstof nano-buise en grafeen, as toekomstige sensor tegnologie geïmplementeer kan word.

Acknowledgments

I would like to express my sincere gratitude to the following people and organizations: Prof. Willem Perold, who acted as my study leader and guided me throughout this study. Also, the Department of Electrical and Electronic Engineering at Stellenbosch University for their financial assistance during this research. I would also like to thank Ulrich Büttner, the laboratory manager of SAND (Superconductors, Advanced Materials and Nano Devices) at Stellenbosch University, for his assistance and motivation throughout this study.

A special word of thanks to Dr. Frik Koch at the University of the Western Cape (UWC), for his assistance with the HRTEM imaging of the nanotube samples and to Prashaan at the Department of Chemistry at Stellenbosch University, for his assistance with the UV- vis -NIR spectral analysis.

I would also like to thank my colleague, Stanley van den Heever, for his assistance with the synthesis of zinc oxide (ZnO) nanowires and also for his friendship in general.

A generous word of thanks to my parents, friends and family, who supported and motivated me throughout this study, especially Nisa Kriek, who also assisted me with the graphic illustrations presented in this work.

Finally, I would like to thank our lord God, for without His grace and blessing, none of my achievements would have been possible.

Dedications

This thesis is dedicated to my parents, Nic and Leonore de Jager.

Contents

List of Figures

List of Tables

List of Abbreviations

AFM	Atomic Force Microscope
CNT(s)	Carbon Nanotube(s)
CVD	Chemical Vapour Deposition
EDX	Energy Dispersive X-ray
HRTEM	High Resolution Transmission Electron Microscope
ITO	Indium Tin Oxide
MEMS	Micro Electromechanical System
NEMS	Nano Electromechanical System
MWCNT	Multi-Walled Carbon Nanotube
SWCNT	Single-Walled Carbon Nanotube
SAED	Selected Area Electron Diffraction
SEM	Scanning Electron Microscope
TEM	Transmission Electron Microscope
XRD	X-ray Diffraction
UV- vis -NIR	Ultraviolet - Visible - Near Infrared

List of Symbols

°C	Degrees Celsius
K	Kelvin
nm	Nanometer
μm	Micrometer
I	Current in Amperes (A)
V	Potential in Volts (V)
Ω	Ohm
sccm	Standard Cubic Centimeters per Minute
%RH	Percentage Relative Humidity

Chapter 1

Introduction

1.1 Motivation for conducting this research

In the modern world, almost every existing manufacturing process implements sensors or requires the application of advanced sensor technologies to optimize various control systems. The demand for higher accuracy, faster processing speeds, improved energy efficiency and enhanced sensitivity, is pushing the boundaries of science and technology to a new frontier. This is in fact the dawning of the nanotechnological era and a revolution in technology and applications await, with major advances foreseen in the fields of science, engineering, medical and industrial processes and even environmental monitoring and product quality control.

The potential to enhance the performance, sensitivity, selectivity and efficiency of sensors, has been demonstrated by numerous nanotechnology related experiments during the past decade. Specifically, the interaction between species at a molecular level, which differs so radically from those in the macro world, is what ultimately drives the enthusiasm for exploring the features of nanotechnology. This also provides the foundation for creating smaller and more sensitive sensors, with unmatched accuracy and efficiency.

Forming the base of most nanosensors, are advanced engineered nanomaterials, which act as highly sensitive receptors for detecting molecules and atomic structures. Such nanomaterials include carbon nanotubes (CNTs) and graphene (a mono-layered carbon structure), which exhibits extraordinary physical, chemical

and electrical properties.

This research was therefore conducted, to investigate the characteristics of carbon nanomaterials like graphene and CNTs and to explore the possible implementation thereof in gas sensing applications.

1.2 Objectives of this study

This research was performed to investigate the feasibility of carbon nanostructured gas sensors and to subsequently endeavour the development of such devices for sensing applications. A further aim was to fabricate carbon-based nanosensors, which could operate at room temperature, as this is a current issue that needs to be addressed.

The carbon nanomaterials which were identified for use in the development of the proposed nanosensors, namely graphene and carbon nanotubes (CNTs), needed to be studied and characterized in various ambient conditions, to determine the potential use thereof for sensing applications. This was performed by executing temperature and relative humidity tests on the nanomaterial film sensors, as well as subjecting the devices to varying gas flow rates. These tests were thus performed to study the effect of such environmental changes on the functioning of the gas sensors.

Initially, the synthesis of carbon nanotubes had to be investigated, to determine whether a viable process could be obtained to efficiently manufacture the CNT material. This was mainly aimed at exploring chemical vapour deposition (CVD) methods, as these techniques are most related to the molecular self-assembly approach of nanomaterial synthesis. Furthermore, in order to expand the development of nanosensor topologies, the fabrication of metallic electrode structures were also investigated.

1.3 Contributions to the field

Pertaining to the synthesis of carbon nanotubes, the results of this research not only confirmed the enhancing effect of water in the chemical vapour deposition of CNTs, but also delivered a possible CVD method for the synthesis of graphene, which was observed at higher process temperatures.

As for pure carbon-based nanomaterials, very little reactivity at room temperature was observed for both single-walled and multi-walled CNTs, as well as for graphene. Furthermore, these nanomaterials were shown to respond in particular to acetylene (C_2H_2) gas, also at elevated substrate temperatures.

During the investigation of functionalized nanomaterial film sensors, the high sensitivity of carboxyl groups on CNT sidewalls were demonstrated and the adverse effects of high temperatures on such organic sensors were highlighted. In addition to creating a carbon nanotube and indium tin oxide (ITO) compound material for sensing gases, this material showed promising results for utilization in other fields such as solar generation and opto-electronics.

Finally, an effective and unique method was developed to fabricate ultra thin aluminium microstructures on silicon dioxide (SiO_2) wafers. A study of the utilization of aluminium for electrode purposes was performed, the results of which was published, together with the fabrication process, in the journal *Thin Solid Films* [87].

1.4 Overview of this work

This section provides a brief summary of the work completed during this research and also highlights some key results. Accordingly, the following chapters entails a comprehensive report on the techniques and methods that were applied in conducting this research.

As mentioned previously, the main objective of this research was to investigate the characteristics of carbon nanomaterials like graphene and CNTs, for gas sens-

ing applications. A general overview of nanotechnology and the various carbon nanomaterials are presented in Chapter 2.

1.4.1 The synthesis of CNTs and graphene

Chapter 3 provides a discussion on the techniques utilized to synthesize carbon nanotubes and also provides an introduction to the "super growth" of CNTs with various growth enhancers, including water. Supplementary information on the purification and functionalization of carbon nanotubes is also presented and discussed.

In this research, a water-assisted floating catalyst chemical vapour deposition (CVD) method was implemented to synthesize both single-walled (SWCNT) and multi-walled carbon nanotubes (MWCNTs). Process diagrams of these experiments are also provided, along with detailed descriptions of the growth mechanisms present during the CVD process. Using electron microscopy (HRTEM) and Raman spectroscopy techniques, the synthesized carbon nanotubes were analyzed.

These CVD growth experiments were mainly aimed at synthesizing carbon nanotubes, but an interesting result was obtained at higher process temperatures, which seemed to favour the growth of few-layered graphene structures. These structures were also analyzed with a high-resolution transmission electron microscope (HRTEM), with additional electron diffraction measurements confirming the presence of graphene.

1.4.2 Pure carbon nanomaterial gas sensors

In order to investigate the properties of the various carbon nanomaterials, spray-coated thin film sensors were fabricated with the nanomaterials in their pure form. The sensing mechanisms were based on changes in film resistivity, upon exposure to different ambient conditions as well as various gas species.

The CNT and graphene films were examined with a scanning electron micro-

scope (SEM) and the fabrication procedures utilized are described in detail in Chapter 4. The fabricated sensors were tested in a custom aluminium chamber and measurements were obtained with an analogue-to-digital converter (LabJack U6 device), which was connected in the Van der Pauw configuration (discussed in Appendix E).

The most notable result of these experiments, were the increased sensitivity observed at higher substrate temperatures and the fast saturation characteristic of these nanomaterials. Furthermore, exposure to acetylene (C_2H_2) gas, predominantly had the highest reactivity at room temperature.

1.4.3 Composite nanomaterial gas sensors

In Chapter 5, the fabrication of three different functionalized carbon nanomaterial film sensors are described. Specifically, the composite materials consisted of a carboxyl-functionalized MWCNT material (MWCNT-COOH), an indium tin oxide (ITO) and MWCNT composite and a graphene and zinc oxide (ZnO) nanowire composite material.

These materials were subjected to the same series of tests, as was performed on the pure carbon nanomaterial film sensors. The results of these composite nanomaterials demonstrated significant increases in sensitivity towards C_2H_2 detection at room temperature, especially for the MWCNT-COOH devices.

The MWCNT-ITO material yielded a faster recovery rate and provided a non-volatile device for gas sensing. Furthermore, the ITO-composite nanomaterials showed interesting UV-vis-NIR characteristics, which proposed the implementation thereof in solar cell technologies and other opto-electronic applications.

For both the MWCNT-ITO and graphene-ZnO composite nanomaterials, a doping effect was observed, which resulted in an inverted sensor response compared to the pure carbon nanomaterial film devices.

1.4.4 Microstructured thin films of aluminium for the integration of nanomaterials

This research also involved the investigation of patterned metal thin films, which are suitable for the integration of nanomaterials like graphene and carbon nanotubes.

Thus, Chapter 6 presents a detailed study of the properties of extremely thin aluminium films. Also presented, is a unique and effective method, which was developed during this research, to fabricate ultra thin aluminium electrode structures on silicon dioxide (SiO_2) substrates. The silicon oxidation process is also discussed in detail, together with the step-by-step lithographic patterning procedure, which was used to generate the metallic structures. The resulting structures were examined via atomic force microscopy (AFM) and was found to be favourable for the integration of nanomaterials.

Finally, it was attempted to manufacture an integrated carbon nanotube sensor, using an aluminium electrode structure and a spray-coating technique, which was followed by a high temperature annealing process. The resulting sensor demonstrated a slight sensitivity towards C_2H_2 and H_2 gas detection at 100°C.

It is however proposed, that this sensor fabrication method be refined and that the development of field-effect transistor (FET) based devices be investigated in future studies.

1.5 Conclusions

This research and the experimental results obtained during this work, indicated that carbon nanomaterials can potentially be utilized as the active elements in gas sensing devices.

It was also demonstrated that the functionalization of carbon nanomaterials are especially of interest for gas detection at lower substrate temperatures. The proposed carbon nanomaterials were thus implemented to fabricate resistive thin film

sensors, which were used to investigate the possible detection of various gases, including C_2H_2, H_2, O_2 and CH_4.

The developed aluminium thin film fabrication process, yielded impeccable electrode structures, which are typically favourable for nanomaterial integration. This method may also benefit the fabrication of other sensor topologies, including FET-based nanosensors. Other recommendations and the full conclusions of this research are discussed in detail in Chapter 7.

Chapter 2

Scientific Literature Review

In the past few decades, nanotechnology and nanoscience has been in a phase of remarkable progress and the implementation of nanotechnical features in modern science and engineering has been acknowledged worldwide. This chapter reviews the basic definition of nanotechnology and briefly discusses the history and physics pertaining to the nanoworld. Subsequently, the evolution of specialized nanofabrication tools and techniques are portrayed and a few modern applications of nanotechnology and nanoscience are discussed. This chapter also includes a short note on the latest developments in nanotechnology, as well as certain non-technicalities of the nanoworld. Finally an in-depth study of the carbon nanomaterials utilized throughout this research is presented.

2.1 Review of Nanotechnology and Applications

2.1.1 The Definition of Nanotechnology

In a broad sense, nanotechnology can be considered as the control and manipulation of material on a molecular and atomic scale. In the nanoworld, devices having at least one functional component with a size below 100 nm, are generally referred to as nanodevices.

It should be clear that nanotechnology is a very diverse and integrated field of science and engineering, which includes the miniaturization of conventional devices, new design approaches incorporating molecular self-assembly processes, the development of nanoscale polymers and other novel and advanced materials

with unique characteristics, as well as investigations into the direct control and manipulation of matter on sub-micron and atomic scales.

Nanotechnology and the future consequences thereof to society has, without any doubt, been a hot topic in scientific councils during the past decade. Not only does nanotechnology and nanoscience have the potential to revolutionize modern applications in electronics, medicine, bio-engineering and energy generation, but concerns regarding the environmental impact and toxicity of engineered nanomaterials and the prospective economic effects of nanotechnology are receiving a great deal of attention on a global level [1].

2.1.2 A Brief History of Nanotechnology

The word "nano" (a prefix denoting 10^{-9}) is derived from the Greek word "nanos", meaning dwarf. Nanotechnology thus refers to things with a general size of one billionth of a meter, or more illustratively, one forty thousandth the average width of a human hair. As early as 1905, Albert Einstein speculated that the diameter of a single sugar molecule is about 1 nm, in a diffusion experiment of sugar in water. It would however be till much later (1974), that the term "Nanotechnology" is coined by physicist Norio Taniguchi in a paper entitled *"On the Basic Concept of Nanotechnology"* [2].

Perhaps one of the biggest notions towards the development on nanotechnology was prompted by Nobel prize winner Richard Feynmann and his mysterious talk at the 1959 Annual American Physical Society banquet. During his enigmatic speech, entitled *"There's Plenty of Room at the Bottom"*, he said: *"I am not afraid to consider the final question as to whether, ultimately in the great future, we can arrange atoms the way we want"* [2].

It wasn't until 1985, when Richard Smalley and his associates discovered the Buckminsterfullerene or so-called "buckyball" (C_{60} molecule), shown in Fig. 2.1, and the discovery of carbon nanotubes (Fig. 2.2) in 1991 by Sumio Iijima, that the field of nanotechnology started to expand almost exponentially.

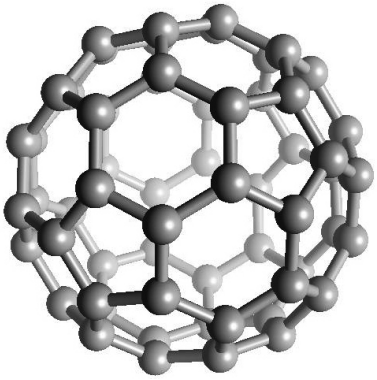

Figure 2.1: The Buckminsterfullerene (C_{60}) molecule [13].

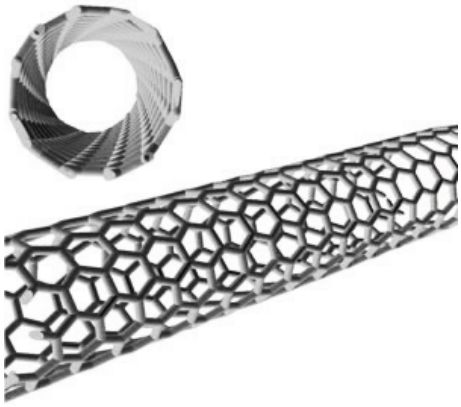

Figure 2.2: A Single-Walled Carbon Nanotube (SWCNT) [14].

We might figure it unfortunate that the great Isaac Newton never saw a buckyball or a nanotube, but it is evident that in order to fully grasp the extent of nanotechnology, we need to understand the objects of the nanoworld such as molecules, atoms, electrons and photons and be able to interpret their behaviour in a quantum mechanical way.

2.1.3 Nanophysics in a Nutshell

Classical or Newtonian physics, from a general perspective, perfectly describe many natural occurring phenomena, but very few (if any) nanoscale phenomena.

Understanding nanoscience and the related technology thus requires an understanding of molecules, atoms and photons and electrons, which are all prevalent "quantum mechanical entities".

Owing to centuries of atomic model refinement, we know that electrons occupy space regions called orbits, which encloses an atom's nucleus. These orbitals are ordered into levels and sub-levels, depending on the energy status of the residential electrons. Analogous to standing waves on a guitar string, electrons can only consist of very specific "wavelengths" or energies [2].

A photon, emitted by an atom when an electron skips from a high-energy level to a lower energy state, is a chargeless "packet" of energy with zero mass. The energy of this photon equals the exact difference between the two distinct energy levels. The emission of photons is a phenomenon which is generally referred to as electromagnetic radiation. The significance of the photon lies in its intrinsic wave-particle duality, in other words, behaving like a wave and a particle simultaneously. This purely quantum effect is also encountered in the event of electrons tunneling through certain nanoscale "barriers".

Molecular recognition, otherwise known as the ability of one molecule to attract and bind to another, is one of the key principles in the development of nanotechnology and nanoscience [3]. Given that many features in the nanoworld are created using a bottom-up approach, the synthesis of self-organizing molecules and molecular structures on supporting surfaces has become an extremely important element of nanotechnological research.

Moving towards the fabrication and characterization of nanodevices, for example superconductors and single nanotube devices, our much relied upon "Ohm's Law" fails desolately and we need to delve into quantum physics theory and Van der Waals force attractions, in order to better our understanding of the functioning of elements in the nanoworld. The most significant concept of quantum theory being that energy, and consequently charge, cannot be added or subtracted continuously. Energy and charge at the nanoscale is thus exchanged in discrete or

finite valued “chunks” or “packets”, called quanta (the plural of quantum) [3].

Due to the anticipated application of nanotechnology on a vast array of scientific fields, ranging from polymer sciences and engineering to bio-medicine, understanding the power of nanoscale inventions ultimately requires the collaboration of knowledge from a very broad scientific spectrum.

2.1.4 Nanofabrication Tools and Techniques

Putting the scales of the nanoworld in another context, the comparative size of a marble to the size of the earth, is similar to that of a nanometer compared to a meter. It therefore seems that it would require the implementation of nanotechnology to manufacture machines and devices that are capable of creating and manipulating nanostructures, thus complicating the evolution of nanotechnology in a remarkable fashion.

Atomic Force Microscope (AFM)

It was in the 1980’s however, that an idea first developed in IBM Laboratories in Zurich, helped to launch the global nanotechnology revolution. Essentially all types of modern scanning probe microscopy instruments are based on this idea [3].

Scanning probe instruments include Atomic Force Microscopes (AFM), Scanning Tunneling Microscopes (STM) and Magnetic Force Microscopes (MFM), where the AFM, depicted in Fig. 2.3, has the capability of scanning both conductive and non-conductive surfaces with nanometer resolutions.

These instruments generally comprise of a micro-machined cantilever with a sharp tip (probe), which scans the sample’s surface. Laser sensors or photodetectors are used to measure the probe’s mechanical or magnetic deflections, which are then assembled into a computer generated image of the scanned surface [4].

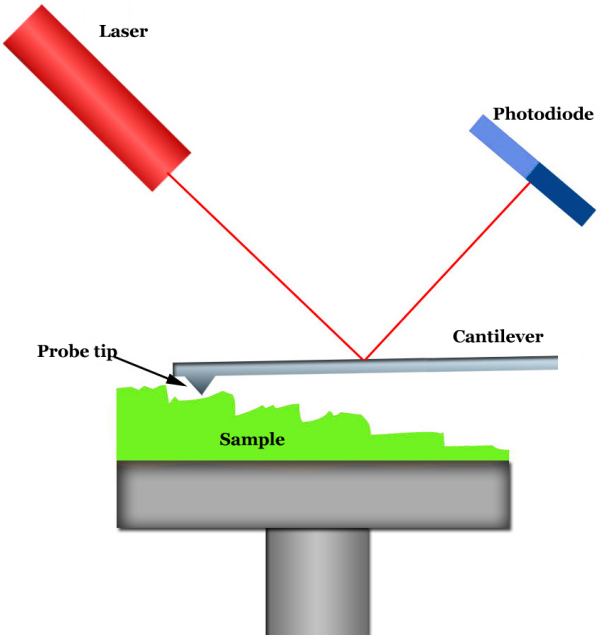

Figure 2.3: Illustration of a surface scan with an Atomic Force Microscope (AFM) [12].

A more general and much older technique named "spectroscopy", is also used in the analysis of nanostructures. Most familiar to the nanoworld is probably the technique called Raman Spectroscopy, where a shift in resonant frequency of the sample material is measured. Although spectroscopy offers many complementary insight when characterizing nanomaterials or engineered nanosurfaces in bulk, most spectroscopy procedures do not yield much information on individual nanoscale structures.

Transmission Electron Microscope (TEM)

With the invention of the Transmission Electron Microscope (TEM) and its successor, the High-Resolution TEM (HRTEM), a new door to the world of nanoscience was opened. Under favourable conditions, TEM and HRTEM captured images can have adequate resolutions to successfully recognize structures with diameters below 0.5 nm. Electron microscopy generates sample images by collecting data on electron scattering, when accelerated electrons are passed through the sample. Similarly to a Scanning Electron Microscope (SEM), a

TEM also comprise of a high-voltage electron gun that focuses the electron beam through a series of lenses, which are housed in a liquid-nitrogen cooled vacuum column.

Scanning Electron Microscope (SEM)

Since the concept of a Scanning Electron Microscope (SEM) was described by Max Knoll in 1935, the SEM has made a huge contribution to scientific research. Modern day SEM instruments boast magnification levels of up to 500 000 times, having high-definition resolutions up to the nanometer range [5].

Contrary to conventional microscopes, SEM and TEM uses electron beams instead of light to form images of the viewed sample. Compared to a "light" microscope, electrons can be accelerated to have much larger momentums than photons, resulting in a smaller De Broglie wavelength, which in turn directly translates into a much higher viewing resolution [6]. Using multiple X-ray and electron detectors, an image of the sample is formed as electrons scatter from the surface of the sample. The locations of these detectors are shown in Fig. 2.4, which illustrates the operation of a typical SEM instrument.

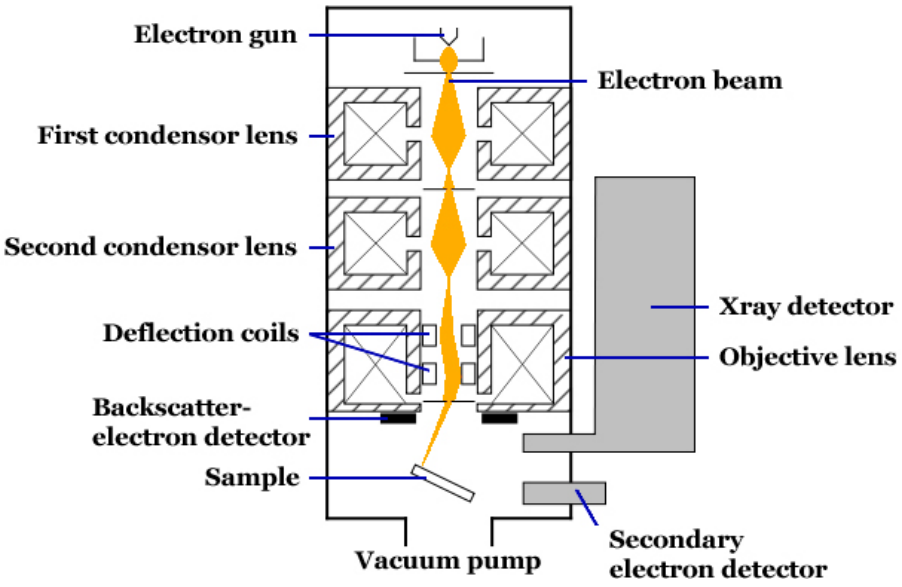

Figure 2.4: An illustration of a typical Scanning Electron Microscope (SEM) [7].

Approach to nanofabrication

For the manufacture of desired nanostructures, two approaches are followed, namely the top-down (miniaturization) approach and bottom-up (molecular self-assembly) approach. The top-down approach, which exploits fabrication techniques similar to those found in the semiconductor industry, is primarily pursued in the fabrication of inorganic nanowires and ultra-thin layer deposition. These semiconductor techniques have been quite successfully miniaturized by using processes like deep ultra-violet (also extreme UV) lithography, e-beam lithography, nano-imprint lithography, focused ion beam lithography and atomic layer deposition via thermal molecular vapour deposition methods. Other processes include Dip Pen nanolithography (DPN), using almost any material as a "nano-ink", as well as Nanosphere lift-off lithography [3].

More direct fabrication techniques have also been introduced, using scanning probes (AFM and STM) to move around and manipulate atoms and molecules, forming complex 3D nanostructures. However, a major drawback of these elegant manufacturing methods, is that they are relatively expensive and rather time consuming, thus limiting these techniques to laboratories and research institutions.

Alternatively, following the bottom-up approach, we enter completely new dimensions of molecular synthesis, molecular self-assembly, nanocrystal growth and polymerization [3]. The self-assembly nanofabrication approach is based on the initiative that molecules and atoms are constantly seeking the lowest level of energy available to them. Therefore molecules will bond and reorient themselves under certain conditions in order to minimize their energy.

Thus by exploiting the energy behaviour of molecules and studying the Coulombic interactions and Van der Waals forces present amongst them, we can provide the ideal environment to synthesize certain nanostructures. An example of such experiments is found with the chemical vapour deposition (CVD) of carbon nanotubes, during which a hydrocarbon feedstock gas (e.g. methane (CH_4) or acetylene (C_2H_2)) is pyrolyzed in the presence of a catalyst material at temperatures ranging from 750°C to 1200°C.

Self-assembly is regarded as one of the most important nanofabrication techniques, due to its relative ease-of-use, moderate low cost and the capability of constructing a wide variety of complex nanostructures over larger areas [3].

2.1.5 Applications of Nanotechnology

We are informed on a daily basis that nanotechnology will entirely change the way we live in the future. Some even envisage nanotechnology as the next "industrial revolution" and like all technological development, nanotechnology is anticipated as an inevitable objective of human advancement [2]. Scientists, physicists, novelists, engineers and noble laureates alike, have promised us electronic paper, palm-sized satellites, digital threads, self-cleaning glass, the cure for deafness and even microscopic cancer-eating robots or the so-called "nanobots" we encounter in science fiction media. In general though, it seems that much that is hyped about the nanoworld is fraught with over-expectations, but a wise man once said that "only time will tell".

Nonetheless, significant progress towards the realization of actual nanotechnological devices and systems have been made. There are numerous claims that have been made and articles that have been published across the globe, referencing terms like *"Smart Nanomaterials"*, *"Nanosensors"*, *"Nanoscale biostructures"*, *"Nano-Optics"* and *"Nano Energy Generation"* to name but a few [3]. Furthermore, prototype carbon nanotube gas sensors (e.g. gas-ionization and FET-based sensors), piezo-electric pressure sensors and various bio-detectors have also been reported in other research work [8].

The intense development of nanotechnology during the past decade has set into motion an international research and study endeavour to obtain efficient, effective and mass-producible nanodevices for applications in a variety of industries, ranging from quantum computers, micro-fluid mechanics and molecular electronics to medical and biological instruments. By observing and manipulating the inherent physical, electrical and mechanical properties of nanomaterials, it is possible to considerably improve the performance of conventional devices by enhancing their sensitivity, selectivity, portability and power efficiency.

Opportunely, in order to help third-world and developing countries obtain clean water and solve many water related health issues, "nano-membranes" or membranes fabricated by woven "nano-fibers" have been proposed, that will be portable and low-maintenance systems, with the ability to desalinate, detoxify and purify contaminated water supplies [9].

2.1.6 Latest Developments in the Nanoworld

In August 2008, the *"Project on Emerging Nanotechnologies"* estimated that there are over 800 manufacturer-identified nanotechnical products, which are publicly available, with new inventions appearing at a rate of three to four per week [10]. Thus according to the given statistic, the consumer market on this day in 2011, should boast nothing less than 1250 purchasable nanotechnology products. Most of the listed products or applications however, are limited to the utilization of so-called "first generation" passive nanomaterials, including UV absorbing titanium dioxide (TiO_2) nanoparticles present in sunscreens and certain cosmetics.

Furthermore, zinc oxide (ZnO) nanomaterials have also featured in sunscreens, cosmetics, surface coatings and outdoor furniture varnishes and paints. Cerium oxide (CeO_2), which is an oxide of the rare earth metal cerium (Ce), is a material of interest for solid oxide fuel cells [11]. Other applications include carbon and its allotropes to manufacture "gecko-tape" and silver nanoparticles in food packaging, clothing, disinfectants and anti-bacterial dressings and common household appliances.

A multitude of proposed applications using both "single-walled" and "multi-walled" carbon nanotubes (SWCNTs and MWCNTs), like CNT-fabrics, nano-memory elements, opto-electronics, digital displays, telecommunications, sports equipment, protective gear and even cartilage regeneration, have been lined up for commercial development. Other studies have included functionalized or decorated CNT-composites with better adsorption characteristics and even magnetic properties for a wide variety of sensor applications [15].

Apart from the vast amount of attention given to CNT applications, a variety of other engineered nanomaterials with promising characteristics have also been produced. These include tin dioxide (SnO_2) nanowires for gas detection, zinc oxide (ZnO) nanowires and nanobelts and indium oxide (In_2O_3) nanomaterials, which are significant transparent oxides that illustrate both insulator and semiconductive behaviour [16]. Last but not least, the now renowned 2010 physics Nobel prize winner, another carbon-based nanomaterial called "Graphene", has yielded a vast array of engineered composite materials with a multitude of possible applications.

Conversely though, due to a number of embellished claims that have been made regarding the potential contributions of nanoscience and nanotechnology and especially the use thereof in warfare and terrorism, quite a few concerns have been raised about the social and environmental effects that nanotechnology will impose on a global scale. Because of the increasing focus on the above-mentioned matters, governments and industries worldwide have initiated nanotoxicology research groups and pro-active agencies to regulate and administer the progress and application of nanotechnology.

These non-technicalities in fact, provide nanotechnology with the capability of being the first technological platform that establishes a culture of sensitivity and environmental consciousness in a hitherto infancy stage of development.

2.2 Nanosensors

In a broad sense, nanosensors are any biological, physical or chemical sensory points which are utilized in conveying information about nanoparticles and their effects to the macroscopic world. Nanosensors are mainly encountered in various medicinal applications or in the building blocks of other nano-assemblies, such as nano-scale computer chips and nanorobots. By measuring changes in concentration, volume, pressure or electrical and magnetic forces, nanosensors may be able to distinguish between entities at a molecular level and allow the monitoring and alteration of those entities.

The most universal functioning nanosensors can be found in the biological world as natural receptors like sense of smell, especially in animals such as dogs, in which the functions using receptors that sense nano-sized particles are particularly strong. Furthermore, nanosensors that detect sunlight are found on certain plants and a variety of fish utilize nanosensors to detect infinitesimal vibrations in the surrounding water. Many insect species also employ natural nanosensors in detecting sex pheromones [4].

One of the first functioning synthetic nanosensors was developed by researchers at the Georgia Institute of Technology in 1999. It involved the measurement of a discrepancy between the vibrational frequency of a carbon nanotube in a "natural" state and when a single particle is attached to it [17]. Thus the researchers were able to determine the mass of the nanoparticle via the difference in resonant frequency. Fig. 2.5 illustrates this concept.

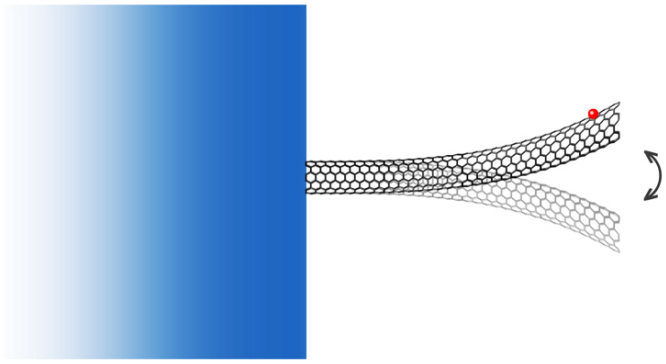

Figure 2.5: Illustration of a SWCNT resonant frequency vibrating mass sensor [17].

The unique properties of nanomaterials like carbon nanotubes (CNTs) are highly attractive for sensor purposes. The cylindrical shape and high aspect ratio of CNTs provides for large surface-to-volume ratio structures that are ideal for the adsorption of chemicals and gases. Carbon nanotube gas sensors are based on various sensing principles such as change in capacitance, resistance, electrical breakdown in a medium and conductance that is induced either within or by the carbon nanotubes themselves. Adsorption is also one of the most fashionable techniques for realizing nanotube gas sensors and since adsorption requires active

sites for the physical attachment of gas molecules, the large surface areas of CNTs are ideal for both physisorption and chemisorption [8].

The detection and observation of gases through a change in the electrical properties of carbon nanotubes has revealed the potential to achieve miniaturization, enhanced performance, acute sensitivity, detection selectivity, as well as chemical stability and the probability of lower operating temperatures.

2.3 Carbon Nanotubes

Since the discovery of carbon nanotubes (CNTs) by Sumio Iijima in 1991 at NEC Semiconductor Corporation [18], the integration of CNTs into micro- and nano-electromechanical systems (MEMS and NEMS) has increased at a quadratic rate.

The major attractions for the utilization of CNTs in micro- and nano-electronic applications are the glorious pool of characteristics and material properties confined in these novel carbon structures. CNTs offer electrical characteristics like a high current-carrying capacity, reduced charge carrier scattering, low effective electron and hole mass, attractive bandgaps and the absence of dangling bonds, which in total anticipates a substantial refinement and improvement of electronic sensory applications. Other mechanical properties of CNTs that make them especially attractive for the employment in NEMS, are the huge resilience or tensile strength provided by the strong covalent C-C bonds of the structures and the high thermal conductivity observed in CNTs [8].

2.3.1 CNT Structure

The basic definition of CNTs lies in the consideration of cylinders formed by graphene sheets, which are mono-atomic layers of honeycomb-like carbon structures. A single "graphene cylinder" is thus referred to as a Single-Walled Carbon Nanotube (SWCNT) and a Multi-Walled Carbon Nanotube (MWCNT) consists of multiple concentric graphene cylinders as depicted in Fig. 2.6.

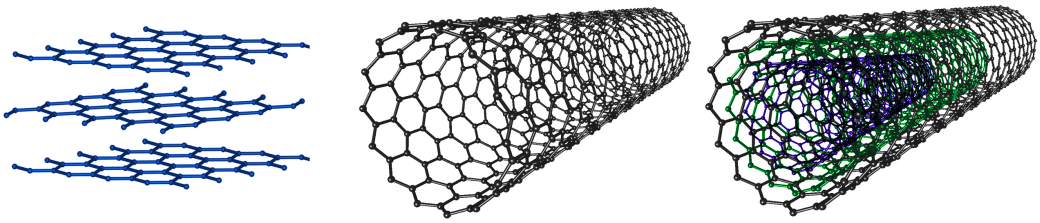

(a) (b) (c)

Figure 2.6: (a) Structure of single graphene layers. (b) Single-Walled Carbon Nano–tube (SWCNT). (c) Multi-Walled Carbon Nanotube (MWCNT) [19].

SWCNTs have typical diameters between 0.7 nm and 2 nm, however diameters of 0.4 nm and 5 nm have been recorded. The bandgaps provided by the various diameters of these SWCNTs (0.8 eV for a 1 nm diameter tube) have attracted great interest in the expansion of transistor and diode applications [8]. Multi-walled carbon nanotubes with diameters of up to 100 nm have been detected, although the average diameter for MWCNTs range between 10 nm and 20 nm. The separation of concentric cylinders in MWCNTs correspond to the 0.34 nm layer separation of graphite (i.e. multiple stacked graphene sheets).

The bond structure of a CNT is expressed via a lattice index (n,m) from which the chirality and circumference of the CNT is determined. Fig. 2.7 illustrates the indexing of the CNTs from a graphene layer and classifies the CNTs as Armchair (n=m), having metallic properties, or as Zigzag (n≠m), in which case the CNTs have semiconductive properties. Fig. 2.8 depicts these different types of CNTs. It is thus notable that the electrical properties of carbon nanotubes are dependent on the chirality and diameter of the structure, defined by the chiral vector

$$C_h = n \cdot a_1 + m \cdot a_2$$

where the index (n,m) and two unit vectors $\mathbf{a_1}$ and $\mathbf{a_2}$ are shown in Fig. 2.7. From a statistical point of view, only a third of the achievable SWCNT formations, regardless the synthesis procedure, are metallic and the remaining two thirds are semiconductive, whilst MWCNTs always inhibit metallic behaviour [8].

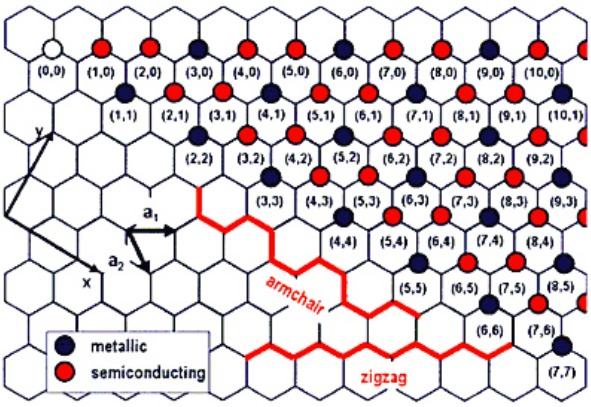

Figure 2.7: A map showing which index (n,m) presents semiconducting and metallic CNTs. The index (n,m) determines the chirality and circumference of the CNT [8].

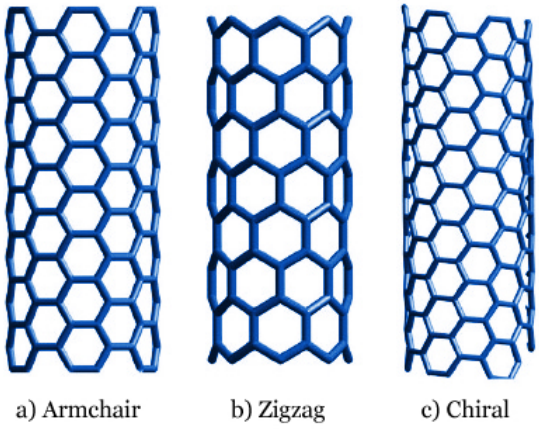

Figure 2.8: The different types of carbon nanotubes [20].

2.3.2 Properties and applications

Following the discovery of CNTs, which were obtained through an arc-discharge procedure, a variety of fabrication methods have been pioneered to manufacture nanotubes. These include laser ablation and the more applicable method for direct MEMS integration, namely "catalyst enhanced chemical vapour deposition" or CCVD. Carbon nanotubes are therefore created through a molecular self-assembly (bottom-up) process and due to the chemical inertness and covalent bonds of the CNT structure, they inhibit a high mechanical stability. CNTs would thus allow the integration with MEMS even at high temperatures.

Micro-electromechanical systems (MEMS) are microscopic systems that coalesce mechanical, electromagnetic, optical, fluidic and thermal elements with electronics and conductors on semiconductor substrates. The integration of CNTs into MEMS (Fig. 2.9), thus providing nano-electromechanical systems (NEMS), are highly dependent on the electrical and mechanical elements of the carbon nanotubes. These elements include the exceptionally high thermal conductivity of CNTs, their ability to undergo massive non-linear deformation without permanent damage and the ability of SWCNTs to conduct electrons at extraordinary current densities, using a form of ballistic conduction [8].

The highly attractive electrical and mechanical properties of CNTs has accordingly led to the possible convolution of CNTs with electronic components like diodes, transistors, power-transistors, flexible and stretchable interconnects and low-k dielectrics. Electromechanical carbon nanotube transducers, including pressure sensors, CNT relays, displacement and force sensors, are all developed on the concepts of piezoresistance of CNTs, mechanical band gap tuning of CNTs, the tight-binding approximation for strained graphene and the electronic structure of carbon nanotubes [8].

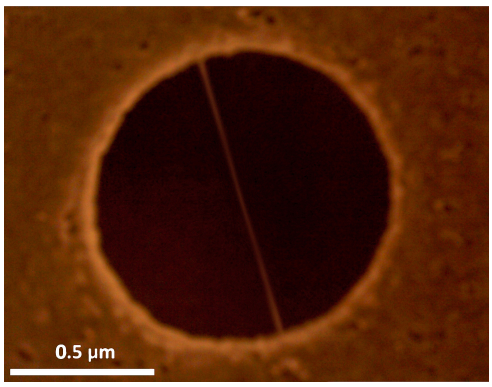

Figure 2.9: Example of a MEMS structure with a horizontally spanned MWCNT, synthesized via a thermal CVD technique at 800°C [8].

2.4 Graphene

For several years scientists and physicists supposed the existence of a theoretical material, consisting of a single atomic layer of sp^2-bonded carbon atoms, that are covalently packed to form a two-dimensional honeycomb-like lattice [21]. Following the actual discovery of graphene by Geim et al. [22] in 2004, a huge wave of scientists have reported some of the most fascinating material properties pertaining to this basic building block of carbon-based nanomaterials in all dimensionalities, as shown in Fig. 2.10.

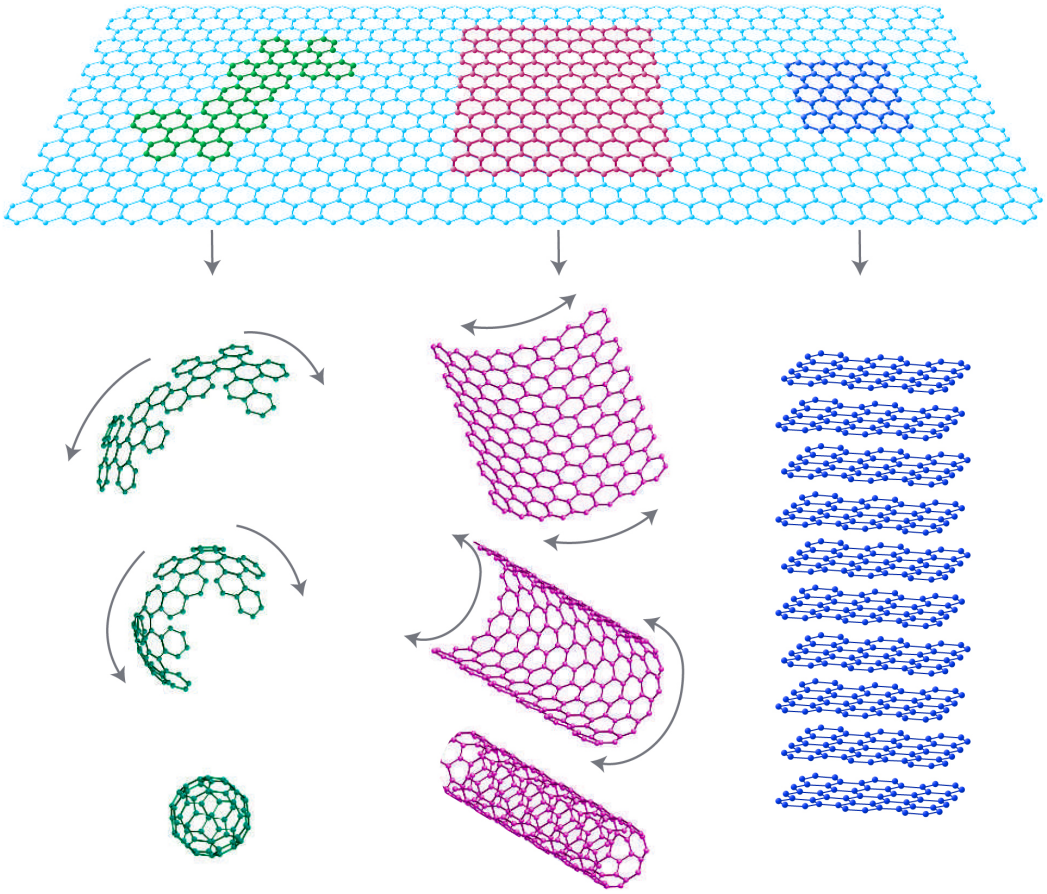

Figure 2.10: Illustration of a 2-dimensional (2D) graphene sheet, forming the basic building block of carbon-based materials. Dimensionalities: Fullerenes (0D), CNTs (1D) and graphite (3D) [22].

2.4.1 Discovery of graphene

Graphite, consisting of hundreds of thousands of stacked graphene layers, was in effect the source to discovering the first mono-atomic graphene layers. Geim et al. [22], implemented a rather unusual method to generate graphene, whereby a piece of graphite was exfoliated using scotch tape. The strands of scotch tape were then dissolved and a silicon substrate was placed in the solution, onto which the graphene flakes then stuck to the surface.

Other methods to fabricate graphene, including the epitaxial growth on SiC (silicon carbide) [23], the epitaxial growth on metal substrates [24] and the rapid heating of graphite oxide [25], as well as chemical vapour deposition (CVD) methods [32], have since been developed.

2.4.2 Properties and applications

Not only is graphene the material with the lowest resistivity, but graphene also exhibits especially high electron mobilities and is the strongest material to date, having a near 1.0 TPa Young's Modulus [26]. Furthermore, graphene boasts an immense thermal conductivity of up to 5300 W/mK, prevailing over all metals, carbon nanotubes and even diamond [27]. Other properties drawing the attention of researchers to the utilization of graphene include the high current density of graphene, as well as the low absorption and reflection coefficients of few layer graphene for a wide spectrum of frequencies [28].

As more of these unusual and extraordinary properties of graphene are revealed, the list of potential applications expand at an astounding rate. Like CNTs, graphene's high electron mobility makes it a prime candidate for replacing contemporary and state-of-the-art transistors to reach new frontiers in processing speed. It is foreseen that graphene-based field-effect transistors (FETs) and molecular electronics incorporating the superior properties of graphene, will ultimately replace our modern day integrated circuit technology, yielding revolutionary electronic devices [29].

The contributions of graphene to the field of opto-electronics is another area of interest, since the current fabrication of thin, optically transparent (especially in the lower nm or UV wavelengths) and conductive films for the use in opto-electronic devices, are quite often very expensive and rather time consuming. Graphene has been proposed as an alternative to ITO (indium tin oxide) and FTO (fluorine doped tin oxide) materials, currently used for touch-screen applications and transparent electrodes in the solar cell industry [30]. Alternatively, the extremely high surface-to-volume ratios of 2D graphene sheets, together with the advanced mechanical and electrical properties it possesses, make the implementation of graphene for sensory applications very attractive [28]. This was demonstrated by Geim et al. [31], when they fabricated a gas sensor from single-layer graphene (produced by the "scotch tape method"), that had the capability to detect an individual gas molecule.

Although we have witnessed some of the most remarkable properties and capabilities of graphene, there are still no commercially available nanodevices that incorporates these superior characteristics. This is mainly due to the fact that all graphene-based nanodevices being developed, are still confined to laboratory experiments and that the complexity of generating continuous and reproducible large-scale graphene films for industrial applications, still need to be overcome.

2.5 Summary

This chapter reviewed the basic definition of nanotechnology and briefly discussed the history and physics pertaining to the nanoworld. It also described some of the nanofabrication tools and techniques that are generally employed in the manufacture and analysis of nanomaterials and nanodevices. Furthermore, a brief note on nanosensors was presented followed by an in-depth study of the carbon nanomaterials utilized throughout this research. The following chapters are thus concerned with detailed procedures utilized to synthesize some of the described nanostructures, as well as the fabrication and analysis of gas nanosensors implementing those nanomaterials.

Chapter 3

Synthesis of Carbon Nanomaterials

It has already been noted that CNT-based gas sensors are constructed on numerous sensing principles, such as changes in resistance and capacitance or electrical breakdown in a medium or induced conductances. Therefore the preparation of carbon nanomaterials and the integration thereof into sensory applications are very important for the improvement of the selectivity and sensitivity of contemporary sensors.

This chapter briefly describes the three most popular techniques for the synthesis of carbon nanotubes (CNTs) and also mention some of the complexities pertaining to them. Subsequently, the role of water in the "super-growth" of carbon nanotubes is presented and a few general rules, governing the highly efficient growth of CNTs, are noted. Furthermore, the purification and functionalization of CNTs for their incorporation in gas sensors are discussed. This chapter is then concluded with the chemical vapour deposition (CVD) procedures, that were developed for the synthesis of carbon nanotubes and graphene during this research.

3.1 Synthesis of CNTs

The three most popular techniques for the production of carbon nanotubes (CNTs) are the *"carbon arc discharge"* method, the *"laser ablation"* method and the various forms of *"chemical vapour deposition"* or CVD methods. The arc discharge and laser ablation methods, involve the evaporation of graphite rods by applying high-voltage AC potentials or a high-intensity pulsed laser source, under constant inert gas flows.

The chemical vapour deposition (CVD) method and its successor, the catalyst enhanced CVD (CCVD) method, are techniques for the synthesis of CNTs, during which a hydrocarbon gas is decomposed into active radical species in the presence of metallic catalysts at high temperatures [8].

CVD synthesis techniques are generally preferred for their moderate simplicity and economical viability. In addition, the resources for hydrocarbons are plentiful in any material state - solid, liquid or gas. Frequently used sources of hydrocarbon gases are methane (CH_4), ethylene (C_2H_4) and acetylene (C_2H_2). Using the CVD technique, Yacaman et al. [33], produced CNTs with lengths reaching 50 μm by using acetylene as hydrocarbon source and iron (Fe) nanoparticles as catalyst at 700°C. Employing a similar catalyst, Endo [34], produced carbon nanotubes from the pyrolysis of benzene at 1100°C. It is also worth noting that the Smalley group [35], invented the HiPco procedure for the mass production (10g/day) of high-purity SWCNTs, which was also based on the hydrocarbon CVD method.

Unfortunately there are several complexities and challenges on the way to realizing integrated CNT-based nanosensors. The attempts to produce high-purity CNT synthesis methods are inevitably floundered by the mixture of carbonaceous and metal nanoparticles (i.e. impurities), that are present in the resulting product. These impurities can greatly reduce some of the fascinating transduction capabilities of CNTs. Xu [36], used a combination of sonication, oxidation and acid washing stages to purify SWCNTs that were synthesized by CVD techniques using carbon monoxide (CO) as a feedstock gas. The purification of carbon nanotubes is discussed in more detail in Section 3.4.

Current state-of-the-art controlled CNT-synthesis procedures have been developed, which utilize sophisticated alignment and location control techniques [37], as well as catalyst patterning procedures [38]. Standard lithographic procedures have also been employed, using either an electron beam or UV light to pattern holes in a resist material, into which a metallic catalyst is deposited. The resist material is subsequently lifted off via a chemical process, yielding isolated catalyst islands on which the CNT growth is then performed.

Ultimately, the key restraints towards the deterministic synthesis of carbon nanotubes, are a lack of diameter and chirality control mechanisms. The lack of control of these factors are attributed to the difficulty in measuring the chirality of CNT samples and the fact that several metallic and semiconductive chiralities have almost identical diameters. However, the above-mentioned catalyst patterning techniques, together with a better controlled growth temperature has, to a certain extent, provided control over the diameters of synthesized CNTs [8].

3.2 Contribution of water to the "super growth" of CNTs

The growth of carbon nanotubes on active catalyst nanoparticles can be greatly enhanced by the addition of water vapour to the hydrocarbon feedstock gas, used in chemical vapour deposition (CVD) processes. This was revealed by Amama et al. [39], who demonstrated the ability of oxygen and hydroxyl species to increase catalyst activity to almost 84%, compared to approximately 6% without the addition of H_2O molecules to the reaction.

Studies by Hata et al. [40], attributed the termination of CNT growth to the formation of amorphous carbon coatings on active catalyst particles, thus limiting the catalyst's lifetime. They have also shown that a water-assisted CVD technique, also referred to as CNT "super growth", can dramatically enhance the activity and lifetime of catalyst particles in the CVD process. They propose that the introduction of a well defined and limited quantity of water vapour (H_2O) into the growth chamber, will decompose into its radical species at high temperatures,

causing rapid oxidation of the amorphous carbon coatings. Due to the high temperatures at which CNTs are formed, the oxidized carbon shells quickly expands and fractures, restoring the activity of the catalyst nanoparticle. A graphical interpretation of this concept is illustrated in Fig. 3.1.

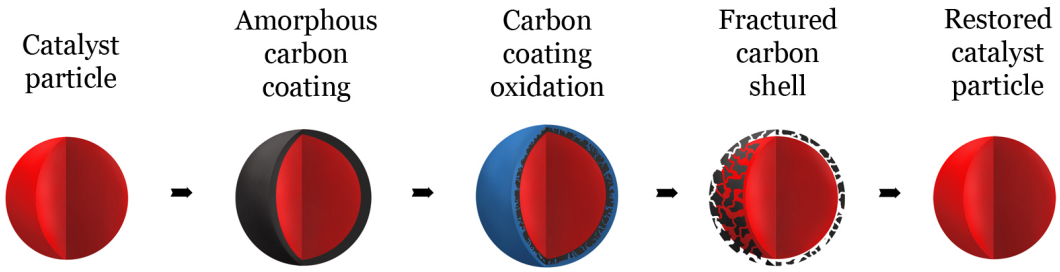

Figure 3.1: Oxidation of amorphous carbon coatings on catalyst particles, during the "super growth" of carbon nanotubes.

Furthermore, it has been observed that through the addition of confined amounts of H_2O to CVD growth procedures, the ability to stabilize small catalyst nanoparticles is acquired, thus suppressing the fusion of catalyst particles and providing a degree of control over the diameter of synthesized CNTs [39].

Although the oxidation mechanism of carbonaceous coatings on catalyst particles is not yet fully understood and other phenomena, like the Ostwald ripening of catalyst particles [39], are also proposed for enhanced catalyst activity, these results reveal that the presence of oxidants in CVD reactions, can generally increase a catalyst's activity and lifetime. A discussion of this revelation is presented in more detail in the following section, together with a few general rules that govern the efficient synthesis of carbon nanotubes.

3.3 General rules governing the highly efficient synthesis of CNTs

In the early years after the discovery of carbon nanotubes, research on the growth mechanisms of CNTs was restricted to theoretical calculations and microscopic analysis techniques, due to the limited availability of CNTs. Since then, numerous methods to synthesize CNTs, especially by chemical vapour deposition (CVD), has drastically advanced our understanding of CNT formation.

As presented in Section 3.2, the concept of CVD synthesis was further expanded by the addition of a "growth enhancer" into the CVD system. The water-assisted CVD technique has demonstrated the growth of SWCNT carpets into millimeter tall forests, with exceptional yields and carbon purities, all with the addition of minuscule levels of H_2O molecules ($\approx$ 100-200 ppm). These results have also extended the list of possible applications for carbon nanotubes, for instance super-strong fibers, high-density super-capacitors, stretchable conductors and 3D micro-electromechanical systems (MEMS) [41].

Extensive research by Futaba et al. [41], recently demonstrated that the highly efficient synthesis of CNTs can also be achieved by the addition of other growth enhancers, including alcohols, esters, ethers, aldehydes, ketones and even carbon dioxide (CO_2). Furthermore, they investigated the effects of various carbon sources on the growth of carbon nanotubes, as well as the effects of combinations of carbon sources and growth enhancers on CVD techniques.

Fig. 3.2 illustrates experimental results obtained by Futaba and his associates, for various growth enhancers used in a CVD process at 750°C with ethylene (C_2H_4) as carbon feedstock gas. These results depict the average length of CNTs, measured by an in situ telecentric height-monitoring system, that were obtained during their experiments. In addition, the performed experiments were only optimized for the level of growth enhancer, thus excluding optimization of other synthesis parameters like carrier gas flow rates, reaction temperatures and growth times.

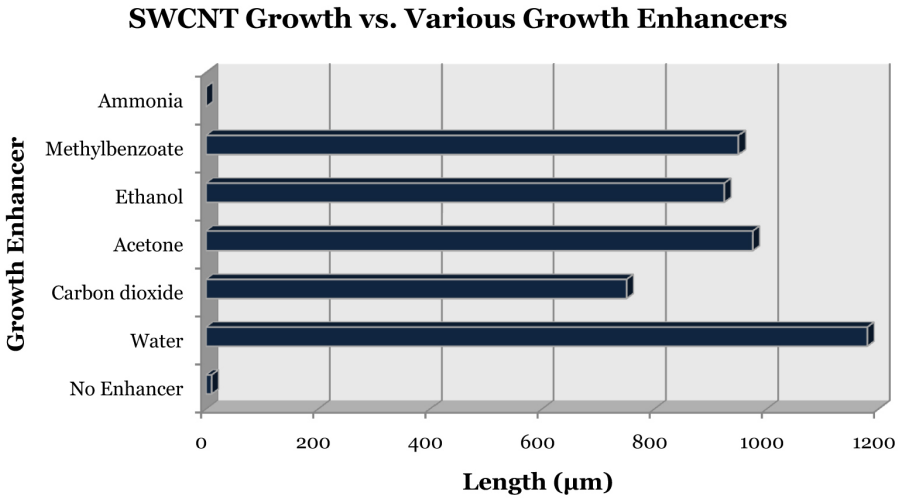

Figure 3.2: Average SWCNT length for various growth enhancers in an ethylene (C_2H_4) CVD process [41].

From the results portrayed in Fig 3.2, it can be observed that the enhanced synthesis or so-called "super growth" of carbon nanotubes is not limited to only water, but include several oxygen-containing substances, such as ethanol (alcohols), acetone (ketones), methylbenzoate (esters) and even CO_2 (an indigenous oxide of carbon). These growth enhancers were found to improve the rate of growth and growth yield, as well as catalyst activity and catalyst lifetime. Similar enhancement patterns were also observed, where the CNT production increased, peaked and then declined again with increasing levels of the various growth enhancers [41].

In stark contrast to the exceptional functionalities of the oxygen-containing substances, ammonia had no enhancing effect on the growth of CNTs via the CVD process. Ammonia (NH_3), a nitrogen-containing species, is often included in plasma-enhanced CVD procedures, but had no visible effect on the atmospheric, carrier-flow CVD technique utilized by Futaba et al. [41].

Furthermore, to investigate the effects of various carbon sources, Futaba and his associates performed a water-assisted CVD experiment, with a fixed level of water vapour ($\approx$ 150 ppm) and different carbon feedstock gases (i.e. acety-

lene (C_2H_2), ethylene (C_2H_4) and carbon monoxide (CO)). From Fig. 3.3, which presents the results for the various carbon source materials, it can be observed that the combination of acetylene and water, prevailed over the ethylene-water combination and that the water-carbon monoxide combination yielded extremely poor CNT growth compared to the other two procedures.

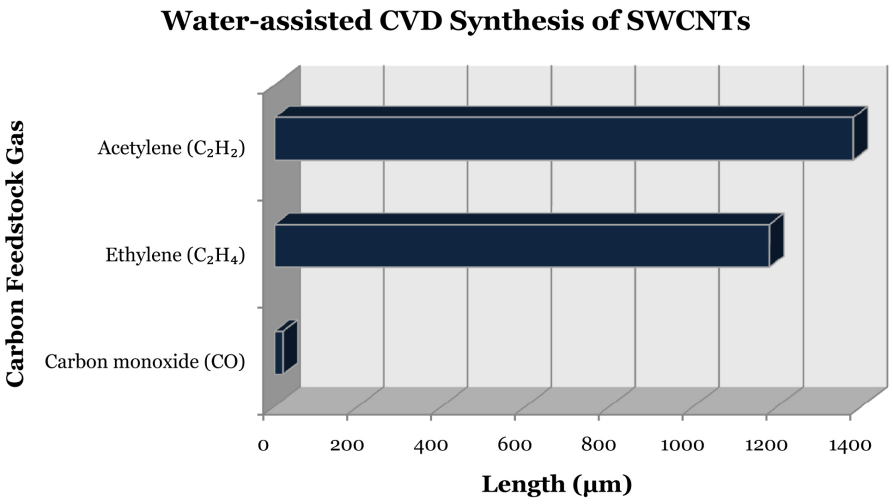

Figure 3.3: SWCNT growth for various carbon source materials [41].

Concluding the research performed by Futaba [41], two fundamental rules were derived for the highly efficient synthesis of carbon nanotubes:

i) An oxygen-containing growth enhancer must be added into the CVD reaction environment, and

ii) A carbon source (feedstock gas) that does not contain oxygen must be used.

These two rules are also explained, in general, by the catalyst encapsulation (amorphous carbon coating) mechanism, that was described in the previous section for water-assisted CVD techniques.

Lastly, the three universal factors pertaining to the implementation of the two

fundamental rules, are:

a) Compared to a normal CVD process (no enhancer), even tiny amounts of growth enhancer (e.g. acetone ($\approx$ 120 ppm), water ($\approx$ 150 ppm) or CO_2 ($\approx$ 1000 ppm)), can drastically improve catalyst activity and CNT production.

b) "Super growth" or enhanced CVD synthesis is strongly dependent on the levels of growth enhancer delivered to the growth environment (i.e. the production increases, peaks and declines again with increasing levels of growth enhancer).

c) The amount of growth enhancer that is required to optimize the CVD process, is considerably less than the corresponding amount of carbon source material, as the presence of excessive amounts of oxygen (as in the case of water and carbon monoxide) will cause superfluous oxidation of the catalyst material, curtailing the efficient synthesis of carbon nanotubes.

3.4 Purification of carbon nanotubes (CNTs)

As the synthesis of carbon nanotubes via chemical vapour deposition (CVD) methods are essentially accompanied by various carbonaceous impurities and residual catalyst particles, efficient and effective purification methods are crucial for applications that require high-purity CNTs. These carbonaceous impurities can range from amorphous carbon and fullerenes to carbon nanoparticles and graphitic polyhedrons [42]. Furthermore, metal catalyst particles present in the CNT product, are generally encapsulated by various forms of carbon layers and may require a multi-phase purification process to remove them. An adaptation of frequently used techniques for the analysis of impurities in CNT materials, as described by Cheng et al. [42], is presented in Table 3.1.

Table 3.1: Common techniques for the analysis of impurities in CNT materials [42].

Technique	*C-I*	*M-I*	*F-G*	*S-D*	*C-F*	Advantages	Limitations
EM	✓	✓		✓		Direct observation	Only small amounts of sample can be analyzed
TGA	✓	✓				Precise content of carbon and metals	CNTs are completely destroyed
Raman	✓			✓	✓	Diameter, quality and conductivity of SWCNTs	Invalid for metal impurities
UV-vis-NIR	✓				✓	Conductivity feature content of SWCNTs	Need 100% pure CNTs as standard
XPS			✓			Accurate assessment of functional groups on CNTs	Invalid to purity assessment
EDS		✓				Elemental contents, special for trace amounts	Invalid to evaluate CNT content

EM	=	Electron Microscopy	***C-I***	=	Carbon impurity
TGA	=	Thermogravimetric Analysis	***M-I***	=	Metal impurity
UV-vis-NIR	=	Ultraviolet-visible-near infrared	***F-G***	=	Functional groups
XPS	=	X-ray Photo-electron Spectroscopy	***S-D***	=	Structural defects
EDS	=	Energy Dispersive Spectroscopy	***C-F***	=	Conductivity feature

Furthermore, the purification methods implemented to purify CNT materials can be divided into three general categories:

i) Chemical oxidation techniques

ii) Physical-based purification techniques, and

iii) Multi-phase purification techniques

3.4.1 Chemical oxidation techniques

Compared to carbon nanotubes (CNTs), the carbonaceous impurities (i.e. amorphous carbon and carbon nanoparticles) usually demonstrate higher oxidation activities, due to the presence of larger structural defects and generally larger curvatures [43]. The purification of CNT materials with chemical oxidation techniques are thus aimed at a selective oxidation process, during which the carbon-based impurities are oxidized more rapidly than the CNTs.

Chemical oxidation techniques are generally subdivided into gas phase oxidation, liquid phase oxidation and electrochemical oxidation. However, several disadvantages of these methods have been documented, which include structural damage to the CNTs and the introduction of various oxygen-containing functional groups (e.g. -COOH, -OH and -C=O) on the carbon nanotubes. The latter formation of functional groups on CNT surfaces, is not necessarily such a disadvantage, as these functionalized CNTs can be implemented as selective chemical reactors in sensory applications [44].

Gas phase oxidation

Gas phase oxidative purification techniques generally consist of the oxidation of carbonaceous impurities in an oxidizing environment at temperatures ranging from 225°C to 760°C. Commonly used oxidants include air, combinations of argon (Ar) and O_2, mixtures of HCl and H_2O, mixtures of O_2, SF_6 and $C_2H_2F_4$, as well as combinations of H_2S and O_2 and also steam [42].

Furthermore, it has been demonstrated that gas phase oxidative techniques require the even exposure of carbon nanotubes to the oxidizing environment [45] and that an enhanced difference in oxidation resistance between the carbonaceous impurities and CNTs, are beneficial for the production of larger purified quantities of nanotube material [46]. Other research [47] has indicated that the effects of gas phase oxidation on MWCNTs and SWCNTs differ quite substantially. These effects were also described by Chiang et al. [48], who attributed the discrepancies to the larger amount of curvature observed for SWCNTs and the fact that metal particles present in the oxidation process, act as a catalyst

towards the oxidation of SWCNTs.

It was therefore concluded by Cheng [42], that gas phase oxidation techniques are primarily applicable to CNT materials synthesized via the arc discharge or laser ablation methods and that purification of MWCNTs or SWCNTs synthesized by CVD techniques, always require acidic treatments to purge metal catalyst particles.

Liquid phase oxidation

In order to surmount the limitations of gas phase oxidative purification, liquid phase oxidation techniques have been developed, allowing the simultaneous removal of both metal catalyst particles and amorphous carbon materials [42].

A number of liquid phase oxidants, including HNO_3 (nitric acid), H_2O_2 (hydrogen peroxide) or mixtures of H_2O_2 and HCl (hydrochloric acid), mixtures of H_2SO_4, HNO_3 and NaOH and also $KMnO_4$, have been applied to purify both SWCNTs and MWCNTs [42]. As mentioned earlier, these liquid based acidic and/or oxidative treatments leads to the formation of several functional groups on the surfaces of carbon nanotubes and may also cause the destruction of CNTs (e.g. cutting and opening of CNTs).

Numerous oxidants have been investigated for the purification of CNTs and various results, regarding the efficiency of the oxidants on particular nanotube materials, have been reported [42]. Nitric acid was found to be the most frequently used reagent for the purification of SWCNTs that were synthesized via laser ablation procedures [48]. This being attributed to the mild oxidation capability of HNO_3, which allows the selective removal of amorphous carbons together with small quantities of metal particles, without the introduction of secondary impurities.

Hydrogen peroxide (H_2O_2) is also considered a mild and "green" oxidant and is a rather inexpensive treatment to oxidize carbonaceous materials. An obvious disadvantage of H_2O_2, is its inability to remove metal catalysts. Subsequently, a

combination of H_2O_2 and HCl was proposed by Wang et al. [49], which dissolved the amorphous carbon coated metal impurities in an aqueous solution of H_2O_2 and HCl at 70°C.

Furthermore, mixtures of concentrated H_2SO_4 (sulfuric acid) and HNO_3 (3:1 by volume), have been found more effective for the purification and parting of long and highly tangled ropes of CNTs [50]. Other methods include the microwave-assisted purification of CNTs, during which inorganic acids (e.g. HCl, H_2SO_4 and HNO_3) rapidly absorb microwave energies, reducing the treatment time and increasing the efficiency of the purification process [51],[52].

Liquid phase oxidation techniques are thus continuous procedures, that can purify CNT materials on a large scale and simultaneously induce surface functionalization on nanotube sidewalls, thus increasing their chemical activity and solubility in aqueous solutions. This in turn, provides for enhanced physical and chemical properties that are attractive for various applications.

Electrochemical oxidation

The electrochemical cyclic voltammetric (CV) oxidation of CNT materials are generally performed in aqueous solutions of medium to strong acids (e.g. H_2SO_4, HNO_3, H_3PO_4 and CH_3COOH), which can readily remove carbonaceous materials as well as metal catalyst particles [42].

Although the electrochemical CV purification methods provide for easy calculation of the optimal process time and degree of oxidation, these methods are insufficient for the removal of polyhedral carbon structures, graphite particles and low-defect carbonaceous catalyst coatings. Furthermore, these oxidation techniques are very limited in terms of batch size, making it inappropriate for large-scale or industrial application.

3.4.2 Physical-based purification techniques

A major drawback of the chemical purification techniques described in the previous subsection, is the inevitable destruction and functionalization of the CNTs. Therefore, in order to extract the natural and intrinsic chemical and physical properties of carbon nanotubes, physical-based purification techniques that exclude acidic or oxidative treatments, have been devised. Due to the morphology and physical attributes of CNTs, including physical size, aspect ratio and solubility, which differs from carbonaceous and metal impurities, the application of physical-based techniques to purify CNT materials is permissible. These techniques vary from filtration, centrifuging and chromatography to high temperature annealing (>1400°C) and electrophoresis [42].

Filtration and centrifuging

The filtration and separation of CNT materials is derived from the differences in morphology (i.e. size, aspect ratio, solubility) of MWCNTs, SWCNTs, fullerenes, carbonaceous nanoparticles, poly-aromatic carbons and metal catalyst particles.

Filtration is usually preceded by the submersion of the as-synthesized CNT material into certain organic solvents (e.g. CS_2, toluene, etc.), which easily dissolve fullerenes and poly-aromatic carbon particles. During the filtration step, small sized particles (smaller than the filter holes) are removed and CNTs (with their large aspect ratios) will remain in the filter. Therefore, filtration techniques also requires the preparation of stable suspensions of carbon nanotubes to avoid CNT aggregation and blockage of the filter membranes [53].

The inherent untainted interactions of carbon structures with amphiphatic molecules and the filter membranes, which leave CNTs undamaged, is thus seen as a great advantage of filtration techniques. However, the pure physical separation by filtration cannot effectively remove carbonaceous particles (e.g. fullerenes) that adhere to the sidewalls of the CNTs.

Differing from filtration, centrifugal techniques rely on differences in the weight of particles, which are separated by gravitational forces during the centrifug-

ing process. This separation is also possible due to the difference in stability of the dispersed carbon products (i.e. CNTs, amorphous carbon and carbon nanoparticles), whereby the differences in stability are produced by different surface charges induced by treatment with nitric acid [54]. Unfortunately, the acid treatment introduces the oxygen-containing functional groups on CNT surfaces as discussed earlier, which limits the application of centrifuging to purify CNTs in a non-destructive way.

High temperature annealing

Briefly stated, the annealing of CNT materials at high temperatures (1400°C to 2000°C) remains one of the most efficient procedures to remove metal catalyst particles at the ends or in the hollow cores of carbon nanotubes [55], and to transform CNT materials form disordered to straight and crystalline structures [56].

In addition to an increase in mechanical strength and thermal stability, the high temperature annealing process also affects the electronic transport properties of CNTs. It was however observed by Hayashi et al. [56], that the complete elimination of amorphous carbons was not achievable and that they become more resistant to removal once graphitization occurred at the high process temperatures.

The high temperature annealing technique is therefore proposed for the removal of metal catalyst particles, residual in CNT materials that have been purified by other methods. Cheng et al. [42], also proposed the high temperature annealing for the removal of metal nanoparticles in CNT materials containing small amounts of carbon impurities or for cases where the existence of carbonaceous contaminants is of little concern.

3.4.3 Multi-phase purification techniques

The formulation of multi-phase purification processes arose from the deficiencies of chemical and physical purification techniques, to simultaneously remove carbonaceous impurities and metal catalyst nanoparticles. Therefore, various combinations of physical and chemical procedures have been investigated to achieve a desired carbon nanotube purity, together with a high product yield.

Examples of these processes include the combination of hydrothermally initiated dynamic extraction (HIDE) with acid treatment [57], microfiltration in combination with chemical oxidation [58], ultrasonication in conjunction with chemical oxidation [59] and also combinations of high temperature annealing and non-destructive polymeric extraction [60].

Based on the brief description of the multi-phase purification of CNTs, it can be concluded that the careful selection and the skillful combination of different physical and chemical techniques, can provide the ability to selectively purify and separate carbon nanotubes, to form functional groups on CNT surfaces or to maintain (or recover damaged CNTs to) undamaged nanotube structures [42].

3.5 Functionalization of CNTs

The functionalization or decoration of carbon nanotubes with functional groups are not limited to the organic oxygen-containing groups (i.e. -COOH, -C=O and -OH) that were encountered during the chemical oxidation procedures presented in Section 3.4. In fact, the functionalization of CNTs and the interactions between carbon nanotubes and other nanoparticles and molecules have been intensively investigated in recent years. This being partly due to the fact that numerous metal-decorated CNT systems have demonstrated inimitable or enhanced sensitivities for gaseous species like H_2, CO, CH_4, NO, NO_2 and H_2S [61]. The possibilities of molecular and biological sensing with functionalized CNT materials have also extended research into nanotube electronics to new dimensions.

Furthermore, the list of metal nanoparticles that are utilized for CNT decora-

tion is growing quite rapidly and includes gold (Au), silver (Ag), platinum (Pt) rhodium (Rh), nickel (Ni), tin (Sn) and iron (Fe). The functionalization of CNTs with iron oxides have also been investigated for producing magnetic CNT composite materials. Wang et al. [62], performed a solvothermal procedure for the fabrication of magnetic Fe_3O_4-CNT composites, by which acid treated MWCNTs were ultrasonically dispersed in a solution of ferrocene ($Fe(C_5H_5)_2$) and benzene. The CNT-solution was subsequently sealed in a stainless-steel autoclave and thermally treated at 500°C for 12 hours to produce a magnetite-CNT material.

Other research [61] reported the application of cathodic electrochemical potentials in metal-salt solutions, to induce the growth of Au, Pt and Rh nanoparticles on SWCNT surfaces, as well as thermal evaporation procedures for decorating CNTs with Ni nanoparticles [63].

Felten et al. [63], demonstrated that the performance of metal decorated nanotube devices are influenced by potential barriers that exist at the metal-CNT junction, which regulates the injection of electrons into the CNTs. Although the concepts of metal-decorated CNTs for gas sensing applications are highly attractive, very little is actually known about the inter-facial potential barriers and the transfer of electrons between the nanotubes, metal particles and impeding gas molecules. This is further complicated by the presence of impurities like carbonaceous particles, metal catalysts and the formation of native oxides of the decorating metal nanoparticles [61].

Nonetheless, the decoration and functionalization of carbon nanotubes forms a key area of interest for the fabrication of sensitive and highly selective CNT-based chemical sensors.

3.6 Water-assisted CVD techniques for the synthesis of CNTs

After investigating the work of Xie et al. [64],[65], who reported a floating catalyst chemical vapour deposition (CVD) method to synthesize random networks of SWCNTs, in conjunction with the work of Wang et al. [66], and taking into consideration the role of water in the "super-growth" of carbon nanotubes, a unique water-assisted floating catalyst CVD process was implemented to synthesize carbon nanomaterials during this research.

3.6.1 Synthesis of MWCNTs

The floating catalyst CVD method described by Xie [64], consisted of a two stage furnace system housing a three-section quartz tube, in which random networks of SWCNTs were synthesized at 1100°C.

Due to the limited availability of custom quartz tube manufacturers locally, a three-section stainless-steel tube was fabricated accordingly for the experimental procedures. The tube was placed horizontally in an electrical furnace and a custom-designed Peltier heating system was fitted to the tube to complete the dual-furnace setup as proposed by Xie et al. [65]. Appendixes A, B and C presents the electrical furnace's temperature profile that was measured, a detailed design of the Peltier heating system and the dimensions of the three-section stainless-steel tube, respectively.

A process diagram of the experimental setup that was constructed for the synthesis of MWCNTs is illustrated in Fig. 3.4. The water-assisted floating catalyst procedure consisted of flowing a carbon feedstock gas, in this case acetylene (C_2H_2), through a humidification stage and into the two stage furnace system. A ferrocene ($Fe(C_5H_5)_2$) catalyst (from Sigma-Aldrich) was sublimed in the first furnace at ≈ 55°C and carried by the hydrolyzed feedstock gas into the reaction zone at 850°C.

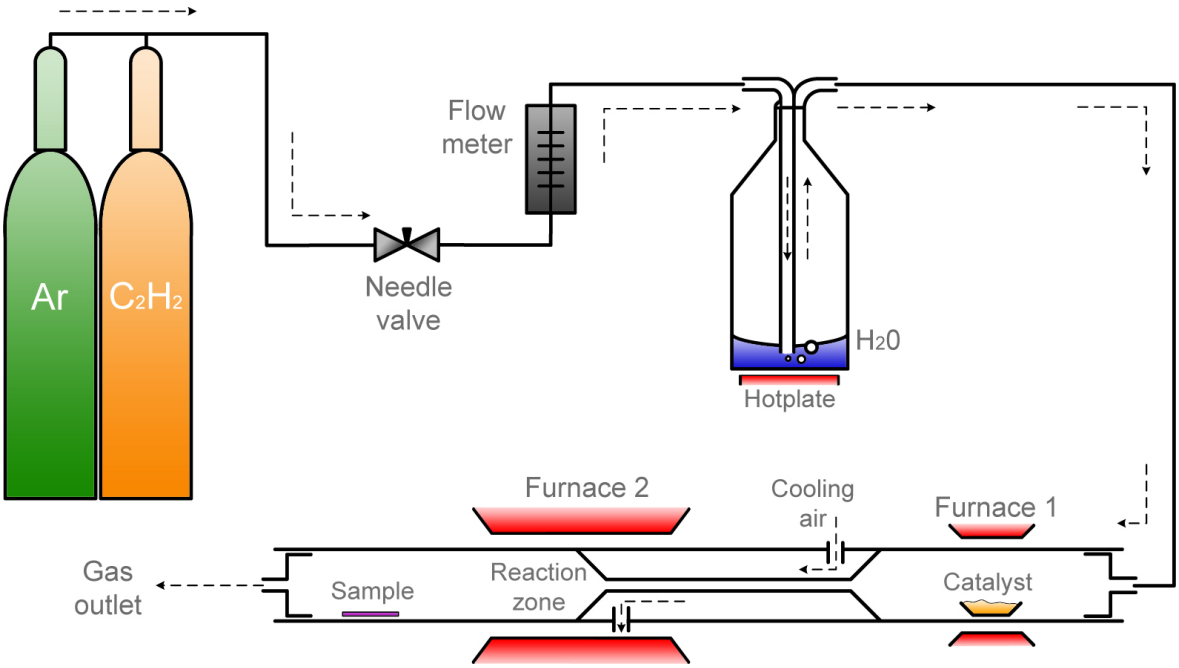

Figure 3.4: Setup for the water-assisted floating catalyst CVD synthesis of MWCNTs.

Once in the reaction zone, the feedstock gas decomposes and reacts with the catalyst particles to form the carbon nanotubes, which float on the carrier gas and deposits further down in the tube. According to Xie [64], the narrower connection tube leading to the reaction zone, effectively controls the quantity of catalyst material delivered to the reaction zone and also accelerates the reactant mixture flowing through this transitional connection segment. These effects are then proposed to reduce the likelihood of catalyst aggregation and the formation of carbonaceous impurities (i.e. amorphous carbons). It is also anticipated that the smaller transition tube (5 mm in diameter) causes a transverse and circumfluent flow of the reagent mixture, which effectively blends the catalyst particles with the radical gas molecules to facilitate CNT growth [64]. Furthermore, cooling air is pumped through the system to prevent the formation of carbon products in the small connecting tube.

A mixture of ferrocene (dicyclopentadienyl iron) and sulfur (16:1 molar ratio) was used as the catalyst source and the experiments were performed with flow rates of 1000 sccm Ar and 1-3 sccm C_2H_2 (acetylene) for 1 hour. The pressure inside the stainless-steel tube was held constant at 1.0 atm for all experiments

and the amount of distilled water vapour added to the process was controlled by the temperature of the hotplate (typically 45°C to 60°C).

Fig. 3.5 shows an optical micrograph of the as-synthesized CNT-product that was collected as pieces of black film on the inner wall of the end parts of the tube.

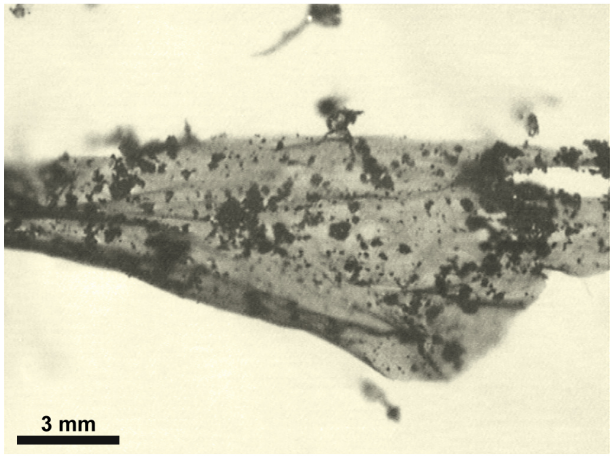

Figure 3.5: Optical micrograph of the as-synthesized MWCNT product.

The as-synthesized CNT material was further observed by high-resolution electron microscopy (HRTEM) at the TEM facility of the University of the Western Cape (UWC) - HRTEM model: FEI Tecnai G2 Spirit. The samples were prepared for TEM imaging by dispersing a small amount of the product in pure ethanol and depositing it onto standard TEM carbon coated nickel grids.

Fig. 3.6 depicts a typical HRTEM micrograph of a MWCNT with a diameter of $\approx$ 25 nm, consisting of roughly 27 or 28 concentric nanotubes, whilst the HRTEM image shown in Fig. 3.7 illustrates the encapsulation of a metal particle by graphitic layers, which exist as impurities in the CNT product. An energy dispersive X-ray (EDX) spectral analysis (Fig. 3.8) of the metal impurities, indicated the presence of iron (Fe), chromium (Cr), nickel (Ni) and manganese (Mn), which are all trace elements of stainless-steel. This implied that slight oxidation of the stainless-steel tube might have occurred at the high process temperatures and lead to the conclusion that a quartz tube might yield less impurities.

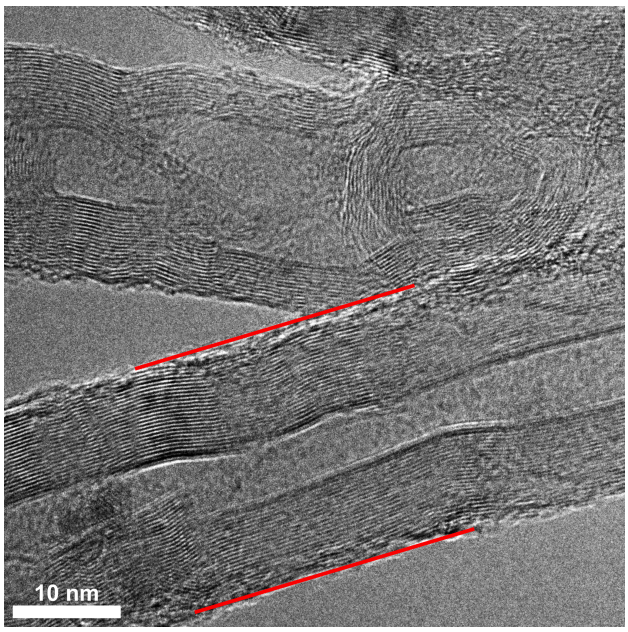

Figure 3.6: Typical HRTEM micrograph of a multi-walled carbon nanotube (MWCNT).

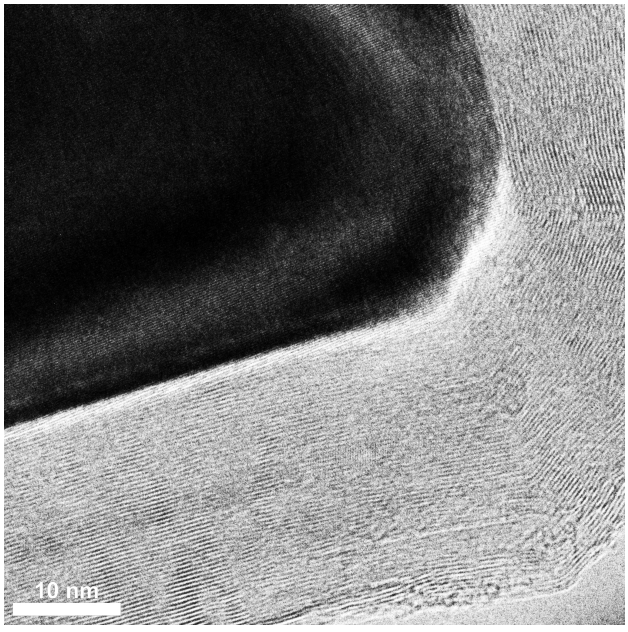

Figure 3.7: HRTEM micrograph of a metal particle encapsulated by multiple graphitic layers.

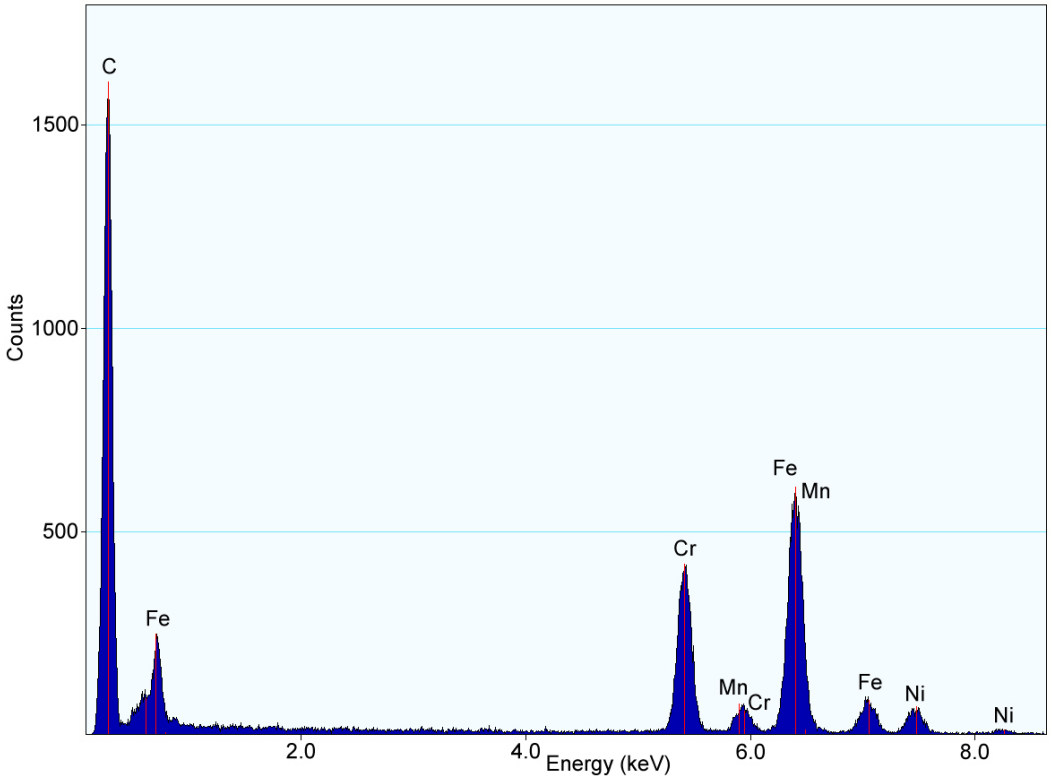

Figure 3.8: EDX analysis of metal impurities in the as-synthesized MWCNT product.

Although the water-assisted floating catalyst method implemented for the synthesis of MWCNTs, produced moderate amounts of carbon nanotube material, some difficulties were experienced in collecting the pieces of film and separating them from what seemed to be amorphous carbon particles. Furthermore, the exact position of the transition section (the section between the small connecting tube and the reaction zone) needed to be determined for optimal growth, since the complete system dimensions were not specified by Xie and associates [64]. It was observed that the dense CNT growth in the reaction zone, causes rapid blockage of the small connecting tube if the transition section is placed too close to the center of the furnace. In addition, during experimental trials with faster carrier gas (Ar) flow rates ($\approx$ 1500-2000 sccm), no growth of CNTs was observed and only a fine black powder was recoverable from the stainless-steel tube. It is anticipated that at these increased flow rates, the catalyst particles move too rapidly to sustain successful nucleation and subsequently the formation of CNTs.

3.6.2 Synthesis of SWCNTs

After a study of the work presented by Wang et al. [66], who demonstrated the fabrication of ultra-long single-walled carbon nanotubes with an enhanced CVD method, the process utilized for the growth of MWCNTs, as described in the previous subsection, was adjusted slightly. Wang [66] described a water-assisted CVD technique to grow ultra-long ($\approx$ 18.5 cm) SWCNTs, by using mono-dispersed Fe-Mo nanoparticles as catalyst and an aqueous mixture of H_2O and ethanol (C_2H_5OH) as the carbon source material.

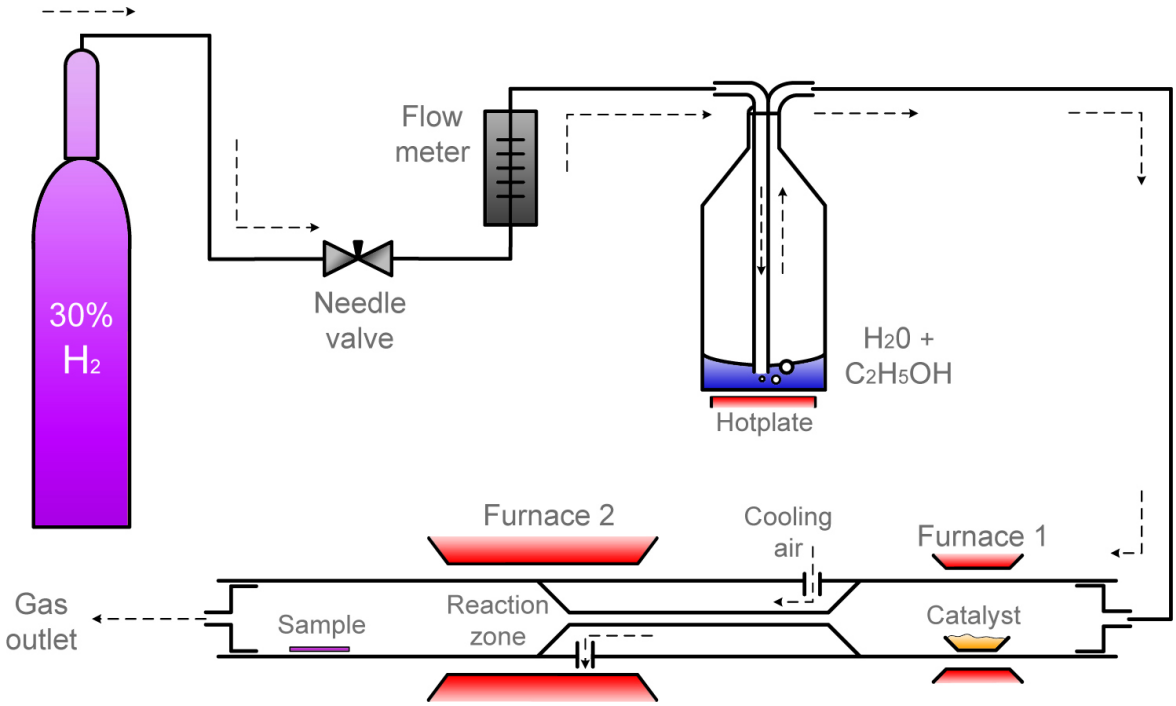

Figure 3.9: Setup for the water-assisted floating catalyst CVD synthesis of SWCNTs.

Subsequently, the argon (carrier gas) and the acetylene feedstock gas for the MWCNT process was replaced by a mixture of Ar and 30% H_2, for the growth of SWCNTs, as shown in Fig. 3.9. Furthermore, the Ar-H_2 carrier gas was bubbled through a water-ethanol mixture (1:4 by volume), which was heated to $\approx$ 40°C. Additional changes to the original MWCNT process, included adjusting the reaction zone temperature to 1000°C and decreasing the carrier gas flow rate to $\approx$ 300

sccm. Due to a complication with the temperature controller fitted to the electrical furnace, an analogue Schmitt trigger temperature controller was designed and manufactured, which is presented in Appendix D. Process parameters that were retained include the stainless-steel tube, the ferrocene catalyst (sublimation at 55°C), the constant 1.0 atm system pressure and the 1 hour growth time.

The as-synthesized CNT material collected from the inner-wall of the stainless-steel tube was sent for Raman spectral analysis at the "National Center for Nanostructured Materials - CSIR". The Raman analysis was performed with a Jobin Yvon LabRAM HR800 spectrometer, using a standard 514 nm (green) excitation laser. A typical result is displayed in Fig. 3.10.

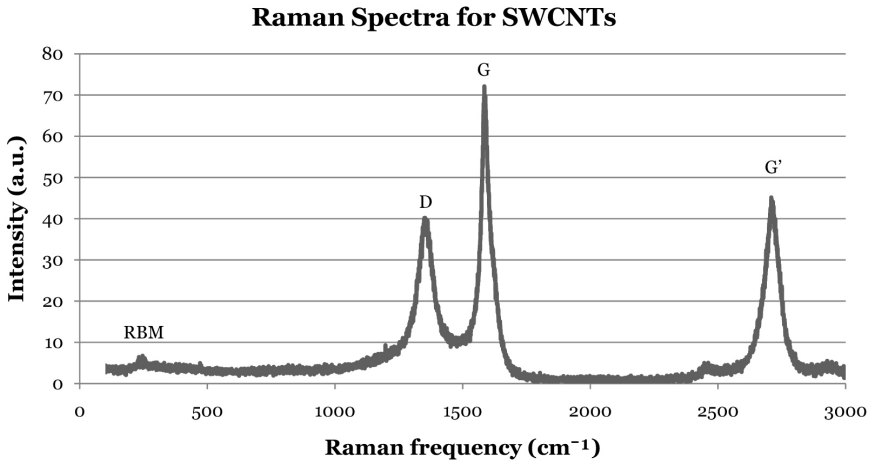

Figure 3.10: Raman spectral analysis of an as-synthesized SWCNT sample.

The Raman spectroscopy of SWCNTs, typically yield 4 main characteristic peaks. These include first order Raman scattering peaks in the G-band and RBM (radial breathing mode) and second order scattering peaks in the D-band and G'-band. The G-band for carbon nanotubes is related to the tangential mode vibrations of the carbon atoms in a wave-vector confinement along the CNT circumferential direction and peaks near the 1580 cm^{-1} Raman frequency [67]. Additionally, the radial breathing mode (RBM) mechanisms are attributed to the coherent vibration of carbon atoms in a radial direction. The RBM features however, are unique to CNTs and Raman scattering generally peaks between 120

cm^{-1} and 350 cm^{-1} for SWCNTs, which corresponds to tube diameters between 0.7 nm and 2 nm. The D-band features correspond to dispersive disorders [68] introduced by structural defects and sample impurities (e.g. metal particles and amorphous carbons) and peaks at $\approx$ 1350 cm^{-1} [67]. Conversely, the G'-band, which peak at $\approx$ 2700 cm^{-1}, is attributed to a two-phonon (intervalley) second order Raman scattering mechanism.

Since the G-band is an intrinsic feature of the sp^2-bonded carbon atoms in CNTs, the ratio between G-band and D-band forms a good qualitative indicator of nanotube samples. A higher G/D ratio is thus indicative of a better sample purity and lower structural defects. It is also noted that CNT samples typically show much higher G-band and RBM peaks if the Raman analysis is performed with a 785 nm (red) excitation laser [68].

The as-synthesized SWCNT samples were further analyzed by the same HRTEM method as described for the MWCNTs. Fig. 3.11 illustrates a HRTEM image of the SWCNT sample, in which multiple SWCNT ropes can be observed, with single tubes having diameters of $\approx$ 2 nm.

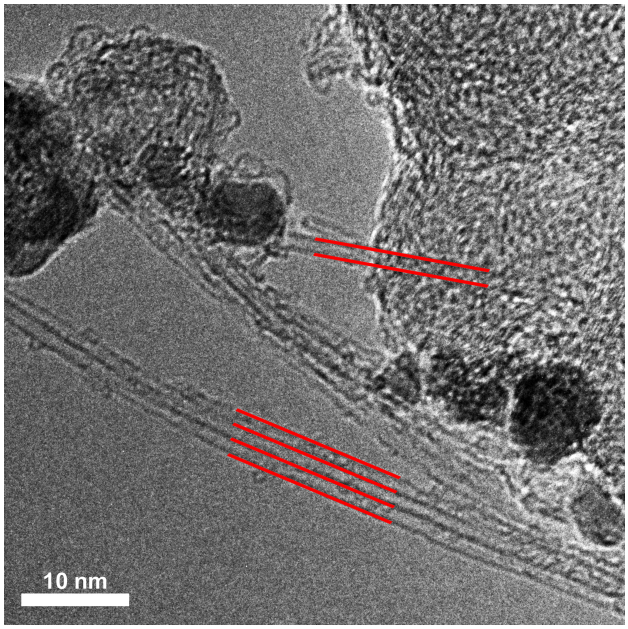

Figure 3.11: Typical HRTEM micrograph of as-synthesized SWCNT-ropes.

3.7 The synthesis of graphene

As the research presented in this work was mainly focused on the synthesis of carbon nanotubes, techniques to fabricate graphene structures were not explicitly investigated. However, the presence of moderate quantities of graphene were observed during HRTEM analysis of sample materials, that were acquired during a CVD experiment at ≈ 1100°C. The system parameters, except for the elevated temperature, were all identical to those described for the water-assisted floating catalyst CVD process that was utilized for the synthesis of SWCNTs. The synthesized material that was collected from the furnace tube was then mechanically transferred (spread by hand) onto standard copper grids, as shown in the optical micrographs in Fig. 3.12, for HRTEM analysis. Fig. 3.13 shows a HRTEM image of a few-layer graphene sheet, with a relatively large surface area.

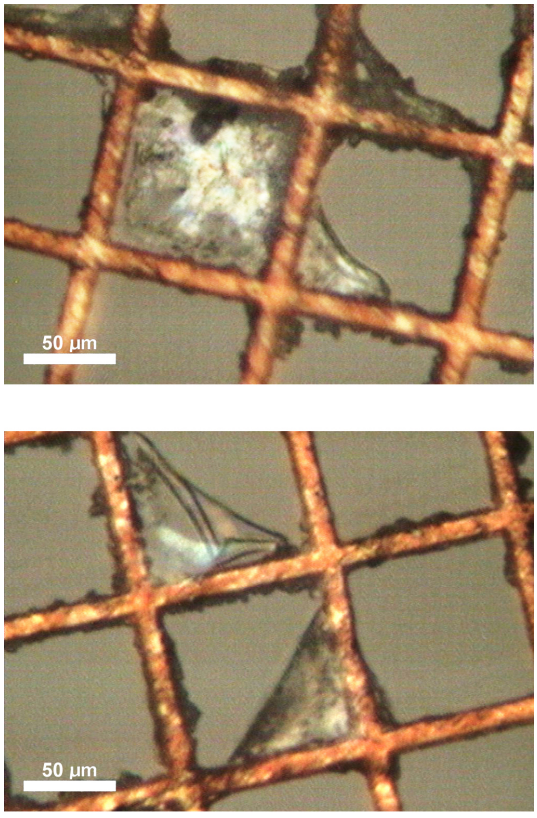

Figure 3.12: Optical micrographs of graphene on standard copper HRTEM grids.

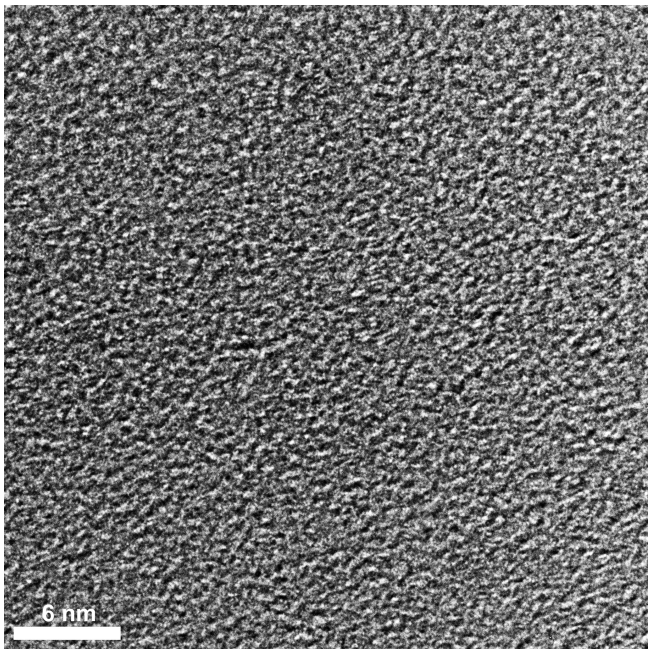

Figure 3.13: HRTEM image of a few-layered graphene sample, with a large surface area.

Additional analysis procedures like EDX (energy dispersive X-ray spectroscopy) and SAED (selected area electron diffraction) were also performed with the HRTEM-instrument, to verify the observed material's characteristics. Fig. 3.14 depicts the EDX results, from which the primary element is specified as carbon, whilst Fig. 3.15 illustrates the measured electron diffraction pattern of the crystalline structure, which is characteristic of few-layered graphene.

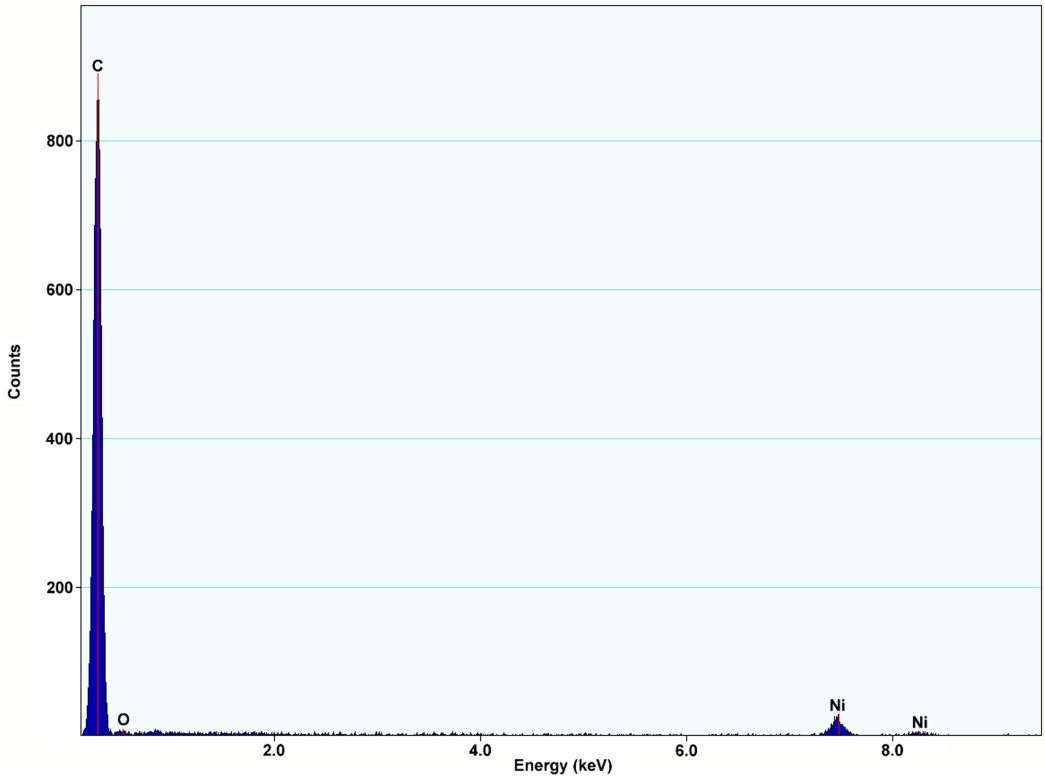

Figure 3.14: EDX analysis of synthesized graphene sample.

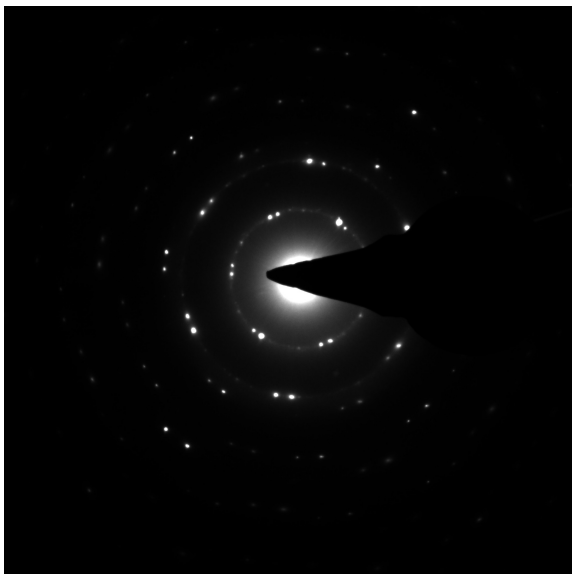

Figure 3.15: The typical electron diffraction pattern for few-layered graphene, obtained by SAED analysis.

It is theorized that the elevated process temperature ($\approx 1100^{\circ}C$), causes the carbon source material to decompose too rapidly to support the growth of CNTs and consequently favours the formation of graphene arrangements. Furthermore, very little impurities were introduced in the resulting product, possibly due to an accurate balance achieved between system temperatures and carrier gas flow rates.

3.8 Conclusions

This chapter briefly described the growth mechanisms present during the synthesis of carbon nanotubes, including the role of growth enhancers in CVD procedures. Furthermore, the general rules governing the efficient growth of CNTs were discussed and the general techniques, pertaining to the purification and functionalization of carbon nanotubes, were presented.

The water-assisted floating catalyst methods, that were implemented during this research, for the synthesis of CNTs were also described in detail. From the experimental results, it was observed that the process temperature and carrier gas flow rates significantly influence the morphology of the resulting carbon nanostructures. As stated earlier, the floating catalyst CVD method derived for the synthesis of carbon nanotubes, was not intensely studied for the fabrication of graphene, but it is believed that further optimization of the process might be promising for the large-scale synthesis of graphene products.

Chapter 4

Pure Carbon Nanomaterial Gas Sensors

This chapter entails the detailed fabrication of three pure carbon nanomaterial (i.e. graphene, SWCNTs and MWCNTs) film sensors, that were manufactured during this research. The tests and results obtained for various gases are also presented and briefly discussed, based upon changes in the measured film resistance for each sensor at both room - and at 100°C substrate temperatures.

4.1 Graphene film sensors

To investigate the properties and effects of various environments and gas species on graphene, pure graphene film sensors were manufactured on clean thermally oxidized silicon (SiO_2) substrates via a spray-coating procedure. These sensors were subsequently subjected to numerous tests, the results of which are presented in this section.

Sensor fabrication

For the fabrication of pure graphene film sensors, a stable graphene solution was spray-coated onto thermally oxidized silicon (1 - 1 - 1) substrates, using a nitrogen-airbrush and spraying at an angle of roughly 75° normal to the substrate surface. The solution was prepared by ultrasonically dispersing pure graphene nanopowder ($\approx$ 0.1 wt%) in a Propan - 2 - ol solvent, with the addition of a tiny amount

of ethyl cellulose to act as a binding agent during the spray-coat procedure.

The spray-coating was followed by a thermal treatment at $\approx 350°C$ for 10 minutes in an argon environment, to remove residual solvent molecules and cellulose particles. Furthermore, it was found that adding the contact wires to the SiO_2 substrate before spray-coating with graphene, reduced contact resistances and also allowed the in situ measurement of the film's resistance. Table 4.1 presents the measurements of a typical graphene film's resistance for increasing film thickness (i.e. increasing number of sprayed layers).

Table 4.1: Graphene Film Resistance vs. Number of Layers

Layers	Resistance
2	∞
4	1.2 MΩ
8	60.3 kΩ
12	8.1 kΩ
16	1.34 kΩ

Using a FEI Phenom II scanning electron microscope (SEM), shown in Fig. 4.1, the spray-coated graphene film morphologies were examined.

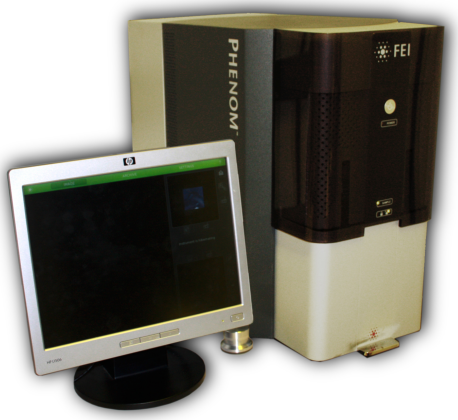

Figure 4.1: The FEI Phenom II Scanning Electron Microscope (SEM).

Fig. 4.2 shows SEM images of a graphene film ($R_{film} \approx 10$ kΩ) at 2500x, 5000x and 18 000x magnification. The pure graphene nanopowder (12 nm flakes) used in these experiments, were obtained from "*Graphene Supermarket.com*".

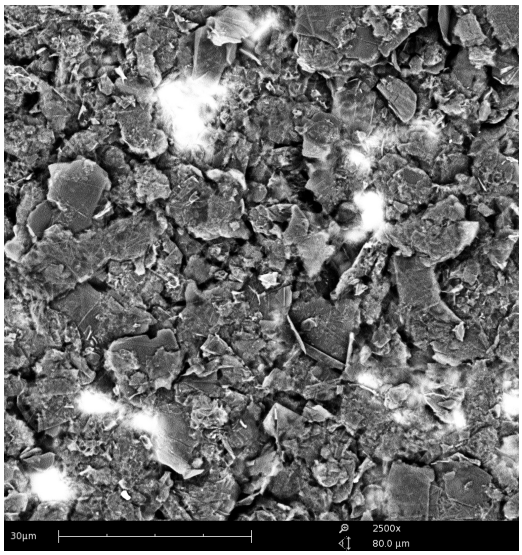

a) 2500x

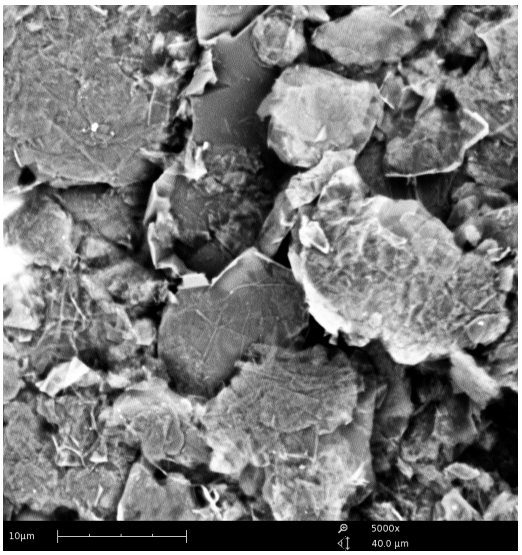

b) 5000x

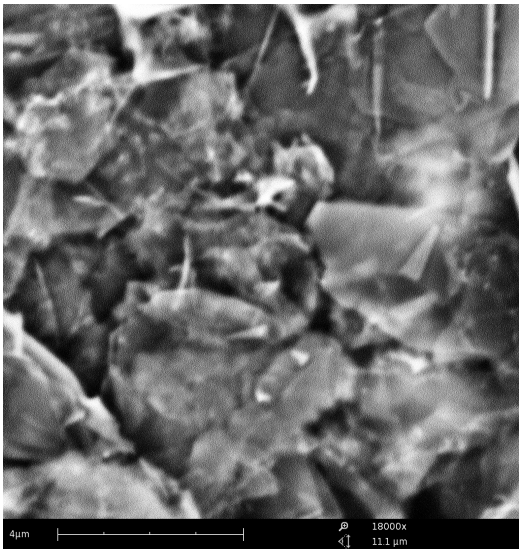

c) 18 000x

Figure 4.2: SEM images of a spray-coated graphene film at a) 2500x, b) 5000x and c) 18 000x magnification.

Providing for sensor heating capabilities and added mechanical strength, the SiO_2/Si substrates (10 x 10 mm) were fixed onto 25 x 25 mm aluminium oxide (Al_2O_3) substrates. The electrical contact wires were then attached to the SiO_2 surface with a conductive silver paint and glued onto the alumina substrate with an epoxy adhesive, prior to the application of the spray-coated graphene solution. Fig. 4.3 displays a photograph of a graphene film sensor that was fabricated by the above-mentioned method.

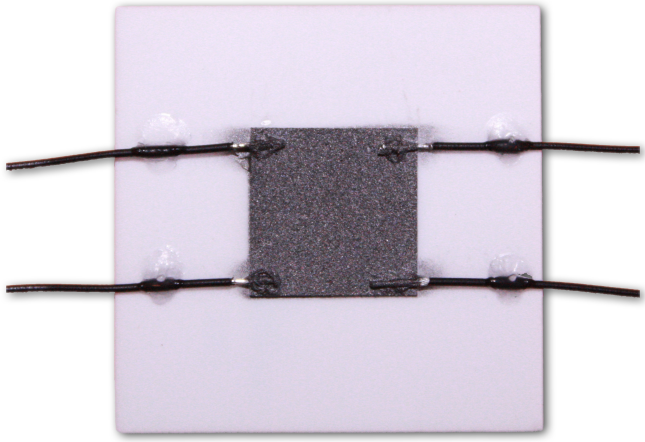

Figure 4.3: Photograph of a spray-coated graphene film sensor.

Tests and measurements

Following the fabrication of the pure graphene film sensor, the device was placed in an aluminium testing chamber, illustrated in Fig. 4.4, to perform the various tests. The testing chamber was fitted with six independent contact electrodes - four contacts at the front, to perform the resistivity measurements and two contacts at the back (not shown in Fig. 4.4), for sample heating and additional measurements (e.g. relative humidity). The film resistivity measurements for all fabricated sensors, during all test phases, were performed using the Van der Pauw 4-point measurement technique [69], which is described in Appendix E.

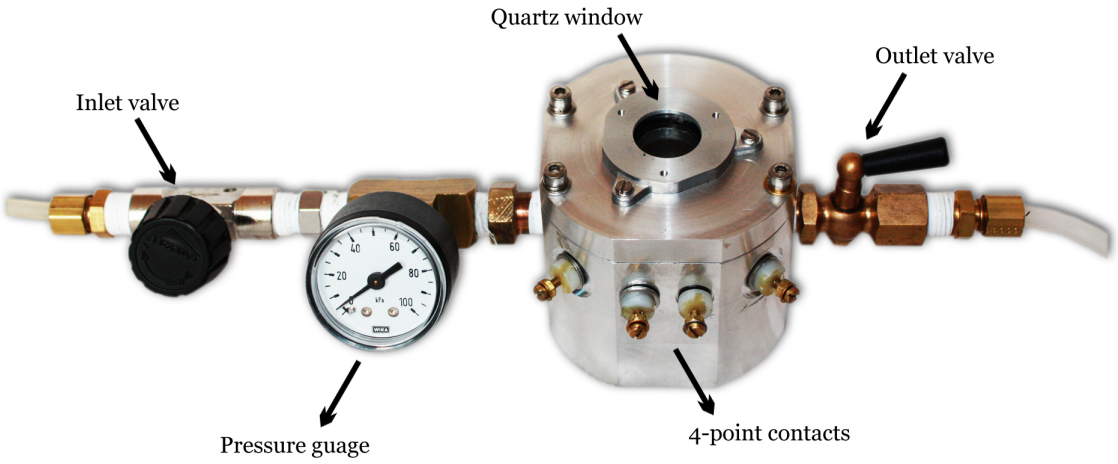

Figure 4.4: Aluminium test chamber.

The first set of tests performed on the graphene film sensor was to characterize the device's behaviour in different ambient conditions. This included measuring changes in the film's resistance for varying substrate temperatures and relative humidities. Fig. 4.5 and Fig. 4.6 illustrates the sensor's responses to increasing substrate temperature and increasing relative humidity (%RH) at room temperature, respectively.

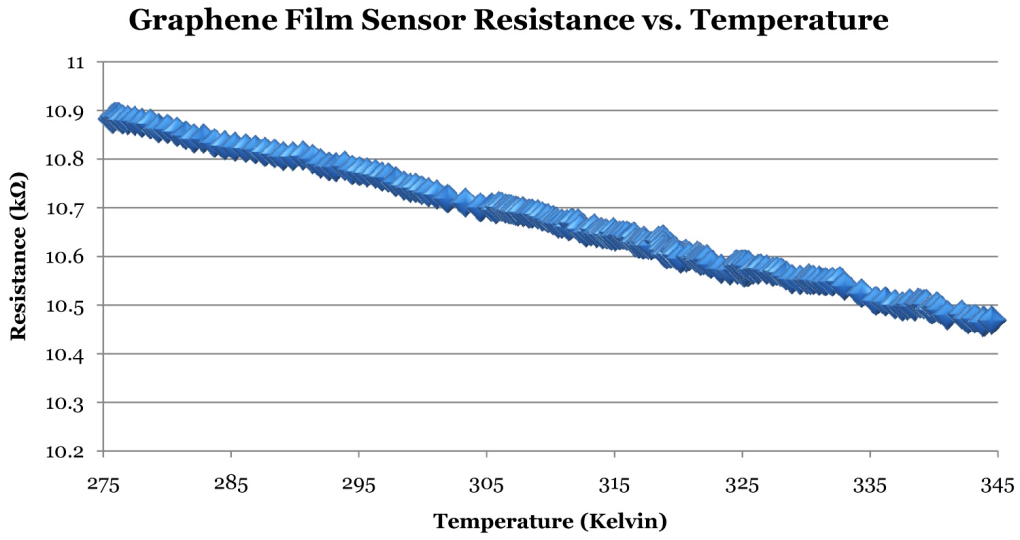

Figure 4.5: Graphene film sensor resistance vs. increasing substrate temperature.

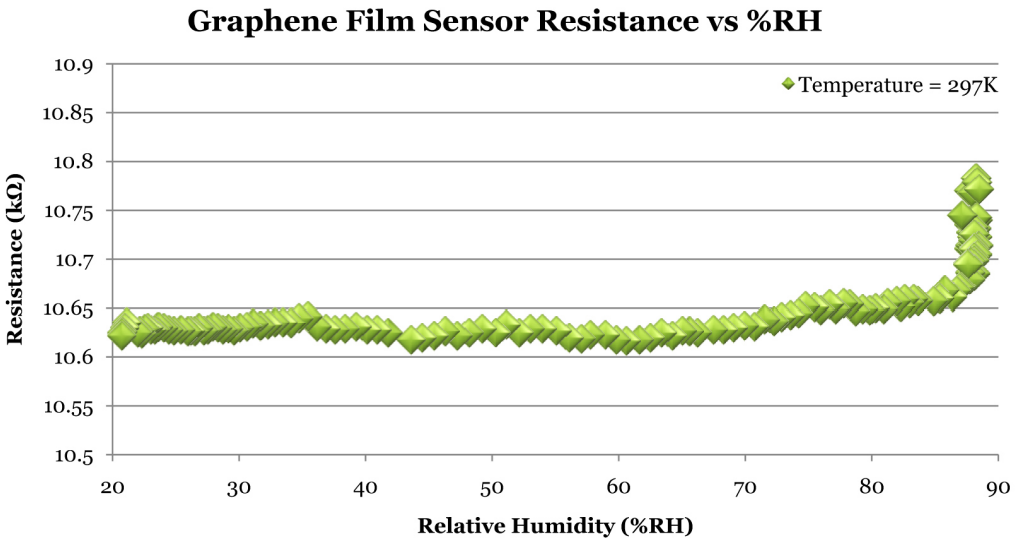

Figure 4.6: Graphene film sensor resistance vs. increasing relative humidity (%RH).

From the experimental results in Fig. 4.5, it was observed that a pure graphene film could be implemented as a linear temperature sensor. However, the future of graphene in temperature sensing applications is quite uncertain, due to the high efficiency and accuracy of modern day thermocouple technologies.

Furthermore, a negligible effect on the film's resistance was observed for low %RH values (Fig. 4.6), with only a small increase for relative humidities between 60% and 85% and a sharp increase for %RH above 85%. The humidity sensor used for the %RH tests, specified a 20 - 90% linear measurement ability. It was therefore concluded that the non-linear response of the graphene film would not be appropriate for humidity sensing applications. It was also deduced that the effects of other gas molecules on the sensor's response, would not be significantly influenced by changes in %RH at levels well below 80%.

All measurements performed during this work, were acquired with a LM335 (ST Microelectronics) precision temperature sensor and a HMZ-333A (Ghitron Technologies) %RH sensing module, which were connected to a LabJack U6 A/D (analogue-to-digital) converter for easy logging of the test data. The LabJack device (shown in Fig. 4.7) accompanied by the "*DAQFactory Express*" software

package from AzeoTech, was also used for the acquisition of all other test data from the sensors that were fabricated during this research.

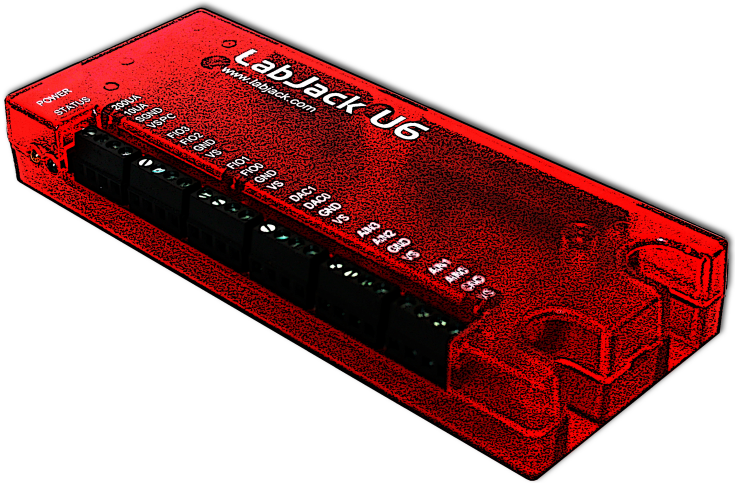

Figure 4.7: LabJack U6 A/D (analogue-to-digital) converter.

Following the temperature and %RH tests, the graphene film sensor was kept in an argon environment for 12 hours, to allow the sensor to stabilize at room temperature. Subsequently, the effects of varying gas flow rates on the graphene film sensor's resistance was investigated at both room temperature and 100°C ($\approx$ 375 K).

The gas flow rate tests were performed by flowing argon (Ar) gas at 100 sccm increments for 5 minute intervals, through the test chamber. Fig. 4.8 and Fig. 4.9 presents the results for the flow rate tests at room temperature and 100°C, respectively. Argon gas was used during these experiments, since Ar is a noble and inert gas and is known to react with very few substances. The increased substrate temperature was obtained with the use of the same Peltier system, that was implemented in the synthesis of the carbon nanomaterials in Chapter 3.

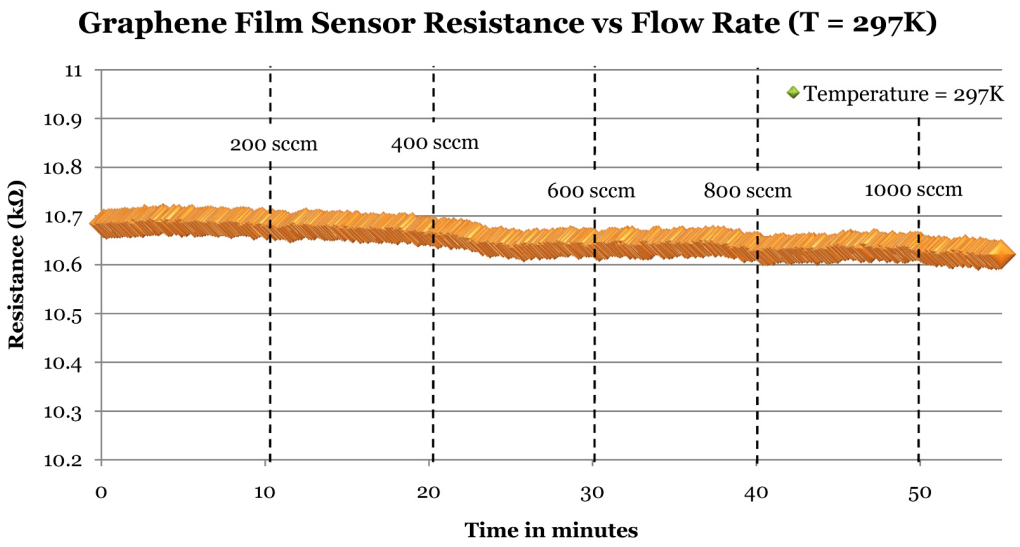

Figure 4.8: Graphene film sensor resistance vs. increasing flow rate (T = 297 K).

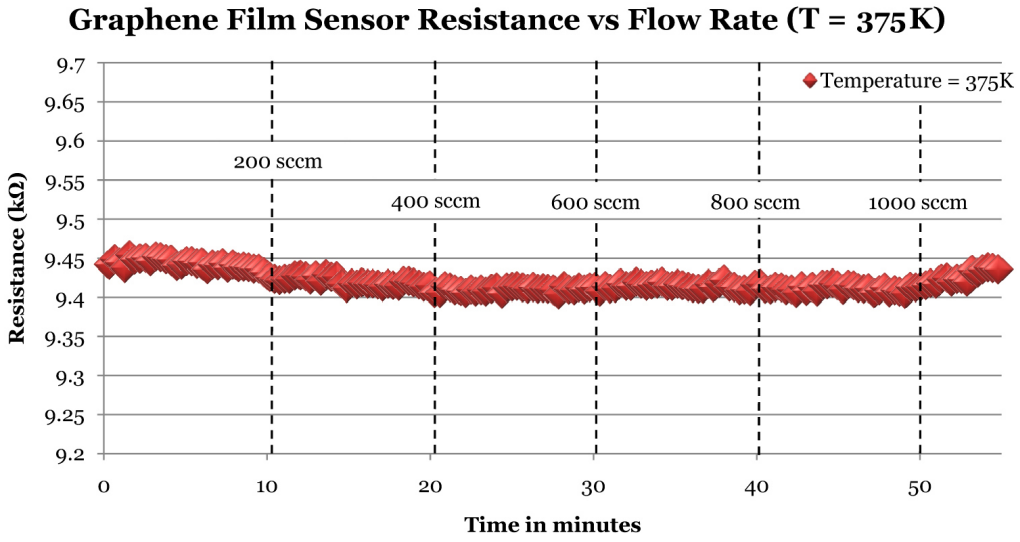

Figure 4.9: Graphene film sensor response vs. increasing flow rate (T = 375 K).

From the flow rate measurements it was evident that an increase in the gas flow rate through the test chamber induced a slight decrease in the graphene film sensor's resistance at room temperature ($\approx$ 24°C) and at 100°C. This small decrease (i.e. $<$ 1% over a 0 - 1000 sccm flow range) can therefore be presumed to

have a negligible influence on the sensing of gas molecules at flow rates between 0 - 400 sccm. Furthermore, the slight increase in film resistance, which occurred above 1000 sccm for the test at 100°C, is most likely due to a decrease in substrate temperature produced by the lower temperature of the flowing gas.

Lastly, the manufactured graphene film sensors were subjected to various gases like CH_4 (methane), C_2H_2 (acetylene), O_2, N_2 and a mixture of Ar and H_2 (30% by volume). These tests were performed by flushing the test chamber with argon, prior to the application of the test gases at increments of 100 sccm flow rates (i.e. 0 - 400 sccm) for 3 minute intervals. The gas flow rate was controlled by a standard flow meter connected to a needle valve, whilst the test data was collected using the LabJack device, which was connected according to the Van der Pauw configuration (App. E).

Fig. 4.10 portrays the gas test results for the graphene film sensor at room temperature (≈ 297 K) and Fig. 4.11 provides the test results obtained at 100°C (≈ 375 K).

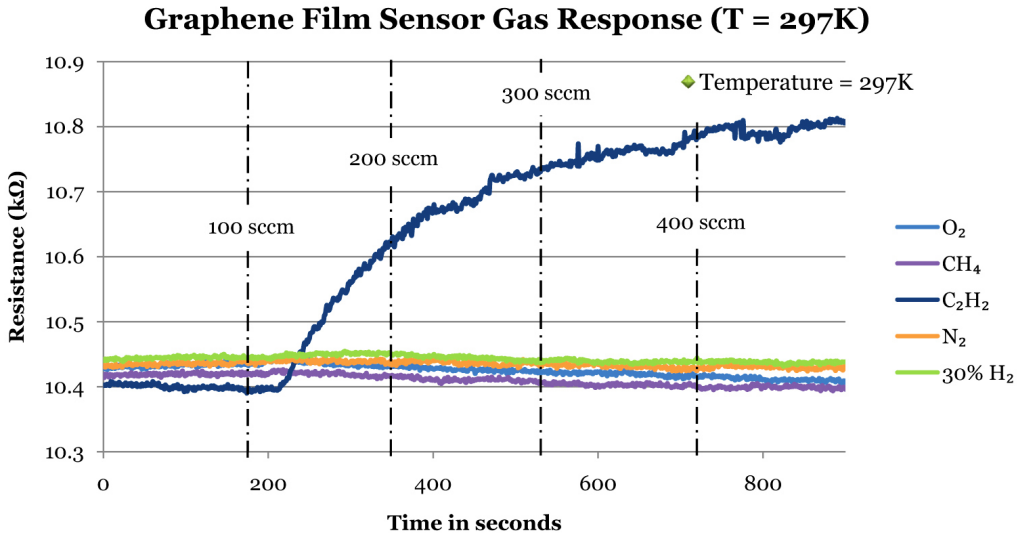

Figure 4.10: Pure graphene film sensor gas response (T = 297 K).

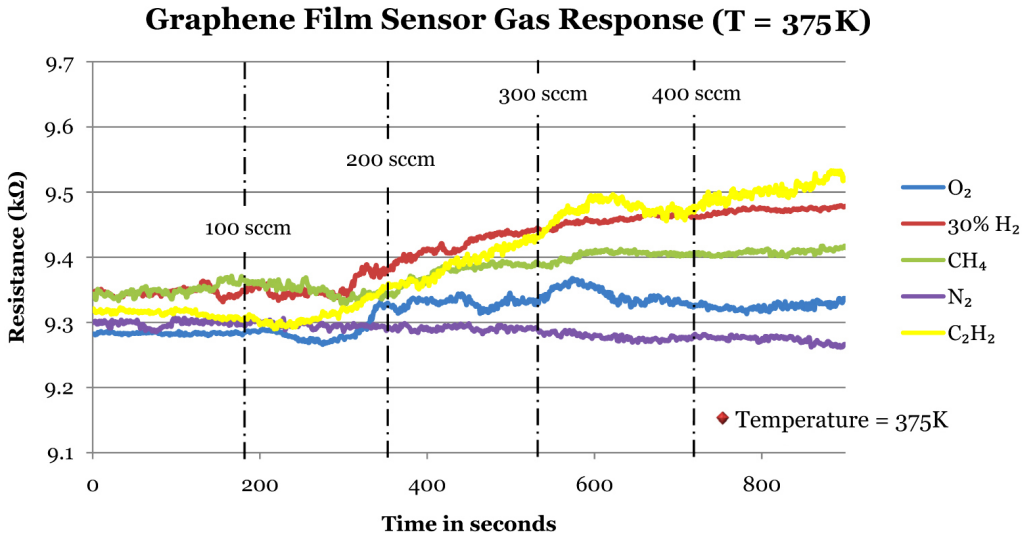

Figure 4.11: Pure graphene film sensor gas response (T = 375 K).

The results from Fig. 4.10 revealed that graphene is not very reactive to gas species at room temperature. Since graphene is basically an inert graphitic material at these low temperatures, this result is not as unexpected. However, a small but definitive increase in resistance was observed for acetylene (C_2H_2) gas (i.e. a change of $\approx$ 3.84% over the 0 - 400 sccm flow range). This result is possibly due to the higher instability and subsequent higher reactivity of C_2H_2 molecules compared to the other gas species.

Conversely, with the substrate temperature increased to 100°C, changes in the graphene film's resistance was measured for acetylene ($\approx$ 2.26%), methane ($\approx$ 0.75%) and also Ar-$_{30\%}H_2$ ($\approx$ 1.39%) and O_2 ($\approx$ 0.74%). Since all of the observed measurements reached a saturated state, it is proposed that the graphene nanomaterial has absorbed the maximum amount of gas molecules at these levels.

Furthermore, the film sensors that were tested at room temperature, exhibited extremely slow recovery times (i.e. a few hours), whilst the sensors recovery times were in the order of tens of minutes at 100°C (with a 100 sccm flow of Ar through the chamber). It was also observed that heating the sensors under an argon flow, reduced the recovery time for room temperature tests to $\approx$ 35 - 45 min.

4.2 MWCNT film sensors

In order to qualitatively compare the gas sensing abilities of carbon nanotubes to that of graphene, it was concurred to manufacture MWCNT film sensors (and SWCNT film sensors) in a similar fashion to that described for the pure graphene film sensors in the previous section. Subsequently, the fabricated MWCNT film sensors were subjected to the same series of characteristic tests that were performed on the graphene sensors, the results of which are presented in this section.

Sensor fabrication

The fabrication of the multi-walled carbon nanotube (MWCNT) film sensors consisted of a similar spray-coating technique, as was described in the previous section. A MWCNT ($\approx$ 0.1 wt%) solution was prepared by ultrasonically dispersing the nanotube material in a Propan - 2 - ol solvent and adding a very small amount of ethyl cellulose to provide better binding to the SiO_2/Si substrates. The spray-coated films were then thermally treated at 350°C for 10 minutes, in order to eradicate residual solvent materials. Furthermore, the MWCNT film sensors were also fixed onto alumina (Al_2O_3) substrates and four contact wires were attached for performing the various measurements.

Table 4.2: MWCNT Film Resistance vs. Number of Layers

Layers	Resistance
2	2.5 MΩ
4	265 kΩ
8	26.2 kΩ
12	4.3 kΩ
16	1.1 kΩ

Table 4.2 presents the equivalent in situ measurements of a typical MWCNT film's resistance for increasing film thickness (i.e. increasing number of sprayed layers). For the fabrication of the pure MWCNT films, high purity ($>$ 95 wt%) MWCNTs, with diameters between 8 - 15 nm and lengths of roughly 50 μm, were

obtained from "*Chengdu Organic Chemicals*". The spray-coated MWCNT films were also investigated by means of electron microscopy, with Fig. 4.12 illustrating typical SEM images of a MWCNT film ($R_{film} \approx 10$ kΩ), at 5000x, 10 000x and 20 000x magnification.

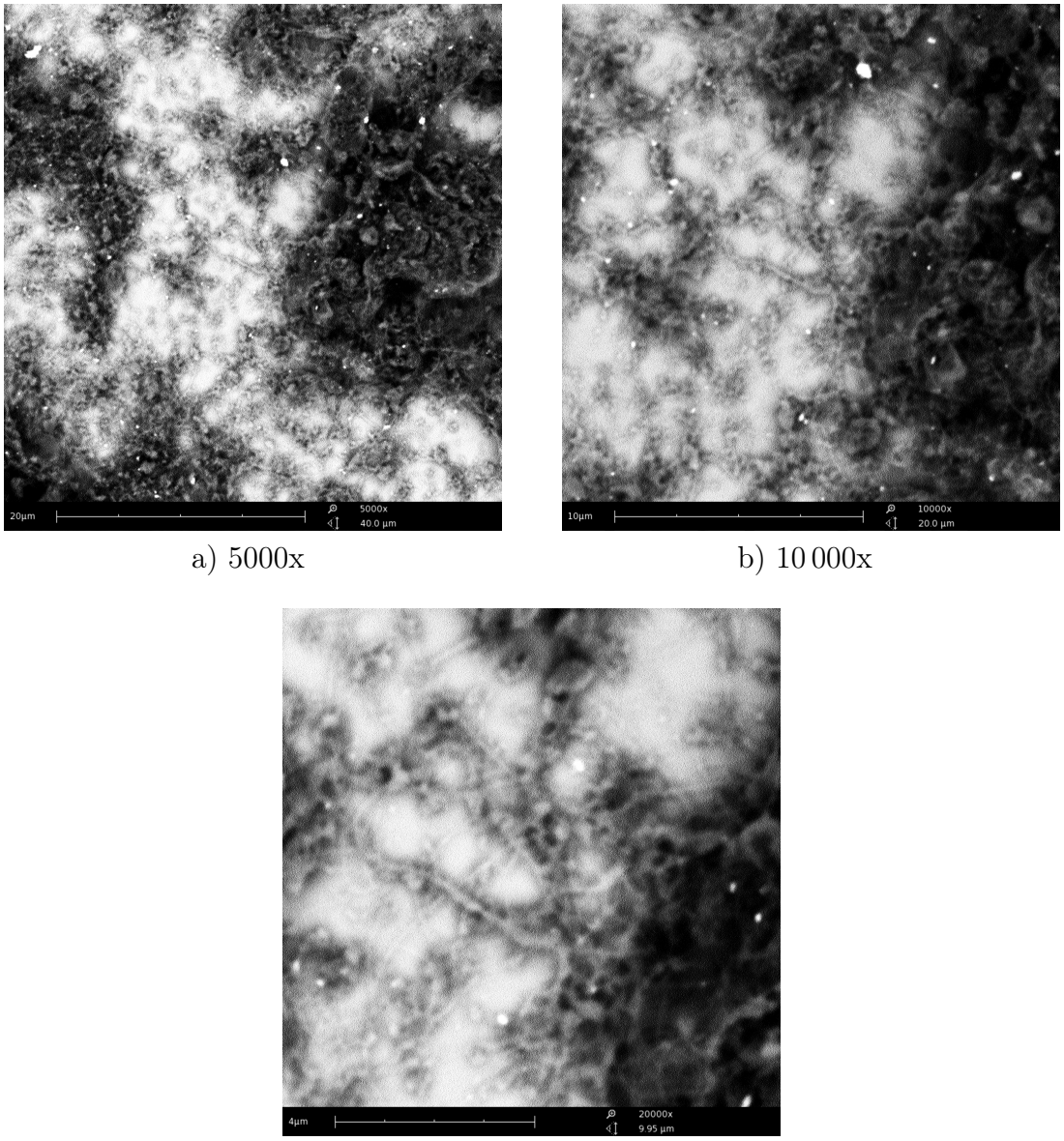

a) 5000x

b) 10 000x

c) 20 000x

Figure 4.12: SEM images of a spray-coated MWCNT film at a) 5000x, b) 10 000x and c) 20 000x magnification.

From the SEM images it was perceived that due to the higher aspect ratios of the MWCNTs (i.e. the longer structures of the nanotubes than the graphene flakes) and the overlapping of the MWCNTs, an electrically conductive path was established sooner than for the graphene film. This observation also corresponds to the film resistance measurements presented in Table 4.2.

Tests and measurements

Following the fabrication of the pure MWCNT film sensors, the devices were subjected to an initial set of tests, to characterize the effects of varying ambient conditions on the MWCNT films. Fig. 4.13 and Fig. 4.14 provides a typical spray-coated MWCNT film sensor's response towards increasing substrate temperature and increasing relative humidity (%RH), respectively.

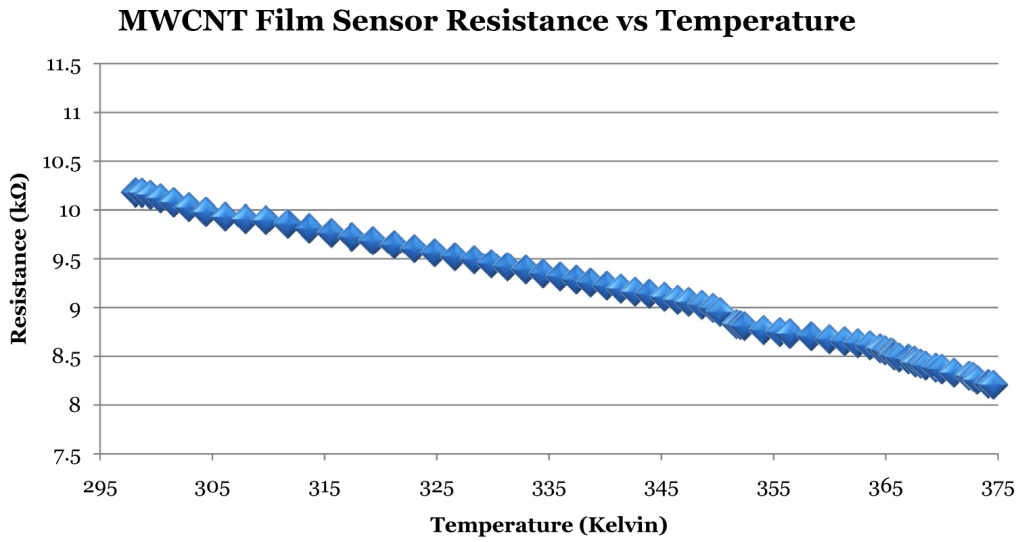

Figure 4.13: MWCNT film sensor resistance vs. increasing substrate temperature.

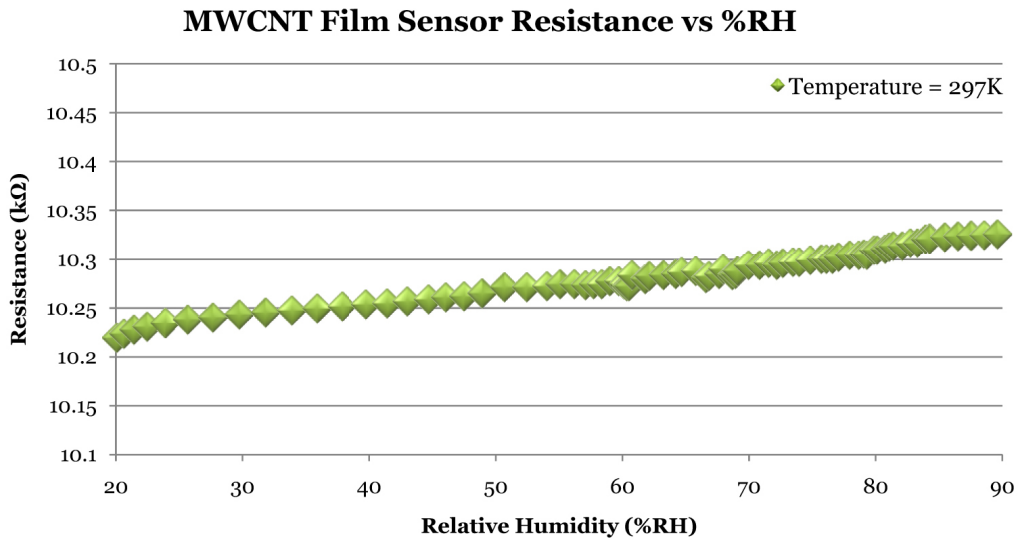

Figure 4.14: MWCNT film sensor resistance vs. increasing relative humidity (%RH).

The MWCNT film sensor demonstrated a near linear decrease in resistance ($\approx$ 19.5% change) over an approximately 80°C increase in substrate temperature. This behaviour was very similar to that observed for the pure graphene film devices presented in Section 4.1. Furthermore, the MWCNT film's resistance increased sightly ($\approx$ 1%) over a relative humidity (%RH) range of 20 - 90%.

From the latter result, it can then also be expected to observe a small decrease in the MWCNT film's resistance during gas test phases, since an applied gas flow through the test chamber will generally cause a reduction in %RH inside the chamber. This in fact, corresponds to the flow rate measurement presented in Fig. 4.15, from which a small ($\approx$ 0.54%) decrease in the film's resistance over the entire flow range, was observed. The flow rate test was performed by flowing Ar gas through the chamber at 100 sccm increments (i.e. from 0 - 1000 sccm) for 5 minute intervals at room temperature.

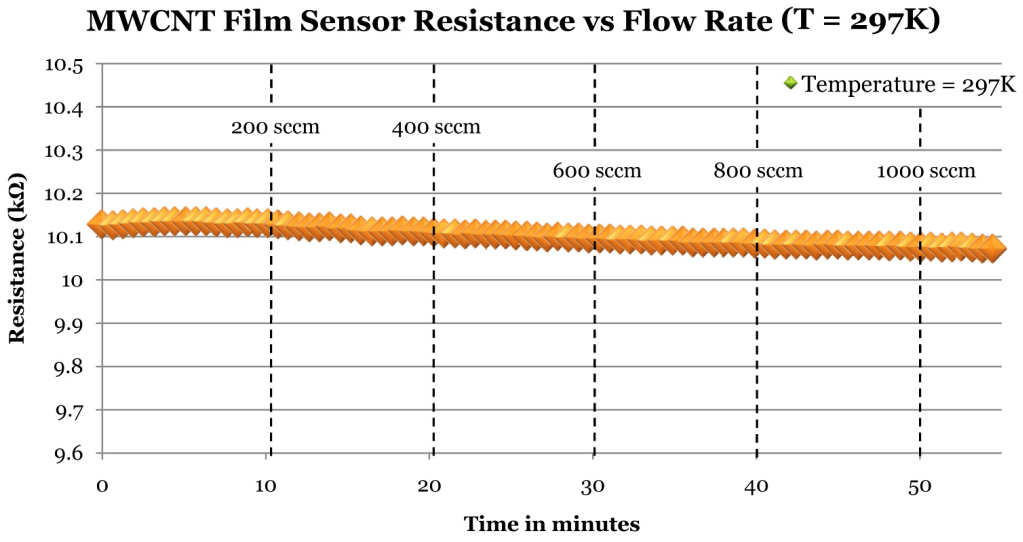

Figure 4.15: MWCNT film sensor resistance vs. increasing flow rate (T = 297 K).

Subsequently, the fabricated MWCNT film sensors were exposed to the various gases, that were implemented during the graphene film gas response tests. The gas response tests were performed by applying the gas flows at 100 sccm increments (from 0 - 400 sccm) for 3 minute intervals. The test chamber was consecutively flushed with argon between the different gases and the tests were executed at both room temperature ($\approx$ 24°C) and 100°C, shown in Fig. 4.16 and Fig. 4.17, respectively.

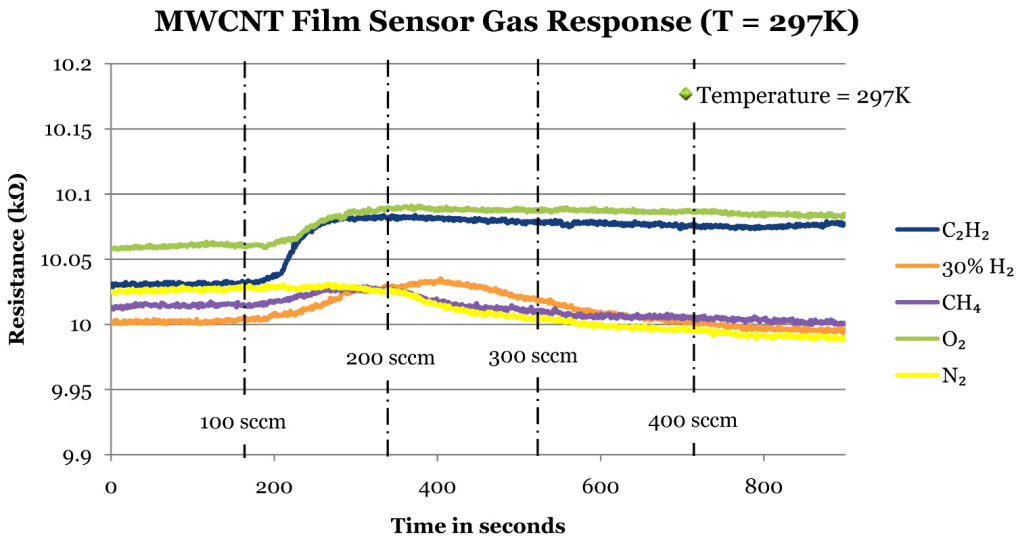

Figure 4.16: Pure MWCNT film sensor gas response (T = 297 K).

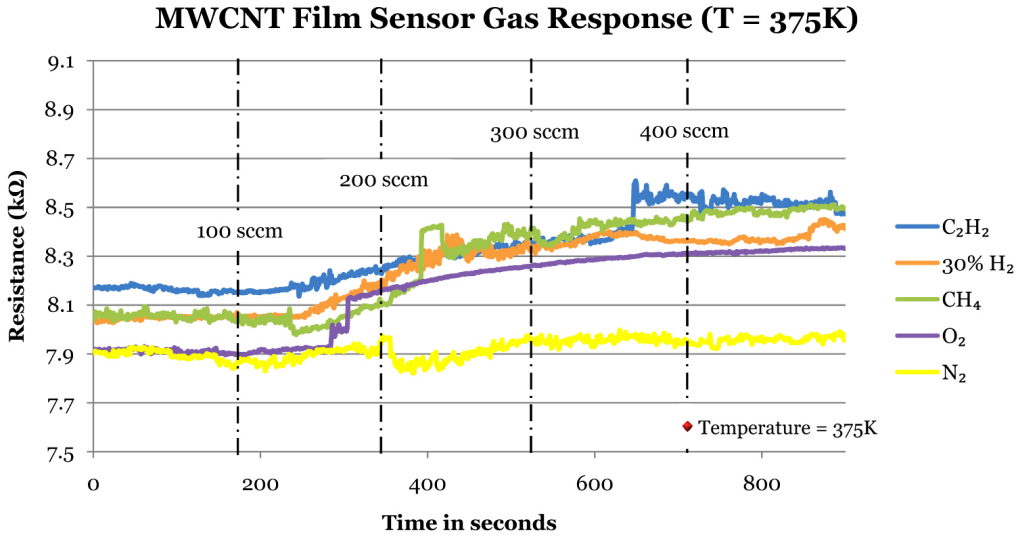

Figure 4.17: Pure MWCNT film sensor gas response (T = 375 K).

The behaviour of the MWCNT film sensor at room temperature (Fig. 4.16), was similar to that of the graphene device, with only acetylene (C_2H_2) inducing a small ($\approx 0.5\%$) increase in the film's resistance. Once more, there were definitive

saturation effects visible for the sensors responses, which contributes to the observations of limited reactivities of carbon nanomaterials at room temperatures.

However, at an increased substrate temperature (i.e. 100°C) the MWCNT film sensor demonstrated a moderate increase in reactivity towards the gaseous species. From the results in Fig. 4.17, a change in the MWCNT device's resistance was measured for C_2H_2 ($\approx$ 5.1%), CH_4 ($\approx$ 5.2%) and $Ar\text{-}_{30\%}H_2$ ($\approx$ 3.96%). The sudden change in resistance observed for O_2 ($\approx$ 2.7%) is in contrast to the slow linear increases observed for the other gases. Although the exact reason for this discontinuity is not known, the device demonstrated similar saturation curves observed for the other fabricated sensors.

Compared to the graphene film sensor, the MWCNT devices also demonstrated recovery times in the order of a few hours, without thermal treatment under an Ar gas flow. It was also observed that the MWCNT film sensors displayed hysteresis effects, which are most likely due to reduced desorption rates of "buried" nanotubes in the thick CNT films.

Furthermore, as the increased substrate temperature was found to yield enhanced sensing capabilities, it was also detected during the performed tests that the increased temperature resulted in a more electrically noisy environment, which is less favourable for high sensitivity applications. The presented test measurements were also acquired by applying the Van der Pauw 4-point technique together with the LabJack A/D device, with a sampling frequency of 1 - 2 Hz.

4.3 SWCNT film sensors

The final assessment of the trio of pure carbon nanomaterials, involved the fabrication and characterization of pure single-walled carbon nanotube (SWCNT) film sensors. Since most of the measurements performed during this research are concerned with changes in the respective films' resistive behaviours, the electron transfer mechanisms employed in the fabricated films, are worth noting. Due to the multiple overlapping of nanostructures, which forms the electrically conductive path, the flow of electrons are mainly governed by two distinct functions, namely:

a) The electron transfer between individual entities (e.g. single nanotubes or graphene layers), also referred to as the "*inter-structural*" electron transfer mechanism, and

b) The electron transfer within each individual entity (i.e between the sp^2-bonded carbon atoms), or the so-called "*intra-structural*" electron transfer mechanism.

Sensor fabrication

In order to produce SWCNT sensors, which would be comparable to the other manufactured carbon-based sensors (i.e graphene and MWCNTs), the same spray-coating technique was adopted in fabricating the pure SWCNT film sensors, as was described for the previous devices.

The pure SWCNT films were also produced by spray-coating a Propan - 2 - ol based solution onto thermally oxidized silicon wafers. The nanotube content in the solution was maintained at ≈ 0.1 wt% as for the previous experiments. Ultrasonication was performed for 30 minutes at 45°C to obtain a well-dispersed SWCNT solution, which was then spray-coated onto the 10 x 10 mm SiO_2/Si substrates. Table 4.3 presents the in situ film resistance measurements that were acquired during the spray-coating procedure.

Table 4.3: SWCNT Film Resistance vs. Number of Layers

Layers	Resistance
2	∞
4	9.9 MΩ
8	403 kΩ
12	5.9 kΩ
16	1.63 kΩ

Evaluating the results from Table 4.3, it was observed that the SWCNT films demonstrated initial resistance values that were significantly higher compared to those found for the pure MWCNT films (Table 4.2). This can be ascribed to the higher semiconductive nanotube content present in the SWCNT product, whereas the MWCNT product mainly consist of carbon nanotubes with metallic properties.

An additional film fabrication procedure was also attempted to generate films with both MWCNTs and SWCNTs. This procedure consisted of spin-coating the dispersed nanotube solutions onto the SiO_2/Si substrates at rotational speeds ranging from 500 - 9000 rpm. This method proved unsuccessful however, since the fabrication of evenly distributed and electrically conductive films could not be achieved. It is theorized that the super smooth and hydrophilic SiO_2 surface, ultimately prevents the attachment of the extremely hydrophobic carbon nanotubes, which simply gyrated off the substrates even at low rotational speeds.

Alternatively, Fig. 4.18 illustrates typical SEM images of a SWCNT film (R_{film} $\approx$ 10 kΩ), that was generated by using the spray-coating technique. For the fabrication of the pure SWCNT film sensors presented in this work, high purity ($>$ 90 wt%) SWCNTs with 1 - 2 nm diameters and 5 - 30 μm lengths, were also obtained from "*Chengdu Organic Chemicals*".

From the SEM images at 5000x, 10 000x and 50 000x magnification, acquired with a Zeiss EVO® MA15 scanning electron microscope, a high degree of SWCNT bundling could be observed, which formed a dense carpet like sheet on the sub-

strates. Furthermore, the intense electron beam-energy, focused on the SWCNTs at very high magnifications, caused electrostatic charging of the CNTs, which resulted in difficulties to capture well-focused images.

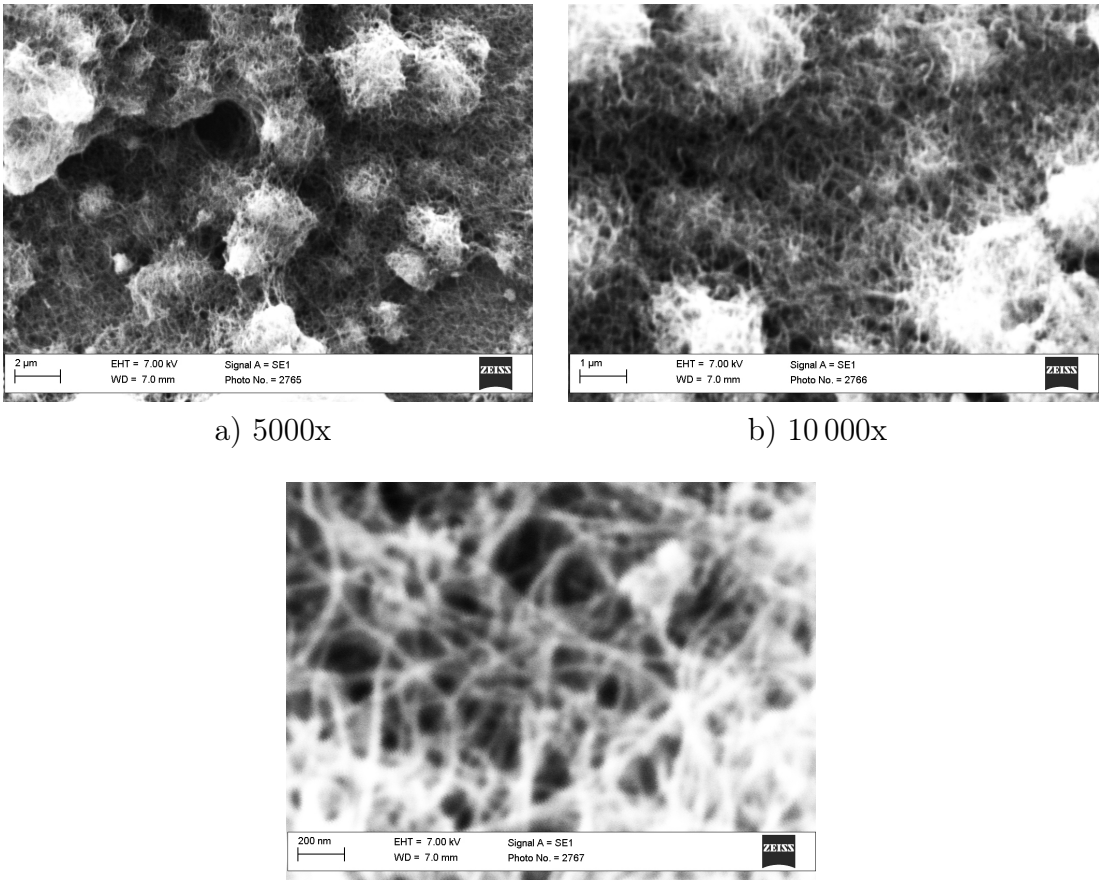

a) 5000x

b) 10 000x

c) 50 000x

Figure 4.18: SEM images of a spray-coated SWCNT film at a) 5000x, b) 10 000x and c) 50 000x magnification.

Tests and measurements

After manufacturing the pure SWCNT film sensor devices, in a similar fashion to that described for graphene and the MWCNTs, the SWCNT sensors were subjected to the various characteristic and gas response tests, which were also performed for the other sensors. To monitor the influences of varying substrate temperatures, the device was heated using the previously implemented Peltier system, whilst simultaneously measuring the sensor's film resistance and the substrate temperature, the result of which is presented in Fig. 4.19. Similar to the graphene and MWCNT film sensors, the SWCNT devices demonstrated a near linear decrease in resistance ($\approx$ 14.85% change) over an approximately 80°C increase in substrate temperature.

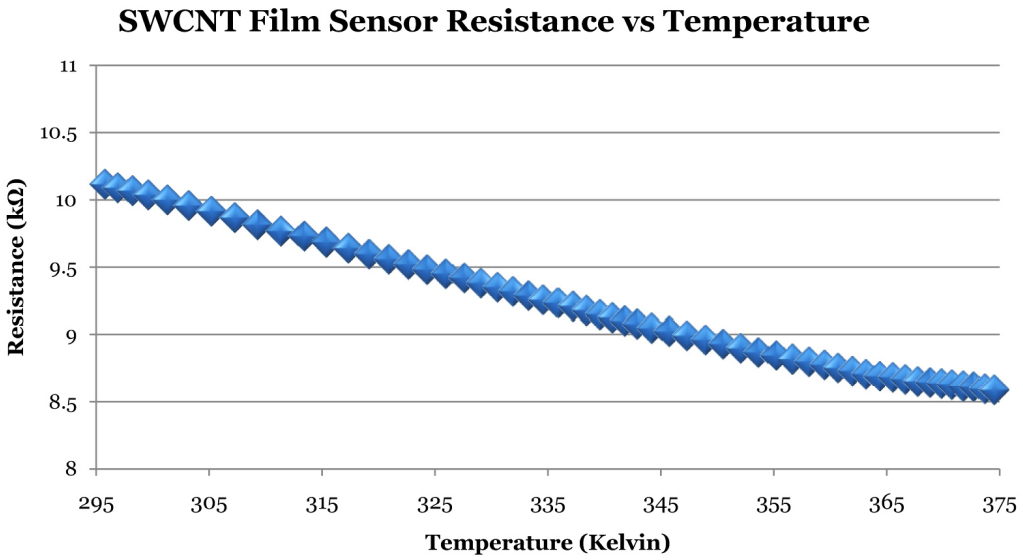

Figure 4.19: SWCNT film sensor resistance vs. increasing substrate temperature.

This was followed by performing the argon flow rate test (Fig. 4.20), during which Ar gas was flown through the chamber at 100 sccm increments (from 0-1000 sccm) for 5 minute intervals. The SWCNT film sensor produced a small change in resistance ($\approx$ 0.77%) over the entire flow range, which is most likely due to a slight decrease in relative humidity inside the test chamber. As well as for the other fabricated film sensors, it is proposed that flushing the chamber

with Ar prior to the application of the other gas species, will effectively prevent the introduction of these secondary effects into the measurements.

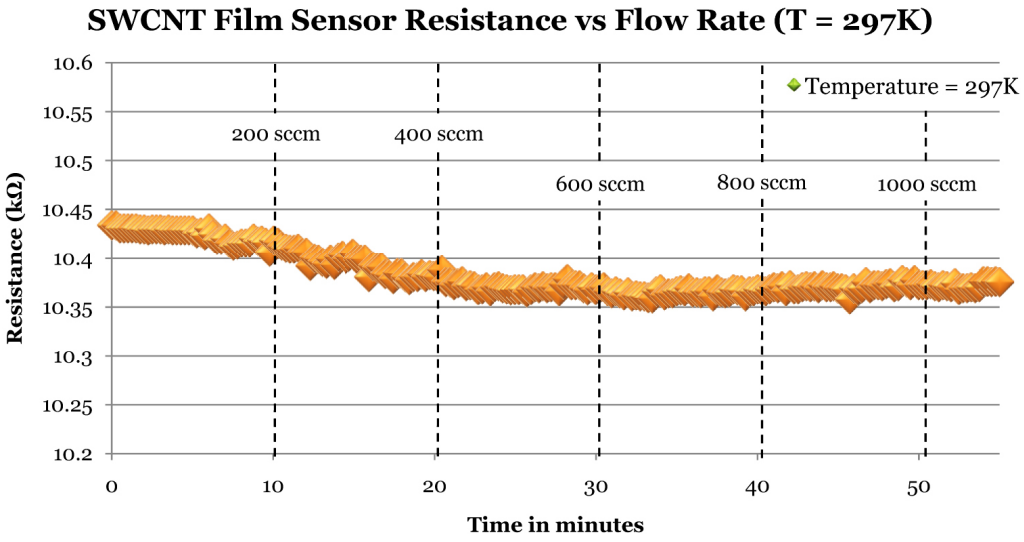

Figure 4.20: SWCNT film sensor response vs. increasing flow rate (T = 297 K).

Lastly, the pure SWCNT film sensors were subjected to the gas response tests, by flowing the various gases at increments of 100 sccm (from 0 - 400 sccm) for 3 minute intervals, through the test chamber. The gas response tests were performed at both room temperature ($\approx$ 24°C) and at 100°C, with the results presented in Fig. 4.21 and Fig. 4.22, respectively.

An analysis of the acquired room temperature measurements, revealed an approximately 2.25% increase in the film's resistance for exposure to acetylene (C_2H_2) and also a small increase ($\approx$ 0.6%) for O_2 exposure. Although the SWCNT sensor demonstrated a higher room temperature activity than the MWCNT device, the sensor's response also swiftly reached a saturated state. The increased activity of the SWCNTs are probably due to the smaller tube diameters, having a greater impact on the intra-structural transfer of electrons and the increased "doping" effect of semiconductive SWCNTs.

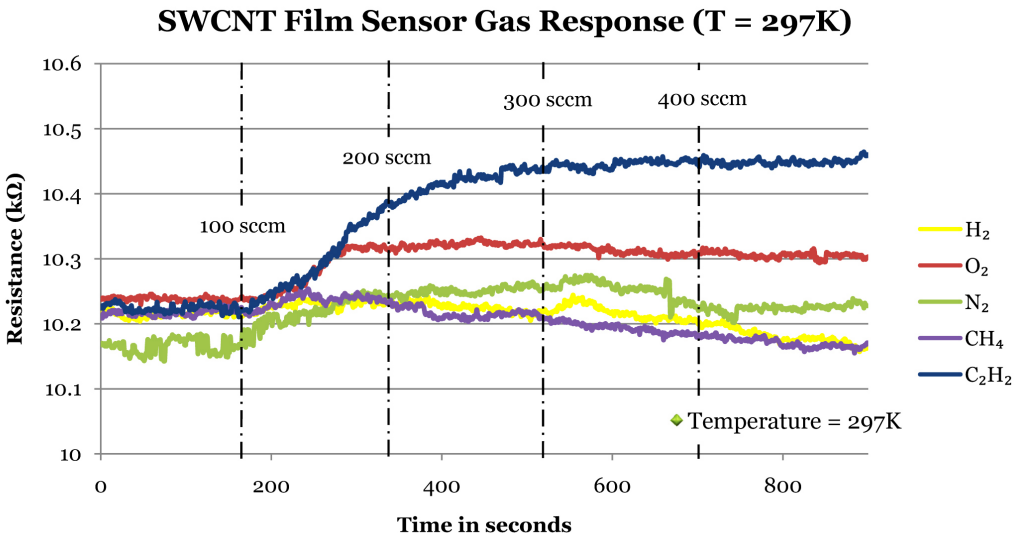

Figure 4.21: Pure SWCNT film sensor gas response (T = 297 K).

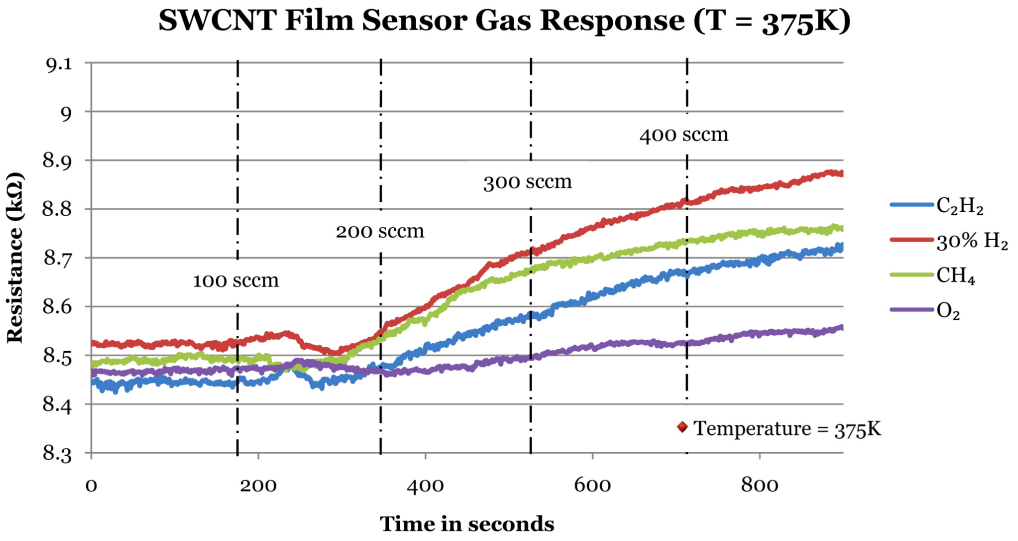

Figure 4.22: Pure SWCNT film sensor gas response (T = 375 K).

For the gas response test performed at the increased substrate temperature (i.e. 100°C), a change in the SWCNT film's resistance was observed for C_2H_2 ($\approx 3.20\%$), CH_4 ($\approx 3.17\%$) and also for O_2 ($\approx 3.17\%$) and $Ar\text{-}_{30\%}H_2$ ($\approx 4.23\%$). These values are comparable to the results obtained for the pure graphene and

MWCNT film sensors, and highlights key factors like the inertness of carbon nanomaterials at room temperatures and an increased reactivity, but a lower selectivity of gaseous species at increased substrate temperatures.

Furthermore, the SWCNT film sensors also demonstrated prolonged recovery times (i.e. a few hours) and required thermal treatment under an Ar flow ($\approx$ 100 sccm for 25 minutes at 100°C), to sufficiently recover to its initial value. The hysteresis effects observed for the MWCNT films, were also detected during the SWCNT film sensor's gas response evaluation.

4.4 Conclusions

This chapter portrayed the fabrication of three pure carbon nanomaterial (i.e. graphene, MWCNTs and SWCNTs) film sensors for gas detection. This included performing various characteristic tests and a qualitative analysis of the measured results. The film sensors were manufactured by spray-coating dispersed solutions of the nanomaterials onto clean SiO_2/Si substrates.

After evaluating the obtained SEM micrographs and resulting film resistances for both the graphene and nanotube film sensors, it is believed that the morphology (i.e. grain size, grain boundaries and also thickness) of the film, may influence its electrical characteristics. This implies that differences in the various films may produce larger or smaller conductivities, due to changes in the inter-structural resistance. Optimization of the respective films morphologies may therefore result in better electrical characteristics of the sensor. Since the alteration of these properties were not fully investigated, it is advised that future studies take into consideration such assessments.

As demonstrated by the gas response measurements, the pure nanomaterials exhibited rather low reactivities at room temperatures, with saturation effects occurring readily. Furthermore, an initial response delay in all device measurements was observed, but this was introduced by the experimental test setup, which implemented a T-connected gas line (typically for Ar and another gas), with a long ($\approx$ 2 meter) inlet tube.

Concluding the results obtained during the fabrication and characterization of the pure carbon nanomaterial film sensors, it was observed that in order to enhance the sensitivity of the devices (at the cost of selectivity), an increase in substrate temperature was necessary. From an efficiency point of view, this is unfortunately not perceived as an efficient process, since the amount of applied power ($\approx$ 8 Watt) to heat the device, is rather vigorous compared to the power consumption of the sensor device itself ($\approx$ 25 - 400 μW).

Chapter 5

Composite Nanomaterial Gas Sensors

With the aspiration to create a gas sensor with the sought after sensitivity and efficiency characteristics at lower temperatures, the functionalization of the proposed carbon nanomaterials were investigated. Accordingly, this chapter presents the fabrication procedures and test results of three composite carbon nanomaterial film sensors, that were constructed during this research.

5.1 Carboxyl-functionalized MWCNT film sensors

As mentioned in Chapter 3, the liquid phase oxidation of carbon nanotubes, results in the formation of various oxygenated functional groups (e.g. -COOH, -C=O and -OH) on the sidewalls of CNTs. These functional groups can have the ability to selectively bind to particular molecules and may provide enhanced levels of sensitivity.

Sensor fabrication

The first step in fabricating a carboxyl-functionalized MWCNT (i.e. MWCNT-COOH) film sensor, entailed the preparation of a MWCNT-COOH compound. Pursuing the purification and subsequent functionalization of CNTs by acid treatment, as described by Wiltshire [50] and Porro et al. [70], a MWCNT-COOH

composite material was produced. The functionalization process was performed by ultrasonically dispersing pure MWCNTs into a 3:1 mixture of concentrated sulfuric and nitric acid ($H_2SO_4 : HNO_3$). The acid solution was kept in an extraction cabinet for 5 hours at 70°C, to execute the functionalization of the MWCNTs. This was followed by several washing stages with deionized water, until the effluent acquired a pH $\approx$ 7. The excess water was extracted via centrifugation at 9000 rpm for 10 minutes and the MWCNT "pulp" was placed on a glass plate and dried in air at 40°C for 12 hours.

After preparing the MWCNT-COOH compound, a stable suspension of the CNT material ($\approx$ 0.1 wt%) was obtained by ultrasonication in a Propan - 2 - ol solvent. The same procedures were incorporated, as was described for the fabrication of the pure MWCNT film sensors in the previous chapter. The MWCNT-COOH solution was then spray-coated onto 10 x 10 mm SiO_2/Si substrates, forming an evenly coated film, which was dried with nitrogen gas at room temperature for 30 minutes. Ultimately, the fabricated MWCNT-COOH film sensors consisted of the same 4-contact device topology as the pure carbon nanomaterial sensors.

Tests and measurements

The characterization of the manufactured MWCNT-COOH film sensors was performed by subjecting the devices to various gas species at room temperature. After placing the sensors into the test chamber and applying an Ar environment for 35 minutes, the sensor obtained a stable film resistance of approximately 1 kΩ. This value is roughly ten times smaller than for the sensors fabricated with the pure carbon nanomaterials, which is most likely due to an enhanced conductivity induced by the -COOH chains.

Fig 5.1 presents the measured film resistance of the MWCNT-COOH device, for exposure to the various gases at room temperature. The gas response tests were performed by flowing the gases at 100 sccm increments (i.e. from 0 - 400 sccm) for 3 minute intervals, through the chamber. Furthermore, argon gas ($\approx$ 100 sccm for 30 min.) was applied repeatedly between the different gas species.

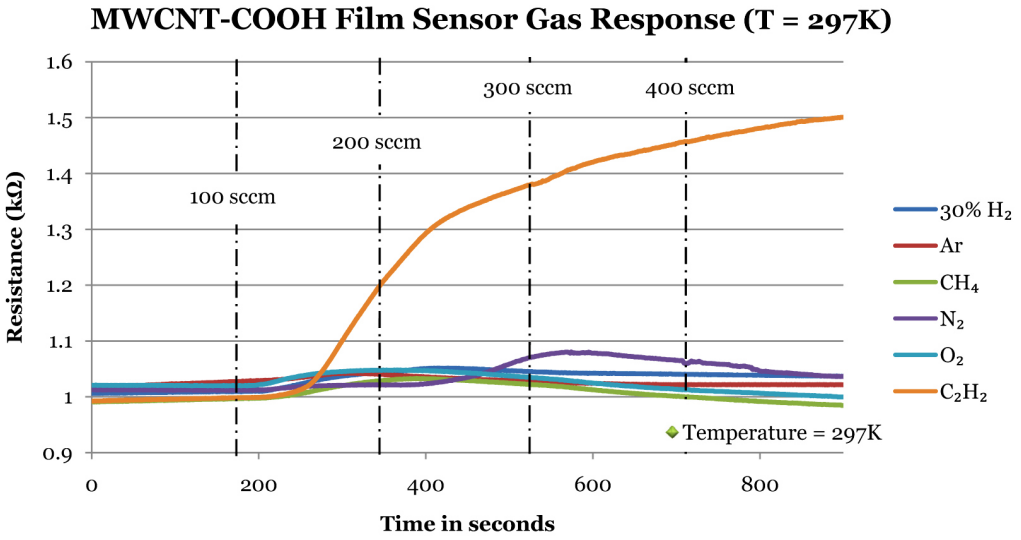

Figure 5.1: MWCNT-COOH film sensor gas response (T = 297 K).

From the measured results (Fig. 5.1), a remarkable 50% increase in the MWCNT-COOH film's resistance was observed for acetylene (C_2H_2), whilst the other gases had an almost negligible effect on the device's performance. It was however, also noted that the MWCNT-COOH film's resistance inclined towards a saturated state over the 0 - 400 sccm flow range. Furthermore, the fabricated film sensor demonstrated an exceptionally slow recovery time in an Ar environment, which is probably due to the stronger bonding mechanisms between the carboxyl groups and the C_2H_2 molecules. The device also displayed a similar hysteresis characteristic, which restrained the film's resistance from recovering to its initial value.

The sensor was subsequently thermally treated at 100°C for 20 minutes under an Ar flow, in order to recover the initial film resistance. It was however noticed, that the thermal treatment produced a significant reduction in the device's sensitivity. It is theorized that excessive heating of the MWCNT-COOH composite material, causes the adhering carboxyl chains to oxidize and subsequently detach from the nanotube structure. This in turn reduces the amount of receptor sites within the CNT film and yields a lower level of sensitivity.

The above-mentioned theory was clearly demonstrated, when the sensor was ex-

posed to successive C_2H_2 tests and allowing the recovery process to occur without any thermal excitation. Fig. 5.2 presents the results obtained for the successive C_2H_2 gas flow tests, also performed at room temperature.

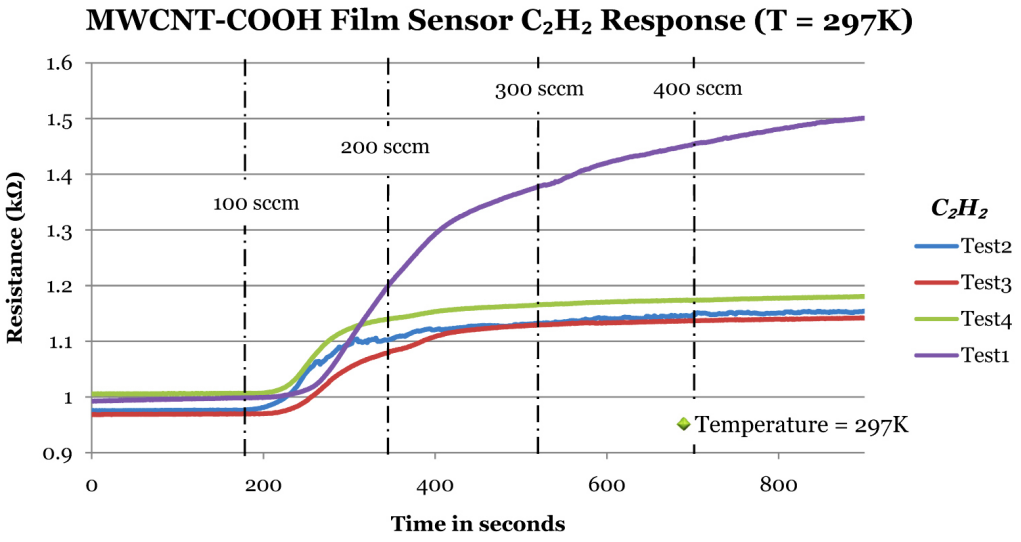

Figure 5.2: MWCNT-COOH film sensor C_2H_2 response (T = 297 K).

The device's first response (prior to thermal treatment) was added to the graph in Fig. 5.2 for comparison. It was observed that the initial 50% increase in film resistance (purple line in the graph), was reduced by $\approx$ 32.5% after heating the sensor. Furthermore, the sensor demonstrated a reproducible effect for the successive C_2H_2 tests, with an approximately 17.5% increase in film resistance. The recovery process was thus allowed to occur at room temperature under an Ar flow, with a successful recovery obtained within $\approx$ 8-10 hours. After performing these tests, the MWCNT-COOH device was subjected to another thermal treatment, which further reduced the device's sensitivity towards C_2H_2 detection to $\approx$ 8%. This confirmed the destruction of active receptor sites within the composite nanotube film during the heating process.

The observed features of the functionalized MWCNT-COOH film sensor, has indeed demonstrated a significant increase in sensitivity towards the detection of C_2H_2 molecules at room temperature. It might therefore be a material of interest

for disposable sensor products, that require a high level of sensitivity. The application of this composite nanomaterial for recuperative sensory devices however, is unfortunately wallowed by the slow recovery times and the evident reduction in sensitivity (i.e. film destruction), produced by increased substrate temperatures.

5.2 MWCNT-ITO composite film sensors

Considering the results of the previously assessed carboxyl-functionalized MWCNT film sensor and venturing towards the synthesis of a non-volatile nanocomposite for gas detection, the implementation of a MWCNT and indium tin oxide (ITO) composite nanomaterial was investigated. The potential of ITO, a transparent and electrically conductive material, for gas sensor applications was demonstrated by Patel et al. [71], who fabricated an ITO thin film methanol sensor, which operated at room temperature. It was therefore devised, that the combination of carbon nanotubes and ITO might yield interesting properties, which could be exploited in detecting gaseous species.

In addition, the properties of carbon-ITO nanocomposites were analyzed via UV-vis-NIR (ultraviolet-visible-near infra-red) spectrometry, to evaluate the possible application thereof in opto-electronic technologies (e.g. solar cells).

Sensor fabrication

In an outline of the work of Zhang et al. [72], who presented the fabrication and characterization of ITO-CNT nanocomposites, a procedure was formulated to synthesize a MWCNT-ITO composite nanomaterial. This was executed in conjunction with the spray-pyrolysis fabrication of ITO films, described by Sawada et al. [73], to manufacture a MWCNT-ITO film sensor.

The aqueous ITO precursor was produced by dissolving 1.12 g of indium (iii) chloride ($InCl_3$) and 0.51 g of tin (iv) chloride ($SnCl_4$) in a 50 ml solution of deionized water and pure ethanol (4:1 by volume). This was followed by magnetic stirring of the solution for 5 hours, to ensure that all solids were dissolved. Subsequently, a

small amount ($\approx$ 0.1 wt%) of the MWCNT-COOH material, that was prepared during the functionalization of the MWCNTs in Section 5.1, was ultrasonically dispersed in the ITO precursor and stirred for a further 4 hours at 60°C. The elevated temperature is proposed to stimulate the decoration of MWCNTs with electrically conductive (i.e. rhombohedral or cubic) ITO nanoparticles [72].

The MWCNT - ITO solution was spray-coated (vaporized) onto clean SiO_2/Si substrates, using a nitrogen airbrush. The substrate temperature was maintained at 350°C during the spray-pyrolysis procedure and was measured via a thermocouple, placed on the substrate surface. This procedure is rather time consuming, since the substrate temperature rapidly drops upon spraying a small amount of the solution onto it. Therefore, the MWCNT - ITO solution was sprayed in small bursts, allowing the substrate temperature to restabilize at 350°C between each sprayed layer (typically 2 - 3 minutes).

After completing the spray-pyrolysis process, the samples were annealed in a quartz tube at 500°C for 1 hour, in a nitrogen environment. The annealing procedure in a reducing ($\approx$ 300 sccm N_2) environment, was found to significantly increase the conductivity of the ITO films. Fig. 5.3 shows a low magnification SEM image of a typical MWCNT - ITO film (thickness = 14 layers), fabricated via the spray-pyrolysis process.

A MWCNT - ITO film sensor (with $R_{film} \approx 1$ kΩ) was manufactured by repeating the spray-coating process 12 - 14 times. A 4-contact sensor was subsequently fabricated by attaching four contact wires with a silver conductive paint and fixing the SiO_2/Si substrate onto an alumina (Al_2O_3) substrate with an epoxy adhesive, similar to the previously described sensors.

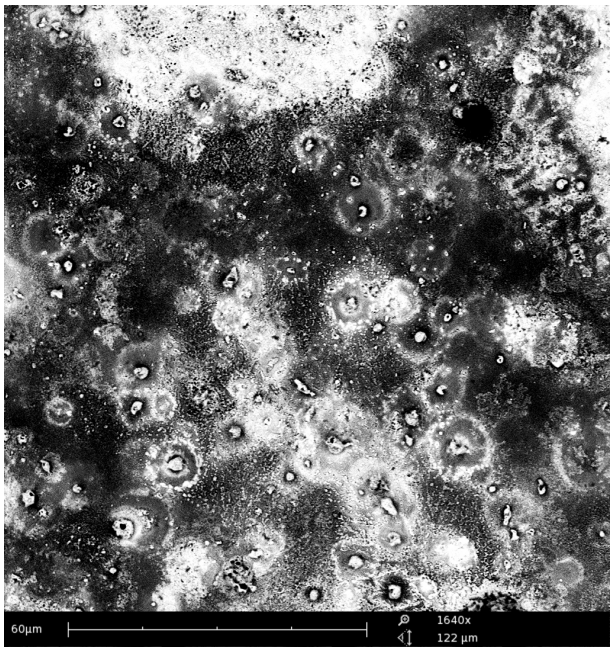

Figure 5.3: SEM image of a MWCNT - ITO composite film on a SiO_2/Si substrate at 1640x magnification.

Tests and measurements

An initial characterization of the ITO and carbon-composite films, produced by the spray-pyrolysis technique, was performed in terms of film resistance versus an increase in film thickness. Table 5.1 presents the measured film resistances for a pure ITO film, a MWCNT - ITO composite film and also a graphene - ITO composite film, that was created by replacing the MWCNT-COOH material with a corresponding amount of pure graphene nanopowder (12 nm flakes).

From the measured film resistances, it was visible that the introduction of the carbon nanomaterials into the ITO films produced lower film resistance values, particularly for very thin films.

Table 5.1: ITO/composite Film Resistance vs. Number of Layers

Layers	ITO	MWCNT - ITO	Graphene - ITO
3	$\approx$ 170 MΩ	93.6 kΩ	1.57 MΩ
7	3.52 kΩ	4.68 kΩ	2.13 kΩ
14	1.21 kΩ	1.08 kΩ	596 Ω
21	658 Ω	372 Ω	349 Ω
28	470 Ω	216 Ω	214 Ω

As mentioned earlier, the prepared ITO - nanocomposites were subjected to a UV- vis -NIR spectral analysis, to determine the possible application thereof in solar cell and other technologies, that require transparent electrodes. For the UV- vis -NIR analysis, the spray-pyrolysis process was repeated for the various film thicknesses, using 25 x 25 mm glass slides instead of the SiO_2/Si substrates. The UV- vis -NIR transmission results are presented for 3, 14 and 28 sprayed layers in Fig. 5.4 to Fig. 5.6. These measurements were obtained with a Specord® 210 Plus UV- vis -NIR spectrometer from Analytik*Jena*, using a clean glass substrate as the reference sample.

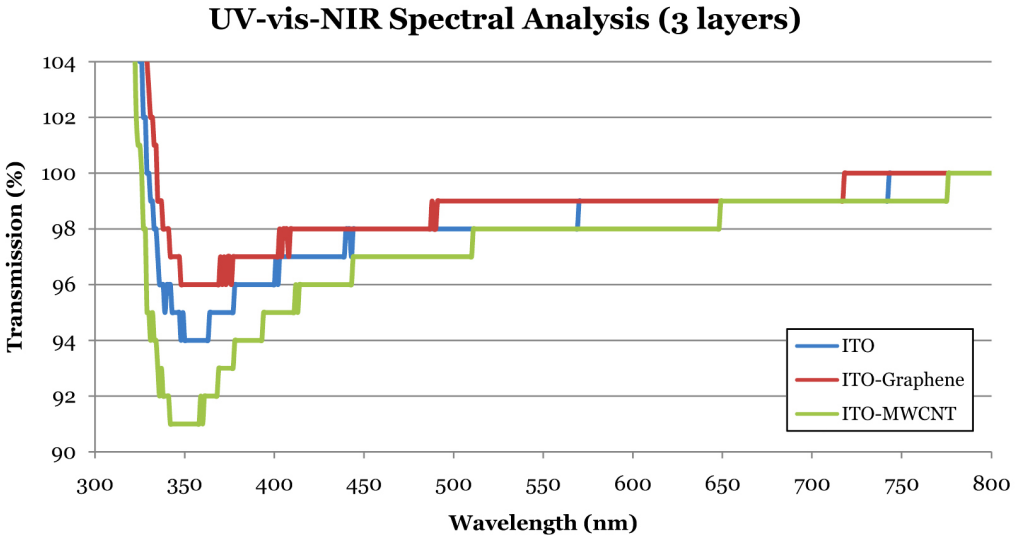

Figure 5.4: UV- vis -NIR transmission of 3 -layer ITO/composite films.

For solar cell applications, the spectral wavelengths between ≈ 380 - 800 nm are typically of interest. Comparing the results in Fig. 5.4 for the transmission of the 3-layer films, it was observed that the films had very good (> 94%) transmission properties, with the graphene - ITO composite prevailing over the pure ITO and MWCNT - ITO materials.

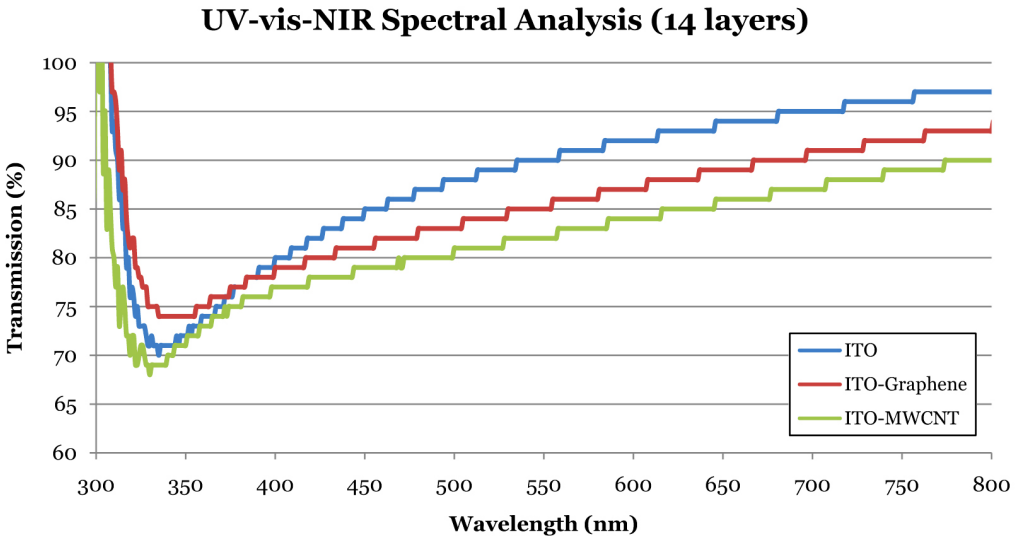

Figure 5.5: UV - vis - NIR transmission of 14 - layer ITO/composite films.

The results for the 14-layer films (Fig. 5.5), presented a similar transmission curve, only with a ≈ 20% decrease in transmission observed for the lower nm wavelengths. However, the small difference in transmission established between the three materials, might promote the addition of MWCNTs and graphene as a favourable method to obtain lower film resistances, especially in the case of very thin films (e.g. 3-layers).

The UV - vis - NIR results portrayed in Fig. 5.6, for the 28-layer films, revealed an interesting effect, whereby the pure ITO film demonstrated a rather weak transmission below 380 nm (i.e. lower than the carbon composite films), but reached a higher peak than the other films between ≈ 410 - 550 nm.

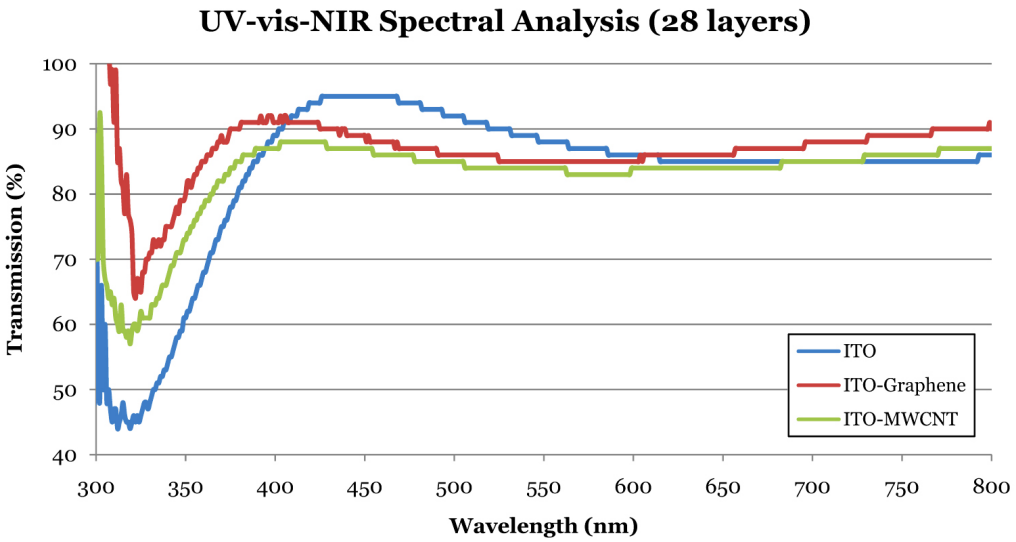

Figure 5.6: UV-vis-NIR transmission of 28-layer ITO/composite films.

Throughout the fabrication process, the MWCNT- and graphene-ITO composites continuously provided lower film resistances, without drastically influencing the transmission efficiency of the films, which can be promising for the utilization of these carbon nanomaterials in opto-electronic applications.

Alternatively, the manufactured MWCNT-ITO film sensor was subjected to various gas species at room temperature, to evaluate the gas sensing properties of the nanocomposite. Fig. 5.7 presents the gas response test results, which was acquired by flowing C_2H_2, CH_4 and $Ar\text{-}_{30\%}H_2$ through the chamber, at 100 sccm increments (0-400 sccm) for 3 minute intervals.

Although the MWCNT-ITO film sensor only demonstrated a small ($\approx 2.26\%$) change in resistance for C_2H_2, this result was in stark contrast with the previous MWCNT test results. The fact that a decrease in resistance was induced by exposure to C_2H_2, instead of an increase as previously observed, suggested that the ITO nanoparticles introduced a "doping" effect on the MWCNTs, creating a n-type semiconductive composite material.

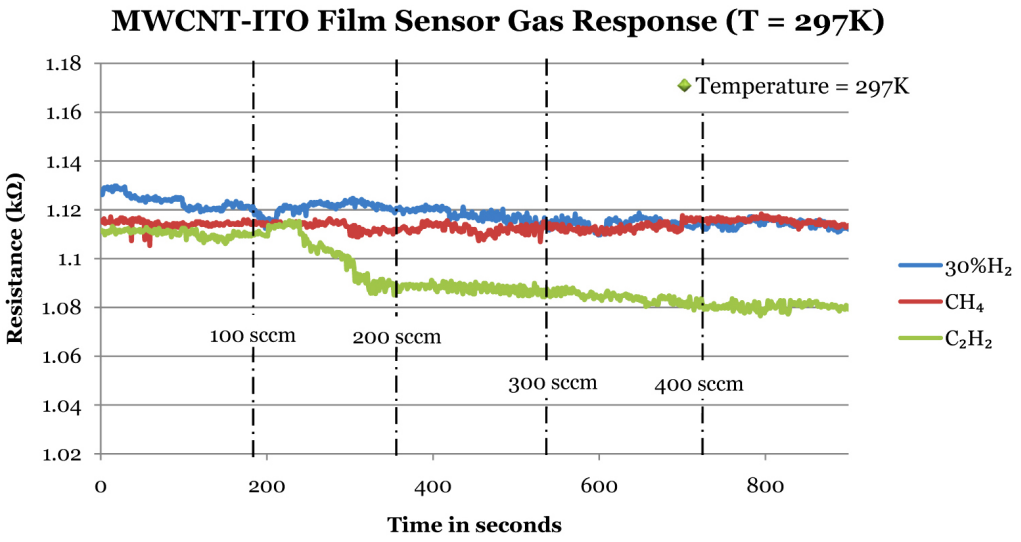

Figure 5.7: MWCNT - ITO film sensor gas response (T = 297 K).

In a different experiment, the same MWCNT - ITO film sensor was exposed to an alternating flow of argon (Ar) and acetylene (C_2H_2) gas at an elevated substrate temperature. Fig. 5.8 portrays the device's response to the alternating gas flow, which was performed by maintaining a constant 200 sccm flow through the test chamber and switching the two gases for 3 minute intervals.

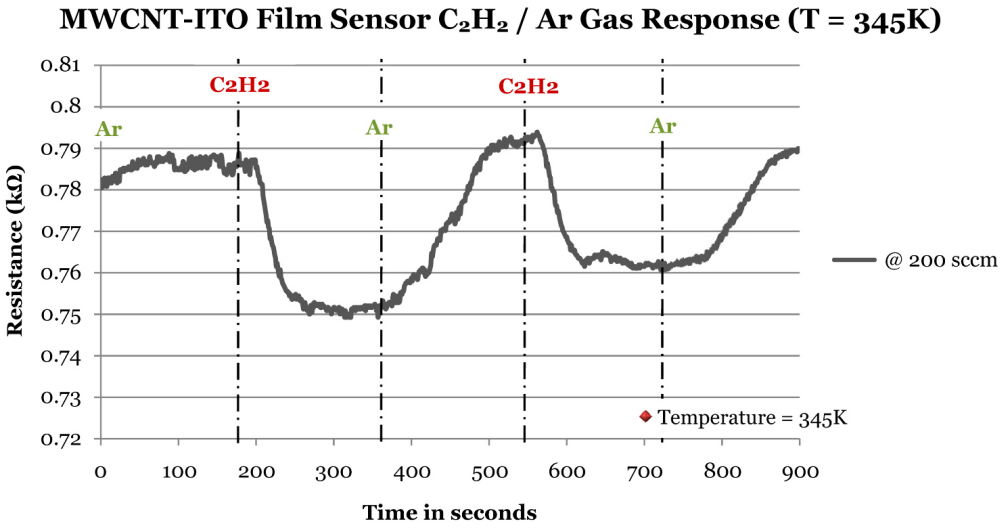

Figure 5.8: MWCNT - ITO film sensor Ar/C_2H_2 response (T = 345 K).

From Fig. 5.8 it can be observed that the MWCNT - ITO film sensor demonstrated a successive decreasing response (by $\approx 4.5\%$) towards exposure of C_2H_2, whilst rapidly recovering to its initial value under the Ar flow. These results not only demonstrated an enhanced sensitivity towards C_2H_2 detection at a higher substrate temperature (i.e. $\approx 70^{\circ}C$), but also that a significant improvement in recovery time as well as a non-volatile functionalized carbon-nanocomposite was obtained.

Due to a limited variety of available test gases, the alternating gas flow experiment could unfortunately not be performed for other gas species. Nonetheless, the utilization of carbon nanomaterial - ITO composites, have been demonstrated to be of interest for various electronic applications and further investigations into the material properties of such composite nanomaterials are advised.

5.3 Graphene-ZnO composite film sensors

Proceeding towards the synthesis of an inorganic "solid-state" graphene-based gas sensor, as was obtained with the MWCNT - ITO device in the previous section, the growth of zinc oxide (ZnO) nanowires on graphene films were investigated. This section presents a 3 -step fabrication procedure to synthesize a graphene - ZnO nanowire film, which was implemented as an acetylene (C_2H_2) gas sensor.

Sensor fabrication

The first step of the graphene - ZnO fabrication, involved the previously described spray-coating technique to produce an evenly coated graphene nanopowder film on a clean SiO_2/Si substrate. This was performed by ultrasonically dispersing the graphene ($\approx$ 0.1 wt%) in a Propan - 2 - ol solvent for 30 minutes at 55°C. Approximately 1 ml of the graphene solution was spray-coated onto the 10 x 10 mm SiO_2/Si substrate, which was dried with nitrogen at 115°C.

The following step consisted of depositing a 5 nm ZnO seed layer on-top of the graphene film, using an inverted cylindrical RF magnetron sputtering unit with a ZnO target [74]. The preparation of a ZnO seed layer was found to radically improve the yield of ZnO nanowires during the growth procedure. This can be observed from the SEM images in Fig. 5.9, which illustrates the ZnO growth on graphene films with and without the deposition of the ZnO seed layer. Furthermore, it was noticed that the size of the ZnO nanoparticles forming the seed layer, generally governed the nanowire diameters and confined the growth orientation normally to the surface of the graphene flakes.

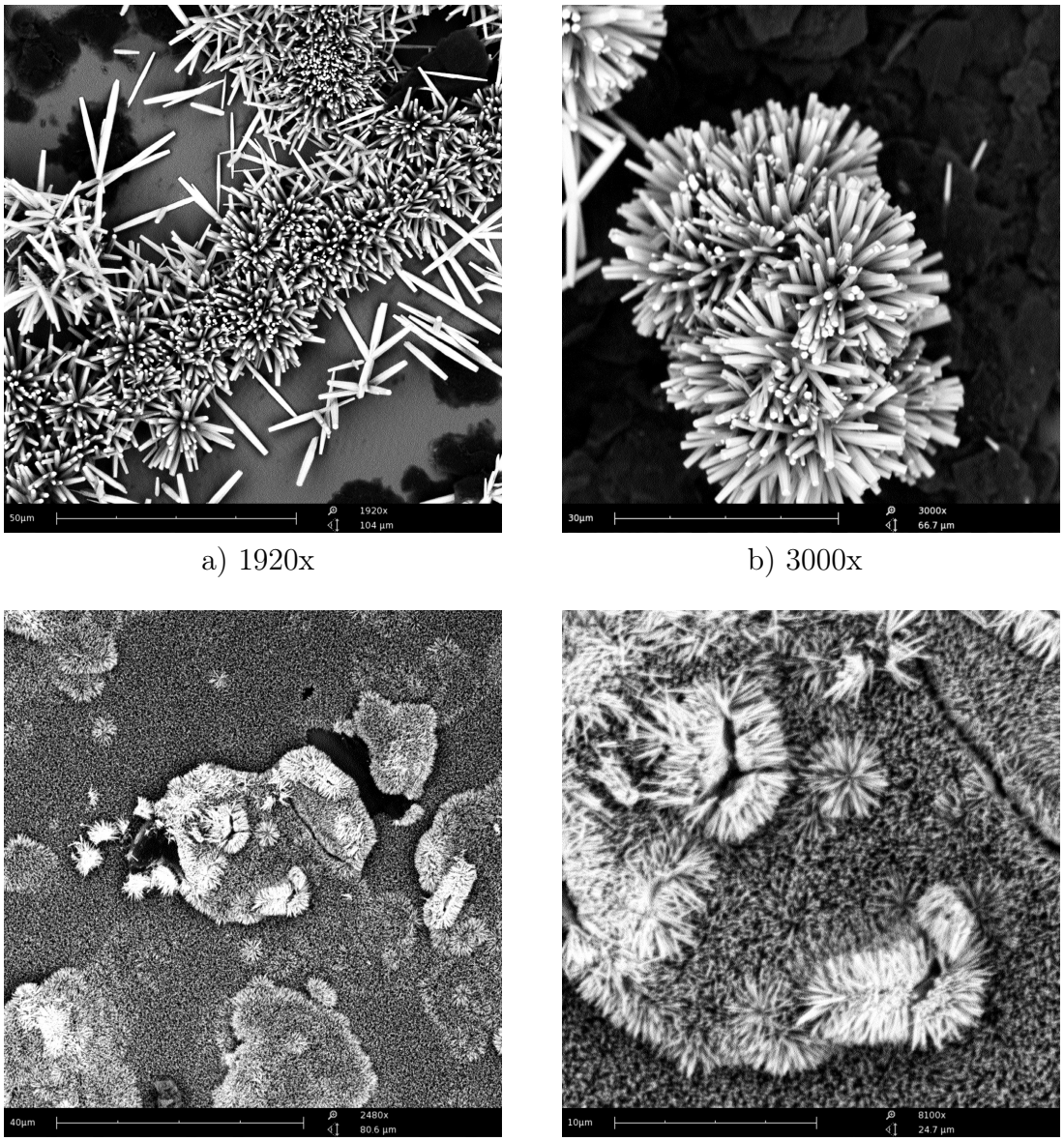

a) 1920x b) 3000x

c) 2480x d) 8100x

Figure 5.9: SEM images of ZnO nanowire growth on a graphene film, without a ZnO seed layer at a) 1920x and b) 3000x magnification, and with the deposition of a 5 nm ZnO seed layer prior to the growth process, at c) 2480x and d) 8100x magnification.

The final phase of the graphene - ZnO film fabrication, comprised the synthesis of the zinc oxide nanowires via a hydro-thermal growth process [74], [75]. The ZnO nanowire synthesis was performed by floating the ZnO_{seed}/graphene coated substrates upside down on an aqueous solution of zinc nitrate hexahydrate (0.1M) and hexamethylenetetramine (0.1M). The used chemicals were all

analytical grade compounds, obtained from "*Sigma Aldrich Chemicals*". The suspended substrates were subsequently placed in a laboratory oven at 85°C for 4 - 5 hours, to stimulate the nanowire growth.

After completing the 3-step ZnO/graphene synthesis procedure, the sample was mounted on an alumina (Al_2O_3) substrate and four contact wires were added with a silver conductive paint, to produce a similar device topology as for the other manufactured sensors.

Tests and measurements

Since most of the previously tested sensors only demonstrated a response towards acetylene (C_2H_2) detection at room temperature, the graphene - ZnO film sensor was also subjected to a C_2H_2 response test. The gas response test was performed by flowing C_2H_2 through the test chamber at 100 sccm increments (i.e. from 0 - 400 sccm) for 3 minute intervals, whilst measuring the film's resistance with the LabJack A/D device (connected in the Van der Pauw configuration). Fig. 5.10 depicts the measured response of the graphene - ZnO device towards the exposure of C_2H_2 at room temperature ($\approx$ 24°C).

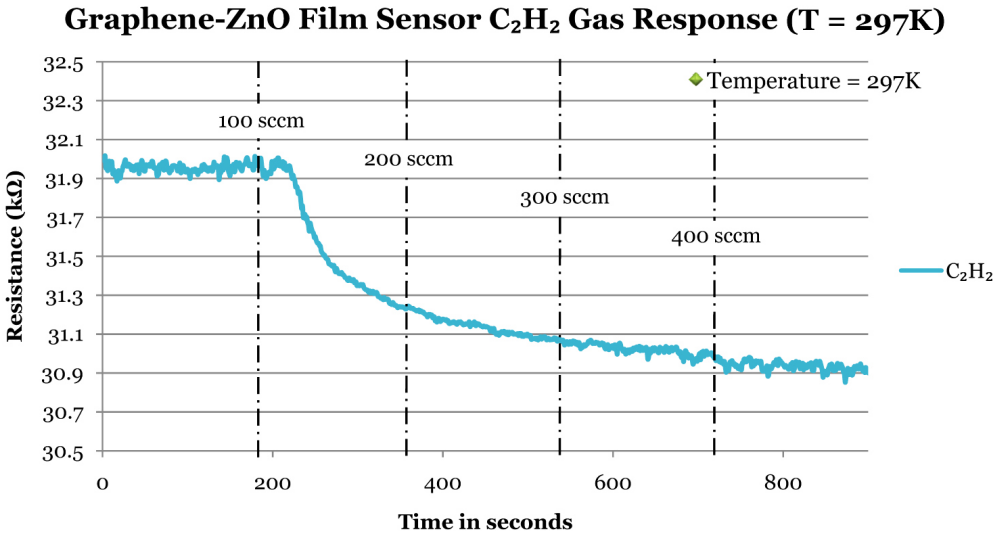

Figure 5.10: Graphene - ZnO film sensor C_2H_2 response (T = 297 K).

From the test results at room temperature (Fig. 5.10), it could be observed that the ZnO nanowires also introduced a similar "doping" effect on the graphene film, as seen for the MWCNT - ITO films. This caused the film's resistance to decrease (by $\approx 3.46\%$) upon exposure to C_2H_2, instead of increasing, as was previously observed for the pure graphene films. Due to the graphene - ZnO film's higher initial value (≈ 32 kΩ), the relative decrease in the film's resistance was comparable to the $\approx 3.84\%$ increase in the pure graphene film resistance (presented in Chapter 4). However, the graphene - ZnO device demonstrated a larger absolute change in resistance, which indicated an enhanced sensitivity.

Additionally, the graphene - ZnO film sensor was heated to 100°C to repeat the C_2H_2 test at an elevated substrate temperature. This test was performed to investigate the effect of the increased temperature on the sensitivity and volatility of the graphene - ZnO device. Fig. 5.11 illustrates the sensor's response to C_2H_2 at 100°C, from which an approximately 28% decrease in the film's initial resistance was noticed (i.e. $R_{initial} \approx 23.1$ kΩ).

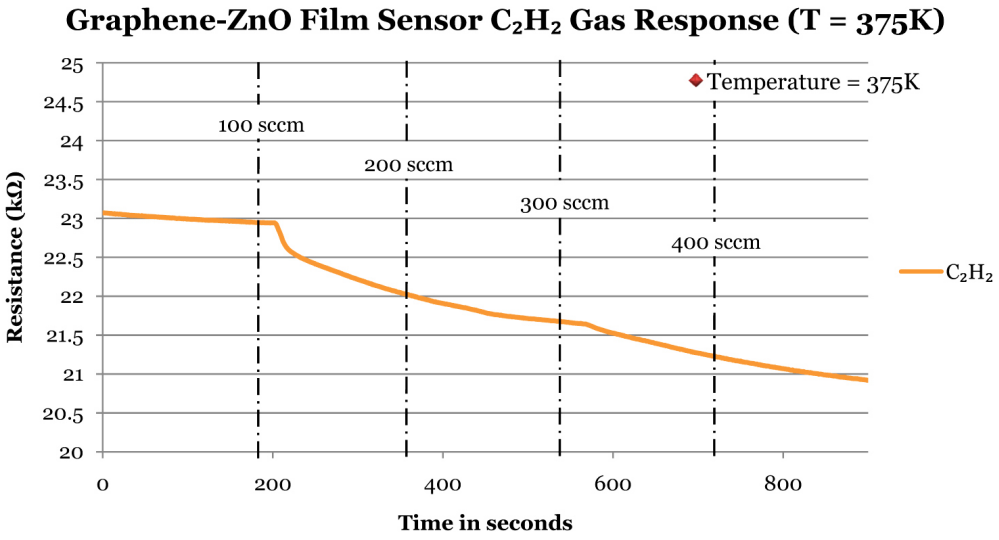

Figure 5.11: Graphene - ZnO film sensor C_2H_2 response (T = 375 K).

Furthermore, the graphene - ZnO device demonstrated a larger change in resistance ($\approx 9.52\%$) over the 0 - 400 sccm flow range, which confirmed an even higher

sensitivity at the elevated substrate temperature. Although the graphene - ZnO film sensor didn't show any signs of degradation after the test at 100°C, the device demonstrated quite lengthy recovery times (i.e. a few hours), even at the higher temperature and under a 100 sccm Ar flow. The latter drawback will therefore probably limit the implementation of graphene - ZnO composites in sensory applications that require a rapid device recovery.

5.4 Conclusions

This chapter presented three functionalized carbon - composite nanomaterials, which were implemented as thin film gas sensors, especially for the detection of acetylene (C_2H_2) at room temperature.

The results obtained during this research, revealed that a changing environment (e.g. an increased temperature) can be detrimental to "organic" functionalized carbon nanomaterials, as was demonstrated for the MWCNT - COOH film sensor. This method however, produced the most significant improvement in device sensitivity towards the detection of C_2H_2 at room temperature. The decoration of MWCNTs with carboxyl groups, was also found to be an effective method to generate a CNT material that is highly soluble in water and other aqueous solutions.

Alternatively, the fabrication of inorganic "solid-state" nanocomposites (e.g. MWCNT - ITO and graphene - ZnO), provided a non-volatile device functioning, but also introduced a "doping" effect on the relevant carbon nanomaterials, causing an inverted sensor response compared to the pure carbon-based film sensors.

Furthermore, it was demonstrated by the UV - vis - NIR spectral analysis (Section 5.2), that the introduction of carbon nanomaterials like MWCNTs and graphene into indium tin oxide (ITO) thin films, may significantly reduce the film's resistance without degrading its transmission properties. This can be beneficial for opto-electronic applications like solar cells, touch screen devices and other transparent electrode technologies.

Chapter 6

Microstructured Thin Films of Aluminium for the Integration of Nanomaterials

This chapter discusses the various effects on the resistivity of thin metal films and describes the dominant factors governing a metal film's resistivity. Accordingly, an innovative procedure for the fabrication of patterned, ultra thin (sub 100 nm thickness) aluminium structures on thermally grown SiO_2 substrates, that was developed during this research, is portrayed. Finally, the preparation of an integrated "carbon nanotube - aluminium structure" sensor for gas detection is presented and briefly discussed.

6.1 The resistivity of nanoscale aluminium films

Although aluminium is a very common electrode metal and is extensively used for discrete devices and integrated circuits, it might also be a promising material for nanostructured devices, because of its relatively low electron-mean-free-path (EMFP) and lower increase in resistivity vs. decreasing film thickness compared to other metals, such as silver, gold and copper.

Aluminium (Al), with a work-function $q\phi_m = 4.1$ eV [76], has generally been used for ohmic contacts and interconnections in the semiconductor industry for many decades and aluminium films can be generated by various physical deposition methods, including thermal deposition or sputtering under vacuum.

From a nanotechnology point of view, with feature sizes in the sub 100 nm range, ultra thin patterned aluminium layers may well be preferred to the thin layers of other commonly used metals. The significance of the proposed metals for the fabrication of ultra thin films, lies in a physical/electrical characteristic referred to as the material's "thickness dependent resistivity".

A thin film's resistivity is influenced by three main factors, namely an external size effect, an internal size effect and impurity scatterings:

External size effect: According to the theory developed by Fuchs and Sondheimer, electrons will be scattered at the external surface of thin metal films as the film thickness is decreased below the EMFP of the material. These scatterings then result in a sudden increase in the film's resistivity [77], [78].

Internal size effect: As the film's thickness, which roughly equals the average grain size for ultra thin layers, decreases below the EMFP, electron scattering at the grain boundaries will be dominant according to the theory developed by Mayadas et al. [78], [79].

Impurity scatterings: Since ultra thin films are more susceptible to the effects of impurities, dislocations and vacancies, an increase in the film's resistivity is expected due to electron scattering at these sites or "defects" [77], [78]. As ultra thin films consist of very little matter compared to the material in bulk, the effects of electron scattering at impurity sites and grain boundaries has a larger influence on the resistivity, since it abruptly changes the "path" in which the electrons flow.

The bulk resistivity at room temperature of aluminium, silver and copper is 2.66, 1.59 and 1.67 $\mu\Omega$-cm, respectively and the corresponding EMFP's are 15 nm, 52 nm and 39 nm [80]. Furthermore, it has been proposed that in order to minimize the size effect on extremely thin films or sub 100 nm thick patterned electrodes, the material with the smallest EMFP and a low-reflective grain boundary will be most efficient [77]. Because the materials have different grain sizes, it becomes hard to separate the effect of EMFP from grain size when the film thick-

ness becomes roughly equal to the EMFP. Therefore aluminium, with the lower EMFP and proposed lower increase in resistivity versus decreasing film thickness, is foreseen to yield a less abrupt change in film resistivity when decreasing the film thickness below the EMFP.

In addition, the annealing of metal thin films may significantly reduce the effects of impurities and dislocations, but as film growth via the physical vapour deposition method will typically yield very low (low ppm) levels of impurities, the latter technique has become the preferred film growth method. Furthermore, it has been observed that aluminium thin films deposited onto SiO_2 have a lower resistivity compared to films grown on pure silicon substrates. This can be ascribed to a better coalescence between Al/SiO_2 and the presence of less sharp grain boundaries in the deposited metal films [78].

George [81] and De Vries [82] have also experimentally verified the electrical resistivity of thin metal films with respect to Matthiessen's rule, given by:

$$\rho_{film} = \rho_{ideal} + \rho_{thickness} + \rho_{impurities}$$

where ρ_{ideal} is a thermal ion motion dependent resistivity part, $\rho_{thickness}$ is a thickness dependent resistivity due to grain boundary scattering of conduction electrons, and $\rho_{impurities}$ is a residual resistivity part dependent on impurities and lattice defects. They have also concluded that grain boundary scattering dominates the contribution to resistivity and that the size effect is mainly independent of ambient temperature [81].

As previously mentioned, many commonly used techniques in the fabrication of semiconductor devices are also implemented and scaled down to produce features for nanodevices, but the growth or deposition of such ultra thin films and the patterning of interconnects and electrodes, remains a non-trivial and complex exercise. In the following sections, a unique and effective method for the fabrication of ultra thin aluminium electrode structures (thickness $<<$ 100 nm) on thermally grown SiO_2 substrates is presented. The results obtained with this proposed method are then also compared to other commonly used procedures

such as dry etching (argon ion milling) and a chemical lift-off process in acetone. Furthermore, the work presented in this chapter, regarding the characterization and fabrication of ultra thin aluminium structures, was published in the journal "*Thin Solid Films*" in September 2011, in an article entitled "*An Effective Fabrication Method for Ultra Thin Aluminium Structures*".

6.2 The silicon oxidation process

For the preparation of electrically isolating SiO_2/Si substrates, prior to the deposition of the thin aluminium films, an approximately 300 nm SiO_2 layer was grown on 2-inch high purity silicon (1-1-1) wafers, via a thermal oxidation process at 1100°C. The oxidation process was performed by placing the Si wafers on a quartz stand in a fused-quartz electrical furnace, in which an oxygen and water vapour environment was established. The chemical reaction that describes the thermal oxidation of Si in water vapour is given by

$$Si_{(solid)} + 2H_2O_{(gas)} \rightarrow SiO_{2\,(solid)} + 2H_{2\,(gas)}$$

For the 300 nm oxide thickness, the required oxidation time was calculated from Sze [76], using the equation

$$x = \sqrt{\frac{2DC_0}{C_1} \times (t + \tau)}$$

where

$$\tau = \frac{\left(d_0^2 + \frac{2Dd_0}{k}\right)}{2DC_0} \times C$$

which represents a shift in time co-ordinates, to account for an initial oxide layer with thickness d_0.

However, for the wet oxidation ($H_2O + O_2$) process, the initial oxide thickness is negligible, which results in

$$\tau \approx 0$$

$$\therefore \; x = \sqrt{\frac{2DC_0}{C_1} \times t}$$

where x = the desired oxide thickness, C_0 = the equilibrium bulk concentration of the oxidizing species at the process temperature (i.e. $C_0 \approx 3{\times}10^{19}$ molecules/cm^3 at 1100°C and atmospheric pressure) , C_1 = the number of molecules of the oxidizing species in a unit volume of the oxide, with $C_1 \approx 4.4{\times}10^{22}/\text{cm}^{-3}$ for H_2O oxidation.

The diffusion coefficient D of the oxidizing species, is calculated from the equation

$$D = \frac{C_1}{2C_0} \times B$$

where $B \approx 6.0{\times}10^{-1}$ μm^2/hr, which was acquired from experimental data regarding the linear rates of oxidation of the different crystal orientations (e.g. 1-1-1 and 1-0-0) of silicon [76].

Thus, for an oxide thickness of x = 300 nm, the required oxidation time was calculated to be

$$t \approx 9 \; minutes$$

Fig. 6.1 illustrates a cross-sectional SEM image (at 18 000x magnification) of a thermally oxidized Si (1-1-1) wafer, which was mounted at a 90° angle. Using the SEM instrument's measuring tool, the oxide thickness was measured to be roughly 300 - 330 nm, which indicated an oxidation rate of

$$\frac{dx}{dt} \approx 35 \;\; \text{nm/min}$$

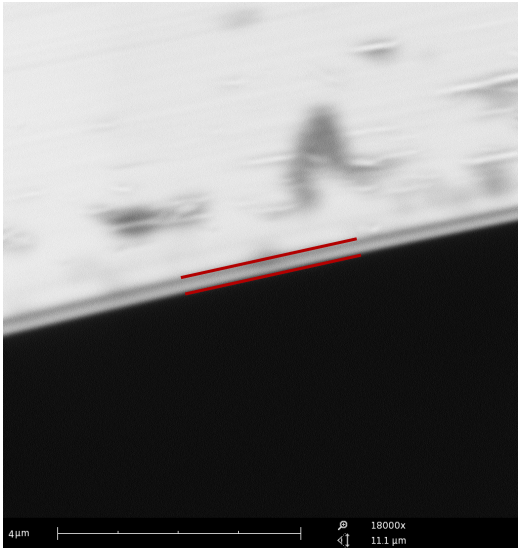

Figure 6.1: Cross-section SEM image of a thermally oxidized SiO_2/Si substrate, with oxide thickness $\approx$ 300 nm.

6.3 Fabrication of ultra thin aluminium microstructures

In order to manufacture the aluminium microstructures, thin layers of aluminium were directly deposited onto 10 x 10 mm SiO_2 substrates, using a vacuum thermal evaporator and a tungsten source boat. The thermal evaporator used during this work is depicted in Fig. 6.2. The thermal vacuum evaporation procedure was implemented to reduce film surface stresses and the effects of islandised growth, to minimize size-effects and to prevent the effect of conduction by the variable range hopping mechanism. It is subsequently assumed that electron scattering at the grain boundaries will be the dominant factor in establishing a film resistivity [78, 83].

The source material used during the film deposition was pure (i.e. 99.999%) aluminium pellets, which were obtained from *Sigma Aldrich Chemicals*. The ultra thin metal layers were thermally evaporated at a system pressure of 200×10^{-9} Pa and at a rate of 0.5 Å/s. The film thickness was measured by a 6 MHz (gold coated) quartz crystal thickness monitor from Inficon (Model: Qpod, S/N 1088).

Figure 6.2: Photograph of the thermal evaporator used to deposit ultra thin aluminium layers.

The implementation of the thermal evaporator requires an initial calibration procedure, to account for the difference in height between the quartz crystal and the sample substrates. This calibration was performed by depositing an initial film, with thickness $d_{initial}$ (typically 50 nm) and measuring the actual film thickness d_{actual}, with an AFM instrument. This information is then used to adjust the tooling factor TF, using the equation

$$TF_{new} = \frac{d_{actual}}{d_{initial}} \times TF_{old}$$

An AFM (Atomic Force Microscope, NanoSurf easyScan 2), shown in Fig. 6.3, was utilized to examine the prepared SiO_2 and patterned aluminium thin film samples. The samples were scanned using non-contact (TAP150Al-G) tips from *Budget Sensors*, with a dynamic force setting in air.

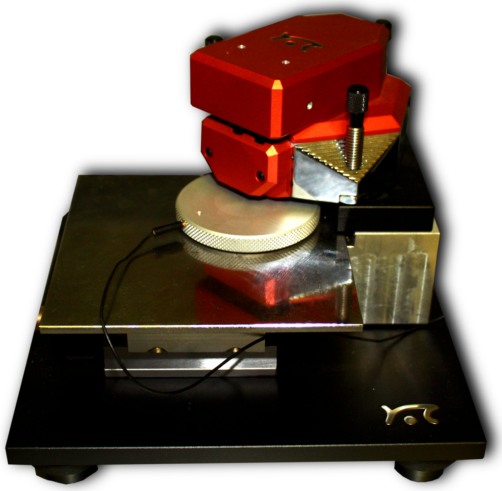

Figure 6.3: NanoSurf easyScan 2 atomic force microscope (AFM).

Fig. 6.4 a) illustrates an AFM image of a thermally oxidized SiO_2 substrate, with a measured surface roughness of about 0.8 nm. Fig. 6.4 b) shows an AFM image of an as-deposited aluminium thin film (thickness $\approx$ 60 nm). The AFM measurements obtained, indicated an average grain size of approximately 35 to 43 nm for the deposited ultra thin metallic film.

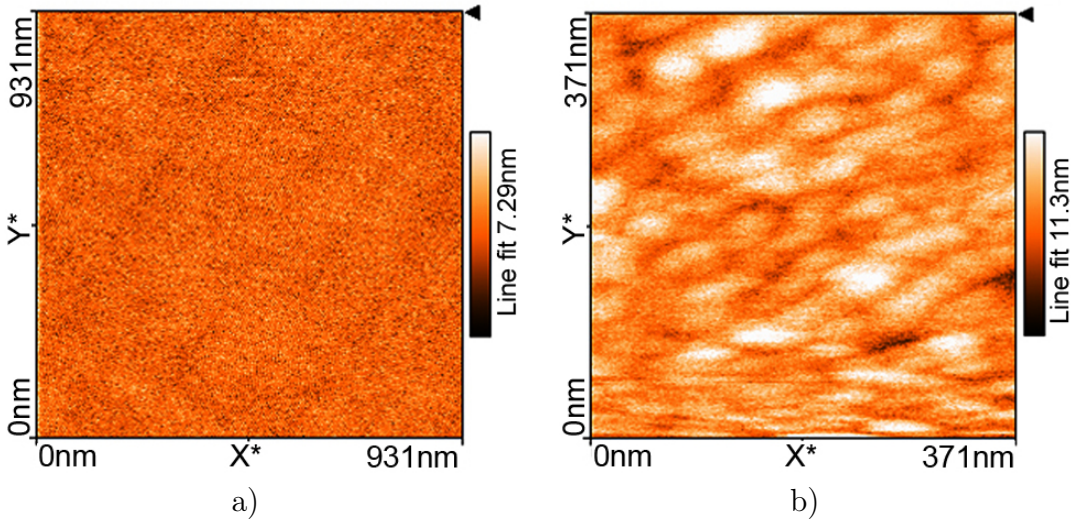

Figure 6.4: AFM image of (a) a 300 nm thermally oxidized SiO_2 layer with measured surface roughness of about 0.8 nm, and (b) a 60 nm thermally evaporated aluminium layer with an average grain size of approximately 35 to 43 nm.

Using a 4-point probe technique, the deposited 60 nm aluminium thin film's resistivity was measured at 5.06 $\mu\Omega$-cm. Although the measured resistivity is higher than the bulk value (2.66 $\mu\Omega$-cm), it is an anticipated result because of the effects described in Section 6.1, and corresponds to the findings of Joshi et al. [78]. In order to perform the 4-point measurement, a constant current source and a low-noise instrumentation amplifier was designed and manufactured, which are presented in Appendix F.

Following the Al film deposition, three different methods were employed to produce patterned aluminium structures. These methods mainly consisted of a lithographic procedure, during which a photoresist pattern is produced on the masked sample surface by exposure to a UV source. The UV lithographic procedure is then followed by different post processing phases, to complete the different patterning techniques.

Firstly, in a chemical lift-off experiment, the photoresist patterning, using a negative photoresist (ma-N 1420), was done prior to deposition of the aluminium thin film. The photoresist layer was spin-coated onto the clean SiO_2 substrates at 5000 rpm for 30 seconds, to produce a resist thickness of ≈ 2 μm. After performing the UV exposure and development, the masked structures remained as trench-like features in the resist material. This was then followed by the Al film deposition and the lift-off procedure was subsequently accomplished by placing the sample in acetone for 24 hours at room temperature.

Fig. 6.5 illustrates an AFM image and the cross-section line view of the patterned Al structures obtained using the chemical lift-off procedure. From the results in Fig. 6.5, the presence of a non-uniform structure surface with spiky edges can be observed. This is attributed to the sharp discontinuities that exist at resist edges, causing an "avalanche effect" during the thermal evaporation process, thus dumping excess deposited material into the patterned resist features.

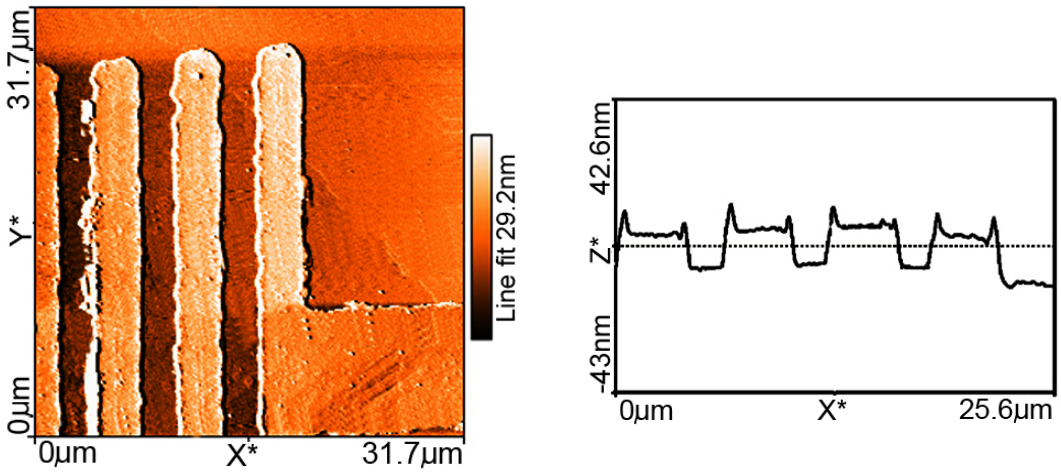

a) b)

Figure 6.5: AFM surface scan and cross-section line view of an aluminium electrode structure (thickness $\approx$ 15 nm) fabricated with a chemical lift-off procedure.

The second aluminium patterning procedure consisted of a dry-etch technique, which was performed with an accelerated argon ion mill. Prior to the milling process, a 2 μm patterned resist mask was generated on-top of the deposited Al thin films, by the same spin-coating and UV lithography techniques.

The samples were also subjected to a hard-bake procedure at 115°C for 10 minutes to cure the photoresist, thus strengthening the resist material and improving its masking ability. Etching of the sample was subsequently performed in the ion mill for 45 minutes at 15 minute intervals. For an approximately 2 nm/min etch rate, the samples were tilted at a 30° angle and placed in the center of the ion beam, which was produced by accelerating the Ar^+-ions through a 1.5 kV/cm electric field. The Ar^+-ions were generated by a high-voltage RF plasma at a system pressure of 3×10^{-6} Pa. The final step in the dry-etch procedure was to ultrasonically rinse the samples in acetone, in order to remove residual resist materials.

Fig. 6.6 depicts the results obtained using the dry-etch technique to generate ultra thin aluminium structures.

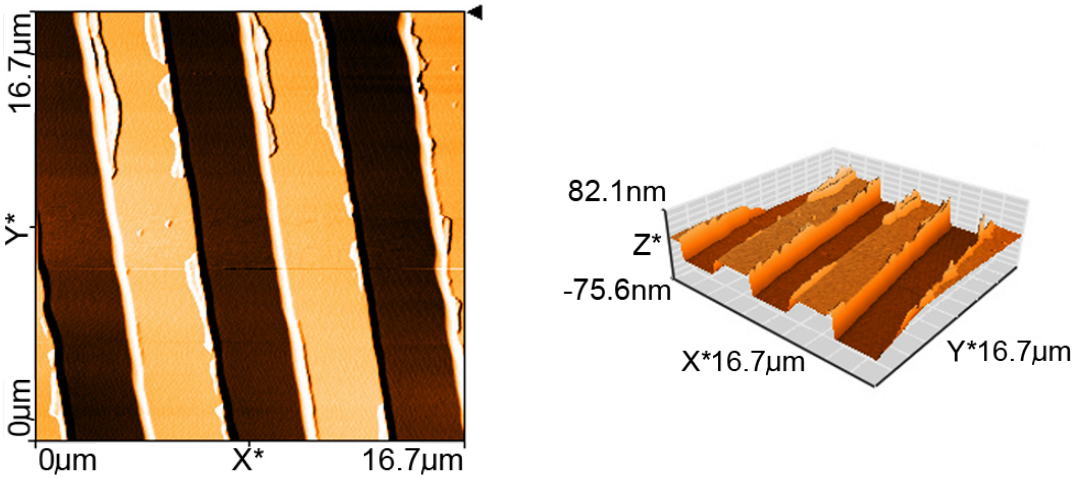

a) b)

Figure 6.6: AFM images of an aluminium electrode structure (thickness ≈ 60nm) fabricated with the dry-etch procedure. a) AFM surface scan. b) A 3D topography illustration.

From the AFM images (Fig. 6.6), it is eminent that the structures produced by the dry-etch technique, is not favourable for the fabrication of exceptionally thin aluminium structures. The notable impurities (residual resist material) and structure deformation can be ascribed to excessive energy that is transferred from the accelerated argon ions during the etch procedure, causing the resist material to fuse onto the underlying aluminium film. These defects are foreseen to adversely affect the efficiency of further processing, especially when integrating nanomaterials such as carbon nanotubes (CNTs) or graphene for nanodevice fabrication.

Finally, after investigating the wet-etching capabilities of strong basic compounds (pH ≈ 13-14) on aluminium, a unique method for fabricating ultra thin aluminium structures was derived. Utilizing a chemical wet-etching procedure does not require high energy ion milling, thus reducing the process time and complexity. Furthermore, a chemical wet-etch procedure can be better controlled to reduce contamination of the samples.

An effective aluminium patterning procedure was thus formulated, by using a negative photoresist and associated developer (ma-N1420 and ma-D533S) to generate

resist patterns on the deposited aluminium thin films. Furthermore, the resist material was spin-coated onto the samples at 9000 rpm for 12 seconds. Although the resulting resist layer was slightly thinner, it was found that the faster rotational speed and reduced time, resulted in a more homogeneous film and reduced edge build-up. This in turn provides a better pattern resolution during the UV exposure process, due to a lower level of diffraction. The resist patterning was performed with the same UV lithographic mask aligner (shown in Fig. 6.7), as for the previous methods.

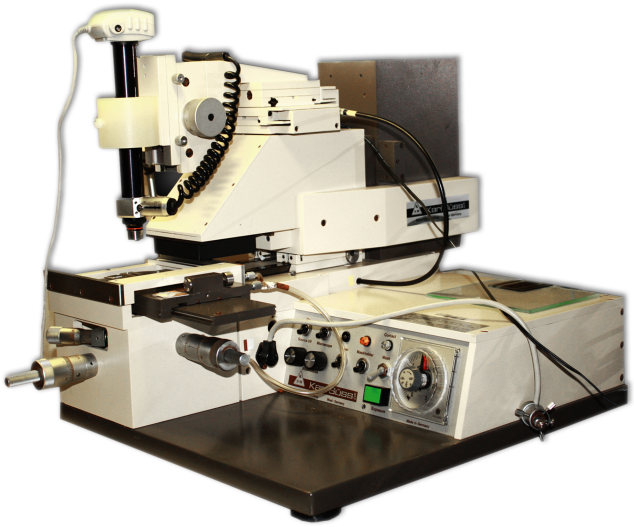

Figure 6.7: The UV lithographic mask aligner (Karl Süss Instruments).

The patterned photoresist samples were then hard-baked at 115°C for 15 minutes. Subsequently, another positive resist developing compound (Microposit MF319) with pH $\approx$ 14 was used to chemically etch the samples. The effective wet-etching procedure for the fabrication of ultra thin aluminium microstructures, developed during this research, is illustrated by the diagram in Fig. 6.8.

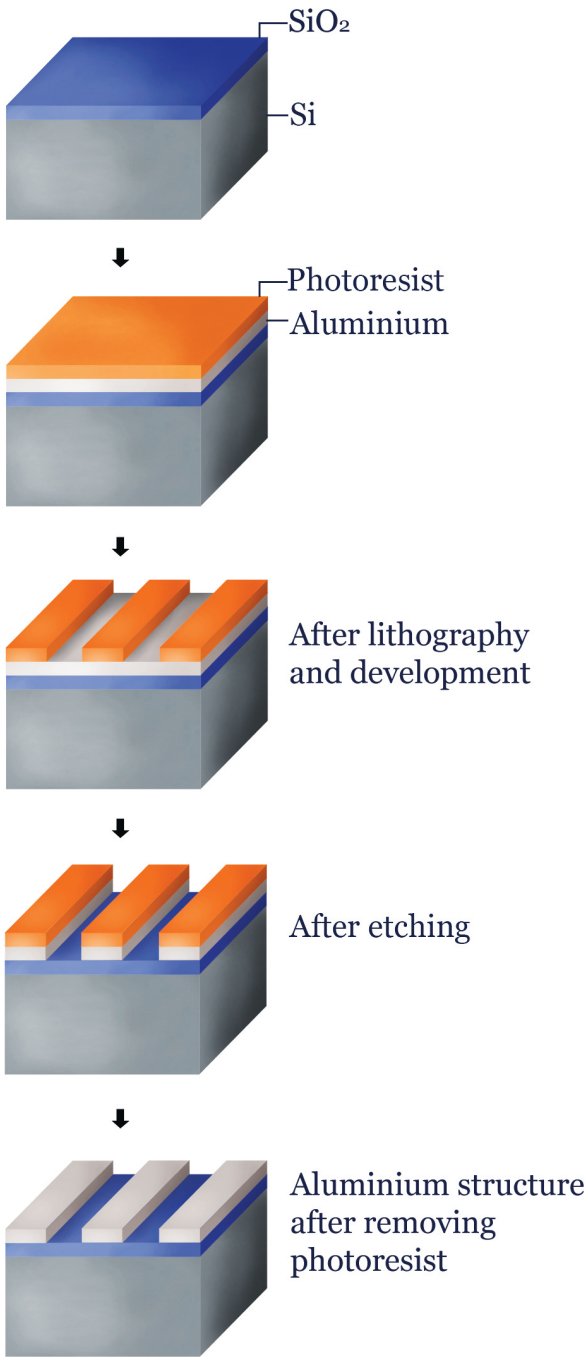

Figure 6.8: A diagrammatic illustration of the unique and effective wet-etch procedure for the fabrication of ultra thin aluminium microstructures, which was developed during this research.

Fig. 6.9 shows optical micrographs of the patterned photoresist layers, which were obtained after completing the lithography and photoresist development procedures.

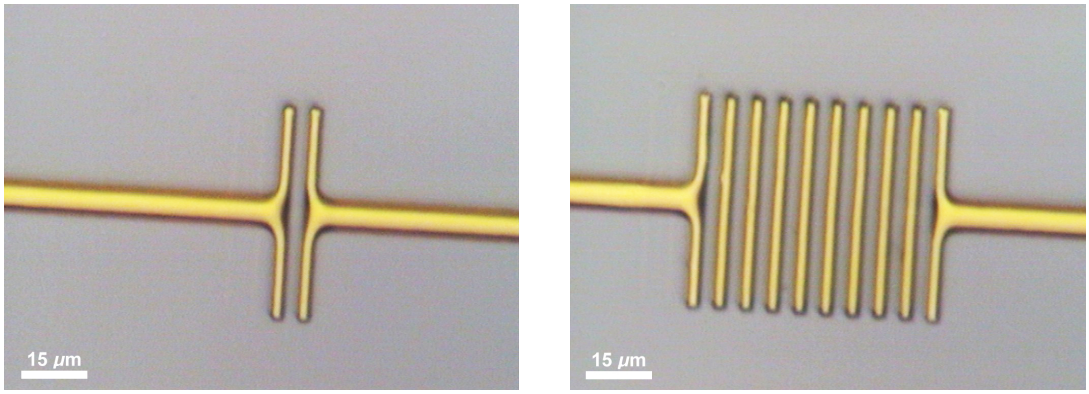

Figure 6.9: Optical micrographs of photoresist patterns on an aluminium film.

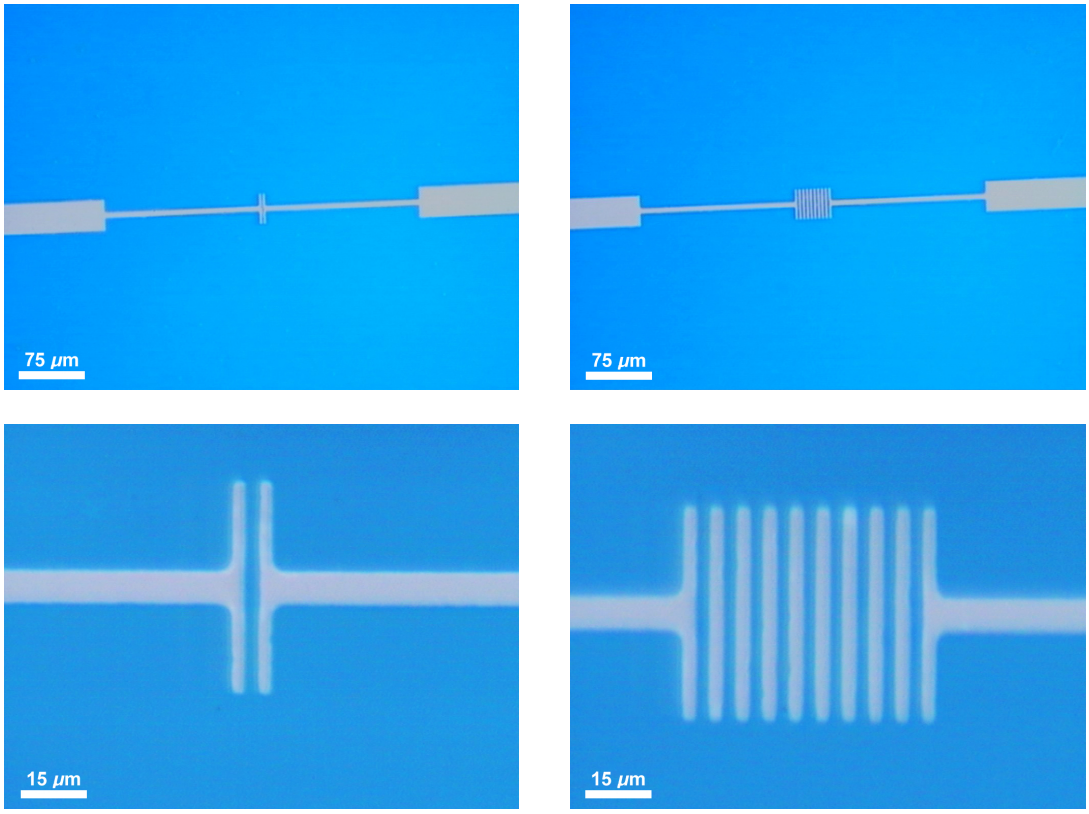

Figure 6.10: Optical micrographs of Al structures (thickness $\approx$ 60 nm) on SiO_2 substrates, fabricated by the unique wet-etch technique.

The resulting Al structures are shown in the optical micrographs in Fig. 6.10, which presents the ≈ 300 nm SiO_2 layer beneath the aluminium as a bright blue background.

Accordingly, an AFM analysis of the generated 60 nm thick aluminium microstructures, produced by the wet-etching process, is presented in Fig. 6.11 (a) to (c). From these figures it is observed, that the latter fabrication technique yielded structures that are well-defined, with a flat topography and presents extremely low levels of contamination or residual resist material.

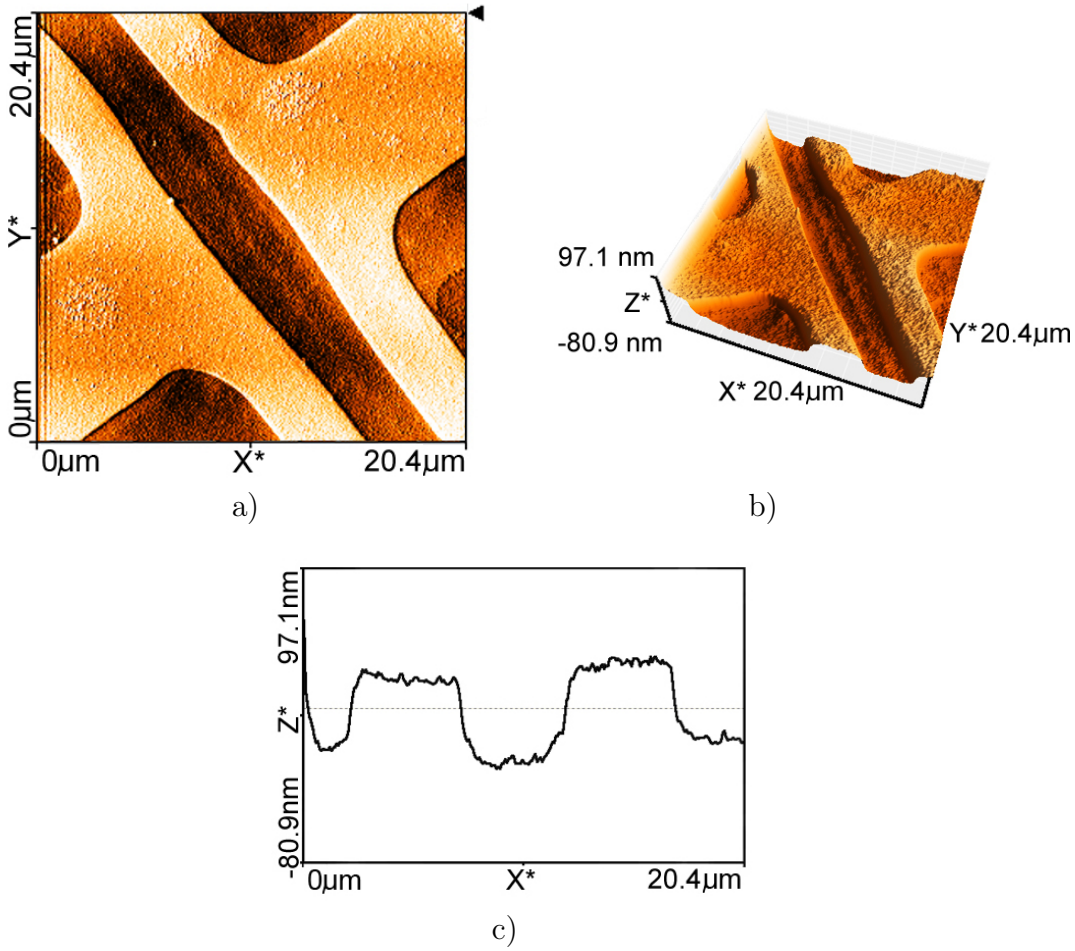

Figure 6.11: AFM analysis of an aluminium microstructure (thickness ≈ 60 nm), fabricated by an effective wet-etch technique. a) AFM surface scan. b) A three-dimensional (3D) topography illustration. c) Cross-section line view.

6.4 An integrated MWCNT-Al microstructure gas sensor

After completing the preceding investigation into the fabrication of patterned aluminium thin film electrodes, an experiment was performed to attempt the integration of multi-walled carbon nanotubes (MWCNT) with the produced 60 nm Al grid structures. A similar gas sensor topology was proposed by Li et al. [84], who demonstrated the gas (i.e. NO_2) sensing abilities of random SWCNT-networks, which were casted onto gold interdigitated electrodes.

By implementing the unique Al patterning procedure, which was developed during this research and described in the previous section, 60 nm thick aluminium electrode structures were produced with typical electrode spacings of 4 - 10 μm. An AFM image of such a single-space electrode was provided in Fig. 6.11. The features of these "grid-type" electrode structures are proposed to allow the integration of CNTs in a defined area, with a small enough electrode spacing to accommodate individual-length nanotubes. The active elements of the sensor are thus also confined to the grid area, which could possibly yield faster recovery rates, if a current is applied to induce self-heating of the nanotube structures. In turn, this would then exclude the need for an external heating device to achieve sensor recovery.

The MWCNT integration was subsequently performed, by spray-coating 2 - 3 layers of a MWCNT solution onto the entire substrate surface. The MWCNT solution was prepared by ultrasonically dispersing a MWCNT-COOH compound ($\approx$ 0.1 wt%) in a Propan - 2 - ol solvent. The latter procedure was fully described in Section 5.1.

The MWCNT coated samples were then annealed at 560°C for 1 hour, in a N_2 environment, to fuse the MWCNTs into the aluminium features. The high annealing temperature is foreseen to destroy all -COOH groups attached to the CNTs, which will cause only the MWCNTs to remain in tact.

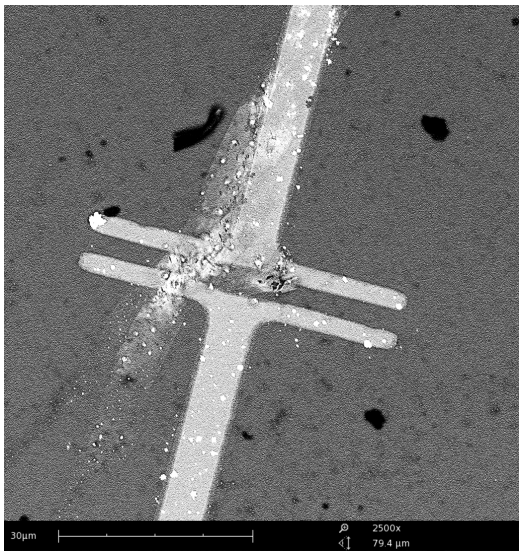

a) 2500x

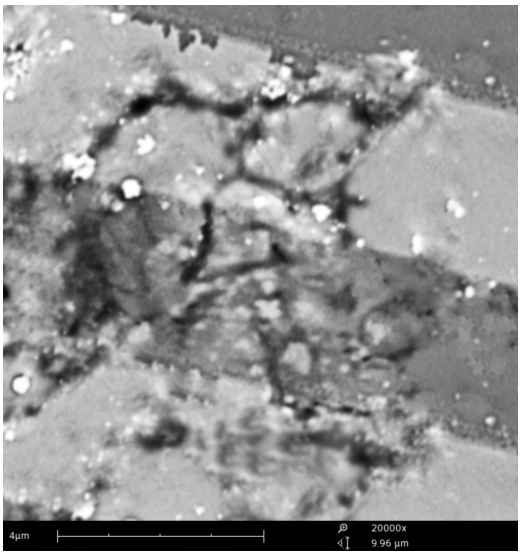

b) 20 000x

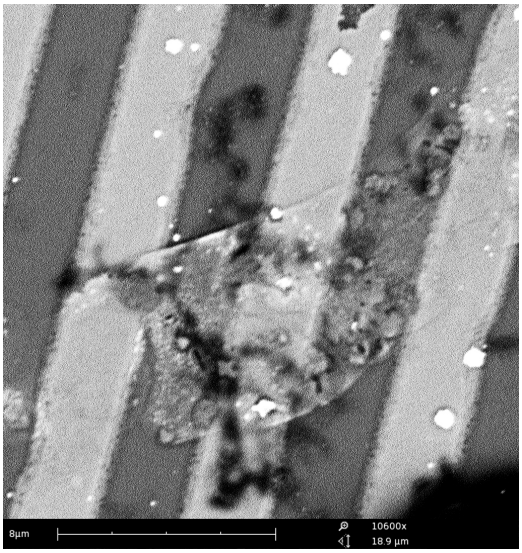

c) 10 600x

Figure 6.12: SEM images of a single-grid integrated MWCNT-Al structure at a) 2500x, b) 20 000x magnification, and c) a SEM image of a multi-grid MWCNT-AL structure at 10 600x magnification..

Presented in Fig. 6.12, are SEM images of the resulting MWCNT-Al structures, that were generated by the above-mentioned technique. Fig. 6.12 a) and b) shows a single-grid electrode structure (i.e. two electrodes separated by a single space) at 2500x and 20 000x magnification, respectively. Fig. 6.12 c) presents a multi-grid structure at 10 600x magnification, with the MWCNT material ran-

domly scattered on the surface. The SEM results demonstrated that the spray-coating technique is a simple method to produce integrated nanomaterial features, however it is evident that this is not a 100% reproducible process, which will limit the application thereof in a large scale fabrication setup.

Following the MWCNT-Al structure fabrication, the 10 x 10 mm samples were fixed onto 25 x 25 mm alumina (Al_2O_3) substrates, and contact wires were added to the structure's pads with a silver conductive paint. A photograph of the MWCNT-Al sensor device is shown in Fig. 6.13.

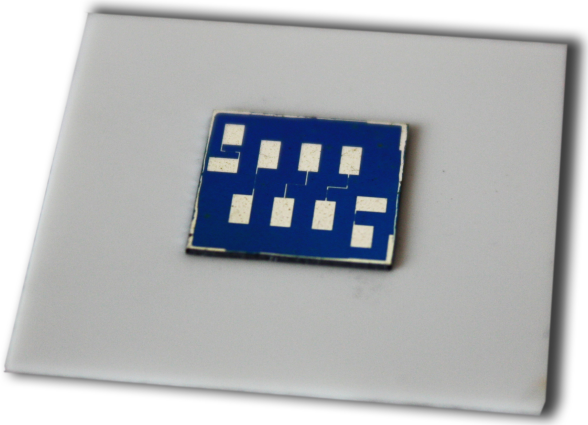

Figure 6.13: Photograph of an integrated MWCNT-Al device.

The MWCNT-Al device was subsequently placed in the test chamber and exposed to acetylene (C_2H_2) and a mixture of argon and hydrogen ($Ar - {}_{30\%}H_2$) gas. The gas tests were performed by flowing the gases at 100 sccm increments (i.e. from 0 - 400 sccm) for 3 minute intervals through the chamber, with the substrate temperature at 100°C. The increased substrate temperature was employed after the initial gas flow tests at room temperature, produced no measurable results.

The MWCNT-Al sensor's response (i.e. change in resistance) towards the C_2H_2 and $Ar - {}_{30\%}H_2$ exposure at 100°C, is illustrated by the graph in Fig. 6.14. Due to the limited electrical connectivity of the other samples, the single-grid feature (Fig. 6.12 a) was utilized for the MWCNT-Al device tests.

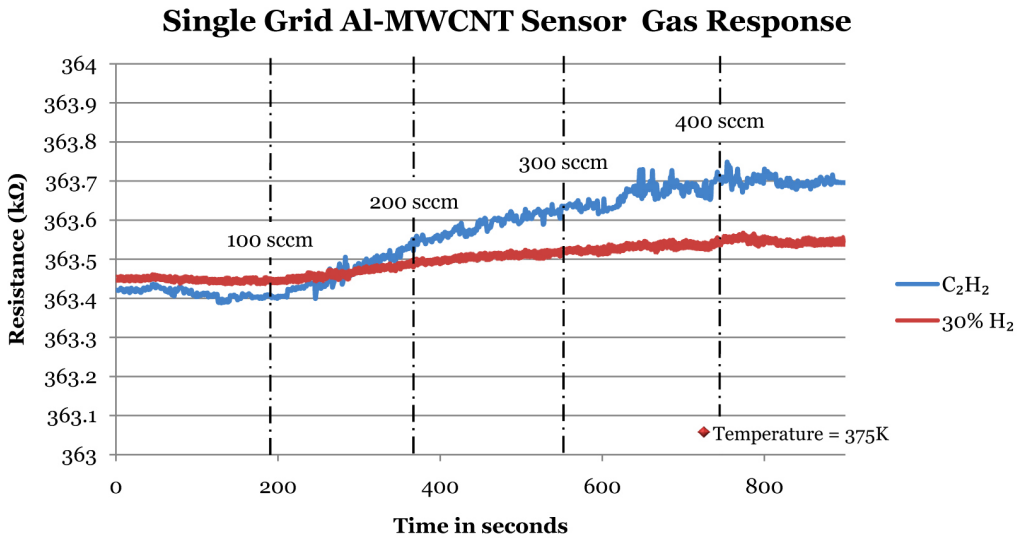

Figure 6.14: MWCNT-Al sensor gas response (T = 375 K).

From the results depicted in Fig. 6.14, a very small change ($\approx 0.1\%$) in resistance was observed for exposure to C_2H_2, with $Ar\text{-}_{30\%}H_2$ producing $\approx 0.04\%$ increase in resistance. These small responses can be attributed to various reasons, which include the very high initial resistance value (≈ 360 kΩ) and the tiny amount of nanotube material (which essentially forms the active elements of the sensory device). The high initial resistance value, is mainly caused by the electrode geometry, whereby the extremely thin and long electrode structures produce a large series resistance. In addition, due to the small effective connection area (i.e. the area where contact wires can be added), contact resistances are most likely introduced, which further increases the measured resistance value.

It is therefore advised that future electrode structures are designed to minimize these secondary resistance effects and that the implementation of a direct integration process, which incorporates catalyst patterning techniques, should be investigated. Furthermore, the construction of CNT-based field effect transistor (FET) sensors have demonstrated enhanced sensitivities towards gas detection [85], [86]. If utilized in conjunction with a catalyst patterning process, the effective aluminium patterning technique presented in this chapter is foreseen to simplify the future fabrication of such FET-based sensors.

6.5 Conclusions

This chapter presented an in-depth study of the resistivity of aluminium thin films for the utilization in nanodevices. The oxidation of silicon in a H_2O and O_2 environment at 1100°C, to form electrically isolated SiO_2/Si wafers, was also described.

Additionally, an investigation into the fabrication of ultra thin patterned aluminium microstructures was presented and an effective wet-etching procedure was developed, which yielded superior results. It is also worth noting that with this procedure, the ability to efficiently produce aluminium microstructures for film thicknesses ranging from approximately 10 - 250 nm, was acquired.

Lastly, an integrated MWCNT-Al sensor was developed and tested. Although the sensor demonstrated a very small response towards the detection of C_2H_2, and H_2, it was found that the electrode topology greatly influences the device's static resistance. The fabrication of CNT-based FET sensors for gas detection was subsequently advised and the implementation of the presented aluminium patterning technique, is foreseen to simplify the realization of such FET-based devices.

Chapter 7

Conclusions

The work performed during this research entailed the characterization and implementation of carbon-based nanomaterials, like graphene and carbon nanotubes, in the field of gas sensing applications and devices. The unique mechanical and electrical properties of these materials, which arise from their large surface-to-volume ratios and their unparalleled physical and chemical properties, have indeed pledged a revolutionary change in sensory and other electronic applications.

The synthesis of these carbon nanomaterials unfortunately remains quite a complex procedure, with numerous system parameters to be controlled. The effects of growth enhancers in the "super growth" of CNTs and the general improvement of the growth environment, has provided a certain degree of control in the fabrication of carbon-based nanomaterials. It is advised that these procedures be further explored, to ultimately generate a controlled and efficient process for the large-scale synthesis of carbon nanostructures.

The purification of carbon nanotubes in particular, as discussed in Chapter 3, is also an intricate process with various side effects, which include the destruction and chemical alteration of the CNTs. Furthermore, it has been found that pure and pristine carbon nanomaterials, more than often behave like graphite at room temperatures, thus yielding minimal gas absorption characteristics. From the results obtained for the fabricated pure carbon nanomaterial film sensors, it was observed that changes in relative humidity and flow rate of the gases had a negligible effect on the device's response, when measuring film resistances.

The gas sensing properties of functionalized carbon nanomaterials were also investigated during this research. This was mainly directed towards composite nanomaterials with either carboxyl functional groups, indium tin oxide (ITO) nanoparticles or zinc oxide (ZnO) nanowires. These additional features may serve as supplementary sensing elements, which exhibit advanced chemical recognition properties. The fundamental carbon nanomaterials (i.e. CNTs and graphene), thus form the carrier substances, which respond to molecular stimulation around these functional sites. It is however advised, that the issues regarding the molecular interactions between the nanostructures and gas molecules be explored further, to gain a deeper understanding of the functioning of nano-sized gas sensors.

From an experimental point of view, this research demonstrated that a carboxyl-functionalized MWCNT film sensor, produced the highest sensitivity towards the detection of acetylene (C_2H_2) gas at room temperature. Unfortunately, it was found that increased substrate temperatures had adverse effects on these sensors, whereby the attached organic functional groups are decomposed, which reduces device sensitivity.

An investigation into non-volatile or "solid-state" functionalized carbon nanosensors was also performed. This demonstrated the "doping" of carbon nanomaterials by ITO (MWCNTs) and ZnO (graphene), which produced inverse but enhanced recovery responses towards the detection of gaseous substances. These functionalized nanomaterials also demonstrated detection capabilities at room temperature, with enhanced sensitivities at higher operating temperatures. As mentioned earlier, the energy efficiency of these nanodevices are drastically reduced when operating at increased temperatures. The functionalization of carbon nanomaterials is therefore considered a necessity for gas detection at room temperature and functionalization techniques should be further explored.

Additional UV- vis -NIR tests, that were performed on the ITO- composite nanomaterials, indicated that graphene and CNTs could produce interesting and superior characteristics for opto-electronic applications. Although not specifically applicable to gas sensors, these results may lead to the development of new solar-cell technologies and transparent conductor applications.

For the fabrication of both the pure and functionalized nanomaterial thin film sensors, the utilized nanomaterials (in pure form) were obtained from two suppliers. Due to certain time constraints in the project and the rather long delay period for acquiring analysis results from external institutions, the nanomaterials (i.e. CNTs and graphene), synthesized via the floating catalyst CVD process, were not specifically implemented in sensory devices.

During this work, a unique and effective method to fabricate ultra thin aluminium microstructures was developed, which was presented in Chapter 6. These microstructures provide a favourable environment for the integration of carbon nanomaterials, in order to generate gas sensor devices. It is advised that the procedures utilized to perform the nanomaterial integration be refined and that direct integration techniques like chemical vapour deposition (CVD), be considered to reduce secondary resistivity effects. The presented aluminium pattering procedure is also foreseen to be useful in fabricating carbon-based field-effect transistor (FET) devices, which may produce an enhanced sensitivity and selectivity for gas detection and identification. As previously stated, the aluminium microstructure patterning process, was published in the journal "*Thin Solid Films*".

Although nanomaterials like graphene and carbon nanotubes have shown abundant potential for utilization in nanostructured gas sensors, several challenges are still to be conquered before large-scale or industrial fabrication of such nanodevices can be realized. This includes finding ways to effectively reduce the recovery times of nanomaterial sensors and realizing procedures that provide reproducible and invariable results. Furthermore, the economical restraints and the lack of public confidence in this revolutionary field of science and technology, is also limiting the implementation of nanostructures in a wide range of applications.

In concluding this research, it is believed that the future generations to come, will inevitably strive towards excelled performance in technological features and that the accomplishment thereof will coincide with the successful development of nanotechnology and nanoscience.

Bibliography

[1] C. Buzea, I. Pacheco, K. Robbie: Nanomaterials and Nanoparticles: Sources and Toxicity. Biointerprises 2: MR17, 2007.

[2] B. Rodgers, S. Pennathur, J. Adams: Nanotechnology: Understanding Small Systems. Mechanical Engineering Series, Vol. 29. CRC Press, Taylor & Francis Group, 2008. ISBN: 0-8493-8207-6.

[3] M. Ratner, D. Ratner: Nanotechnology: A Gentle Introduction to the Next Big Idea. Prentice Hall, PTR, 2003. ISBN: 0-13-101400-5.

[4] M. Köhler, W. Fritsche: Nanotechnology: An Introduction to Nanostructure Techniques. 2nd Edn. Wiley-VCH, 2007. ISBN: 978-3-527-311871-1.

[5] B. Breton: The Early History and Development of the Scanning Electron Microscope. [Online]. Available: http://www2.eng.cam.ac.uk/~bcb/history.htm.

[6] A. Nouailhat: An Introduction to Nanoscience and Nanotechnology. Wiley, 2008. ISBN: 978-1-84821-007-3.

[7] "Scanning Electron Microscope". [Online]. Available: http://en.wikipedia.org/ wiki/Scanning_electron_microscope.

[8] C. Hierold: Carbon Nanotube Devices: Properties, Modeling, Integration and Applications. Advanced Micro & Nanosystems, Vol. 8. Wiley-VCH, 2008. ISBN: 978-3-527-31720-2.

[9] N. Savage, M. Diallo, J. Duncan: Nanotechnology Applications for Clean Water. Norwich, NY. William Andrew Publishing, 2008.

[10] The Project on Emerging Nanotechnologies. [Online]. Available: http://www.nanotechproject.org/inventories/consumer/analysis_draft.

[11] Nanotechnology Information Center, American Elements. [Online]. Available: http://www.americanelements.com/nanotech.htm.

[12] "Atomic Force Microscope". [Online]. Available: http://comp.uark.edu~jchakakafm-draw-1-c-1.jpg1.

[13] "Buckminsterfullerene". [Online]. Available: http://www.asu.edu/clas/csss/NUE/img/Gallery/Buckyball.jpg.

[14] "Single-Walled Carbon Nanotube". [Online]. Available: http://www.biomedme.com/wp-content/uploads/2010/01/single-walled-carbon-nanotubes2.jpg.

[15] A. Busnaina: Nanomanufacturing Handbook. Northeast University, Boston, USA. CRC Press, Taylor & Francis Group, 2007. ISBN: 0-8493-3326-1.

[16] L. Zhang, X. Fang, C. Ye: Controlled Growth of Nanomaterials. Chinese Academy of Sciences, China. World Scientific, 2007. ISBN: 10 981-256-728-3.

[17] P. Poncharal, Z.L. Wang, D. Ugarte, W.A. de Heer: Electrostatic Deflections and Electromechanical Resonances of Carbon Nanotubes. Science (p.283), 1999. [Online]. Available: http://www.sciencemag.org/cgi/reprint/283/5407/1513.pdf.

[18] H. Seunghun, S. Myung: Nanotube Electronics: A Flexible Approach to Mobility. Nature Nanotechnology (2), 2007. [Online]. Available: http://www.nature.com/nnano/journal/2/n4/abs/nnano.2007.89.html.

[19] "Graphene and Carbon Nanotubes". [Online]. Available: http://en.wikipedia.org/wiki/File:Allotropes_of_Carbon.png.

[20] "Carbon Nanotubes". [Online]. Available: http://www.robaid.com/tech/nanotechnologies-carbon-nanotubes.htm.

[21] K.S. Novoselov, A.K. Geim, J.V. Morozov, D. Jiang, Y. Zhang, S.V. Dubonos, I.V. Grigorieva, A.A. Firsov: Electric Field Effect in Atomically Thin Carbon Films. Science, Vol. 306 (p.666), 2004.

[22] A.K. Geim, K.S. Novoselov: The Rise of Graphene. Nature Materials, Vol. 6 (p.183-191), 2007.

[23] K.V. Emtsev, A. Bostwick, K. Horn, J. Jobst, G.L. Kellog, L. Ley, J.L. McChesney, T. Ohta, S.A. Reshonov, J. Rhrl, E. Rotenberg, A.K. Schmid, D. Waldmann, H.B. Weber, T. Seyller: Towards Wafer-size Graphene Layers by Atmospheric Pressure Graphitization of Silicon Carbide. Nature Materials, Vol. 8 (p.203), 2009.

[24] K.S. Kim, Y. Zhao, H. Jang, S.Y. Lee, J.M. Kim, K.S. Kim, J. Ahn, P. Kim, J. Choi, B.H. Hong: Large-scale Pattern Growth of Graphene Films for Stretchable Transparent Electrodes. Nature, Vol. 457 (p.706), 2009.

[25] H.C. Schiepp, J. Li, M.J. McAllister, H. Sai, M. Herrera, D.H. Adamson, R.K. Prud'homme, R. Car, D.A. Saville, I.A. Aksay: Functionalized Single Graphene Sheets Derived from Splitting Graphite Oxide. J. Phys. Chem. B, Vol. 110 (p.8385), 2006.

[26] C. Lee, X. Wei, J.W. Kysar, J. Hone: Measurement of the Elastic Properties and Intrinsic Strength of Monolayer Graphene. Science, Vol. 321 (p.385), 2008.

[27] A.A. Balandin, S. Ghosh, W. Bao, I. Calizo, D. Teweldebrhan, F. Miao, C.N. Lau: Superior Thermal Conductivity of Single-layer Graphene. Nano Letters, Vol. 8 (p.902), 2008.

[28] C. Soldano, A. Mahmood, E. Dujardin: Production, Properties and Potential of Graphene. Carbon, Vol. 24 (p.2127), 2010.

[29] K. Bullis: TR10: Graphene Transistors. [Online]. Available: http://www.technologyreview.com/read_article.aspx?ch=specialsections&sc.emerging08&id=20242.

[30] X. Whang, L. Zhi, K. Mullen: Transparent, Conductive Graphene Electrodes for Dye-Sensitized Solar Cells. Nano Letters, Vol. 8 (p.323), 2008.

[31] F. Schedin, A.K. Geim, S.V. Morozov, E.W. Hill, P. Blake, M.I. Katnelson, K.S. Novoselov: Detection of Individual Gas Molecules Adsorbed on Graphene. Nature Materials, Vol. 6 (p.652), 2007.

[32] M. Terrones, A.R. Botello, J. Campos, F. Lopez, Y.I. Vega, F.J. Rodriguez, A.L. Elias, E. Munoz, A.G. Cano, J.C. Charlier, H. Terrones: Graphene and Graphite Nanoribbons: Morphology, Properties, Synthesis, Defects and Applications. Nano Today, Vol. 5 (p.351-372), 2010.

[33] M.J. Yacaman, M.M. Yoshida: Catalytic Growth of Carbon Microtubes with Fullerene Structures. Appl. Phys. Letters, Vol. 63, 1993.

[34] M. Endo: The Production and Structure of Pyrolytic Carbon Nanotubes. J. Phys. Chem. Sol., Vol. 54, 1993.

[35] M.J. Bronikowski, P.A. Willis, D.T. Colbert, K.A. Smith, R.E. Smalley: Gas Phase Production of Carbon Single-Walled Nanotubes from Carbon Monoxide via the HiPco process: A Parametric Study. J. Vac. Sci. Technol. A, Vol. 19, 2001.

[36] C. Xu, E. Flahaut, S.R. Bailey, G. Brown, J. Sloan, K.S. Coleman, V.C. Williams, M.L.H. Green: Purification of Single-Walled Carbon Nanotubes Grown by a Chemical Vapour Deposition (CVD) Method. Chemical Research in Chinese Universities, Vol. 2 (p.130), 2002.

[37] M.E. Roberts, M.C. LeMieux, Z. Bao: Sorted and Aligned Single-Walled Carbon Nanotube Networks for Transistor-Based Aqueous Chemical Sensors. ACSNano, Vol. 3 (p.3287), 2009.

[38] B.Q. Wei, R. Vajtai, Y. Jung, J. Ward, R. Zhang, G. Ramanath, P.M. Ajayan: Assembly of Highly Organized Carbon Nanotube Architectures by Chemical Vapour Deposition. Chemical Materials, Vol. 15 (p.1598), 2003.

[39] P.B. Amama, C.L. Pint, L. McJilton, S.M. Kim, E.A. Stach, P.T. Murray, R.H. Hauge, B. Maruyama: Role of Water in Super Growth of Single-Walled Carbon Nanotube Carpets. Nano Letters, Vol. 9 (p.44), 2009.

[40] K. Hata, D.N. Futaba, K. Mizuno, T. Namai, M. Yumura, S. Iijima: Water-Assisted Highly Efficient Synthesis of Impurity-Free Single-Walled Carbon Nanotubes. Science, Vol. 306 (p.1362), 2004.

[41] D.N. Futaba, J. Goto, S. Yasuda, T. Yamada, M. Yumura, K. Hata: General Rules Governing the Highly Efficient Growth of Carbon Nanotubes. Advanced Materials, Vol. 21 (p.4811), 2009.

[42] P.X. Hou, C. Liu, H.M. Cheng: Purification on Carbon Nanotubes. Carbon, Vol. 46 (p.2003-2025), 2008.

[43] H.P. Chang, A.J. Bord: Scanning Tunneling Microscopy Studies of Carbon Oxygen Reactions on Highly Oriented Pyrolytic-Graphite. J. Am. Chem. Soc., Vol. 113 (p.5588), 1991.

[44] S. Banerjee, T. Hemraj, S.S. Wong: Covalent Surface Chemistry of Single-Walled Carbon Nanotubes. Advanced Materials, Vol. 17 (p.17), 2005.

[45] Y.S. Park, Y.C. Choi, K.S. Kim, D.C. Chung, D.J. Bae, K.H. An: High Yield Purification of Multi-Walled Carbon Nanotubes by Selective Oxidation During Thermal Annealing. Carbon, Vol. 39 (p.655), 2001.

[46] Y.J. Chen, M.L.H. Green, J.L. Griffin, J. Hammer, R.M. Lago, S.C. Tsang: Purification and Opening of Carbon Nanotubes via Bromination. Advanced Materials, Vol. 8 (p.1012), 1996.

[47] I.W. Chiang, B.E. Brinson, R.E. Smalley, J.L. Margrave, R.H. Hauge: Purification and Characterization of Single-Walled Carbon Nanotubes. J. Phys. Chem. B, Vol. 105 (p.1157), 2001.

[48] E. Dujardin, T.W. Ebbesen, A. Krishnan, M.M.J. Treacy: Purification of Single-Shell Nanotubes. Advanced Materials, Vol. 10 (p.611), 1998.

[49] Y.H. Wang, H.W. Shan, R.H. Hauge, M. Pasquali, R.E. Smalley: A Highly Selective, One-Pot Purification Method for Single-Walled Carbon Nanotubes. J. Phys. Chem. B, Vol. 111 (p.1249), 2007.

[50] J.G. Wiltshire, A.N. Khlobystov, L.J. Li, S.G. Lyapin, G.A.D. Briggs, R.J. Nicholas: Comparative Studies on Acid and Thermal Based Selective Purification of HiPco Produced Single-Walled Carbon Nanotubes. Chem. Phys. Lett., Vol. 386 (p.239), 2004.

[51] C.M. Chen, M. Chen, Y.W. Peng, H.W. Yu, C.F. Chen: High Efficiency Microwave Digestion Purification of Multi-Walled Carbon Nanotubes Synthesized by Thermal Chemical Vapour Deposition. Thin Solid Films, Vol. 498 (p.202), 2006.

[52] F.H. Ko, C.Y. Lee, C.J. Ko, T.C. Chu: Purification of Multi-Walled Carbon Nanotubes Through Miggtffgcrowave Heating of Nitric Acid in a Closed Vessel. Carbon, Vol. 43 (p.727), 2005.

[53] J.M. Bonard, T. Stora, J.P. Salvetat, F. Maier, T. Stockli, C. Duschl: Purification and Size-Selection of Carbon Nanotubes. Advanced Materials, Vol. 9 (p.827), 1997.

[54] A.P. Yu, E. Bekyarova, M.E. Itkis, D. Fakhrutdinov, R. Webster, R.C. Haddon: Application on Centrifugation to the Large-Scale Purification of Electric Arc-Produced Single-Walled Carbon Nanotubes. J. Am. Chem. Soc., Vol. 128 (p.9902), 2006.

[55] R. Andrews, D. Jacques, D. Qian, E.C. Dickey: Purification and Structural Annealing of Multi-Walled Carbon Nanotubes at Graphitization Temperatures. Carbon, Vol. 39 (p.1681), 2001.

[56] Y.A. Kim, T. Hayashi, K.Osawa, M.S. Dresselhaus, M. Endo: Annealing Effects on Disordered Multi-Walled Carbon Nanotubes. Chem. Phys. Lett., Vol. 380 (p.319), 2003.

[57] K. Tohji, H. Takahashi, Y. Shinoda, N. Shimizu, B. Jeyadevan, I. Matsuoka: Purification Procedure for Single-Walled Carbon Nanotubes. J. Phys. Chem. B, Vol. 101 (p.1974), 1997.

[58] S. Bandow, A.M. Rao, K.A. Williams, A. Thess, R.E. Smalley, P.C. Eklund: Purification of Single-Walled Carbon Nanotubes by Microfiltration. J. Phys. Chem. B, Vol. 101 (p.8839), 1997.

[59] Y. Wang, L. Gao, J. Sun, Y.Q. Liu, S. Zheng, H. Kajiura: An Integrated Route for Purification, Cutting and Dispersion of Single-Walled Carbon Nanotubes. Chem. Phys. Lett., Vol. 432 (p.205), 2006.

[60] H. Zhang, C.H. Sun, F. Li, H.X. Li, H.M. Cheng: Purification of Multi-Walled Carbon Nanotubes by Annealing and Extraction Based on the Difference in Van der Waals Potentials. J. Phys. Chem. B, Vol. 110 (p.9477), 2006.

[61] D.R. Kauffman, D.C. Sorescu, D.P. Schofield, B.L. Allen, K.D. Jordan, A. Star: Understanding the Sensor Response of Metal-Decorated Carbon Nanotubes. Nano Letters, Vol. 10 (p.958), 2010.

[62] X. Wang, Z. Zhao, J. Qu, Z. Wang, J. Qiu: Fabrication and Characterization of Magnetic Fe_3O_4-CNT Composites. J. Phys. Chem. Solids, Vol. 10 (p.1016), 2010.

[63] C. Bittencourt, A. Felten, J. Ghijsen, J.J. Pireaux, W. Drube, R. Erni, G. Van Tendeloo: Decorating Carbon Nanotubes with Nickel Nanoaprticles. Chem. Phys. Lett., Vol. 436 (p.368-372), 2007.

[64] Z. Zhou, L. Ci, L. Song, X. Yan, D. Liu, H. Yuan, Y. Gao, J. Wang, L. Liu, W. Zhou, G. Wang, S. Xie: Random Networks of Single-Walled Carbon Nanotubes. J. Phys. Chem. B, Vol. 108 (p.10751), 2004.

[65] S. Xie, L. Song, L. Ci, Z. Zhou, X. Dou, W. Zhou, G. Wang, L. Sun: Controllable Preparation and Properties of Single-/Double-Walled Carbon Nanotubes. Science and Technology of Advanced Materials, Vol. 6 (p.725), 2005.

[66] X. Wang, Q. Li, J. Xie, Z. Jin, Y. Li, K. Jiang, S. Fan: Fabrication of Ultralong and Electrically Uniform Single-Walled Carbon Nanotubes on Clean Substrates. Nano Letters, Vol. 9 (p.3137), 2009.

[67] M.S. Dresselhaus, G. Dresselhaus, R. Saito, A. Jorio: Raman Spectroscopy of Carbon Nanotubes. Physics Reports, Vol. 409 (p.47), 2005.

[68] S. Costa, E. Borowiak-Palen, M. Kruszynska, A. Bachmatiuk, R.J. Kalenczuk: Characterization of Carbon Nanotubes by Raman Spectroscopy. Material Science, Vol. 26 (p.433), 2008.

[69] L.J. Van der Pauw: A Method of Measuring Specific Resistivity and Hall Effects of Disks and Arbitrary Shapes. Phillips Research Reports, Vol. 13, 1958.

[70] S. Porro, S. Musso, M. Vinante, L. Vanzetti, M. Anderle, F. Trotta, A. Tagliaferro: Purification of Carbon Nanotubes Grown by Thermal CVD. Physica E., Vol. 37 (p.58), 2007.

[71] N.G. Patel, P.D. Patel, V.S. Vaishnav: Indium Tin Oxide (ITO) Thin Film Sensor for Detection of Methanol at Room Temperature. Sensors and Actuators B, Vol. 96 (p.180), 2003.

[72] Q. Zhang, M. Zhu, Q. Zhang, Y. Li, H. Wang: Fabrication and Characterization of Indium Tin Oxide-Carbon Nanotube Nanocomposites. J. Phys. Chem. C, Vol. 113 (p.15538), 2009.

[73] Y. Sawada, C. Kobayashi, S. Seki, H. Funakubo: Highly-Conducting Indium-Tin-Oxide Films Fabricated by Spray CVD Using Ethanol Solution of Indium(III)Chloride and Tin(II)Chloride. Thin Solid Films, Vol. 409 (p.46), 2002.

[74] T.S Van den Heever, U. Büttner, W.J. Perold: A Novel Method to Measure the Generated Voltage of a ZnO Nanogenerator. Nanotechnology, Vol. 22, 2011

[75] L.E. Greene, B.D. Yuhas, M. Law, D. Zitoun, P. Yang: Solution-Grown Zink Oxide Nanowires. Inorg. Chem., Vol. 45 (p.7535), 2006.

[76] S.M. Sze: Semiconductor Devices, Physics and Technology. Wiley Int., 1985. ISBN: 0-471-83704-0.

[77] W. Zhang, S.H. Brongersma, O. Richard: Influence of the Electron Mean Free Path on the Resistivity of Thin Metal Films. Microelectron. Eng., Vol. 76 (p146.), 2004.

[78] N. Joshi, A.K. Debnath, D.K. Aswal: Morphology and Resistivity of Al thin films grown on Si(111) by Molecular Beam Epitaxy. Vacuum, Vol. 79 (p.178), 2005.

[79] A.F. Mayadas, M. Shatzkes, J.F. Janak: Electrical Resistivity Model for Polycrystalline Films. Appl. Phys. Lett., Vol. 14 (p.345), 1969.

[80] N.W. Ashcroft, N.D. Mermin: Solid State Physics. WB Saunders, Philadelphia, 1976.

[81] J. George, V.U. Nayar, E.C. Joy: The Effect of the Annealing of Electrode Films on the Electrical Resistivity of Thin Aluminium Films. Thin Solid Films, Vol. 47 (p.121), 1977.

[82] J.W.C. De Vries: Temperature and Thickness Dependence of the Resistivity of Thin Polycrystalline Aluminium, Cobalt, Nickel, Palladium, Silver and Gold Films. Electronics and Optics. Thin Solid Films, Vol. 167 (p.25), 1988.

[83] P. Quintana, A.I. Oliva, O. Ceh: Thickness Effects on Aluminium Thin Films. SMC. SYV., Vol. 9 (p.280), 1999.

[84] J. Li, Y. Lu, Q. Ye, M. Cinke, J. Han, M. Meyyappan: Carbon Nanotube Sensors for Gas and Organic Vapour Detection. Nano Letters, Vol. 3 (p. 929), 2003.

[85] T. Someya, J. Small, P. Kim, C. Nuckolls, J.T. Yardley: Alcohol Vapor Sensors Based on Single-Walled Carbon Nanotube Field Effect Transistors. Nano Letters, Vol. 3 (p.877), 2003.

[86] A. Goldoni, L. Petaccia, S. Lizzit, R. Larciprete: Sensing Gases with Carbon Nanotubes: A Review of the Actual Situation. J.Phys. Condens. Matter, Vol. 22, 2010.

[87] N.J. de Jager, W.J. Perold, U. Büttner: An Effective Fabrication Method for Ultra Thin Aluminium Structures. Thin Solid Films, 2011.

Appendix A

Electrical Furnace Temperature Profile

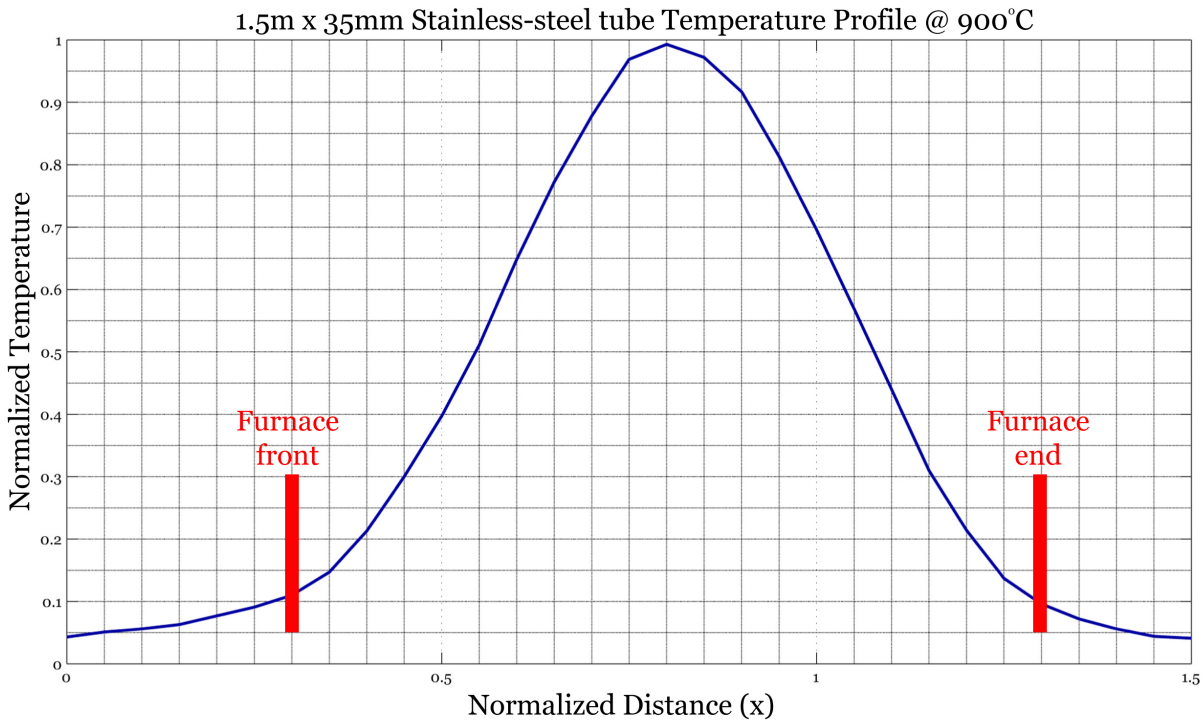

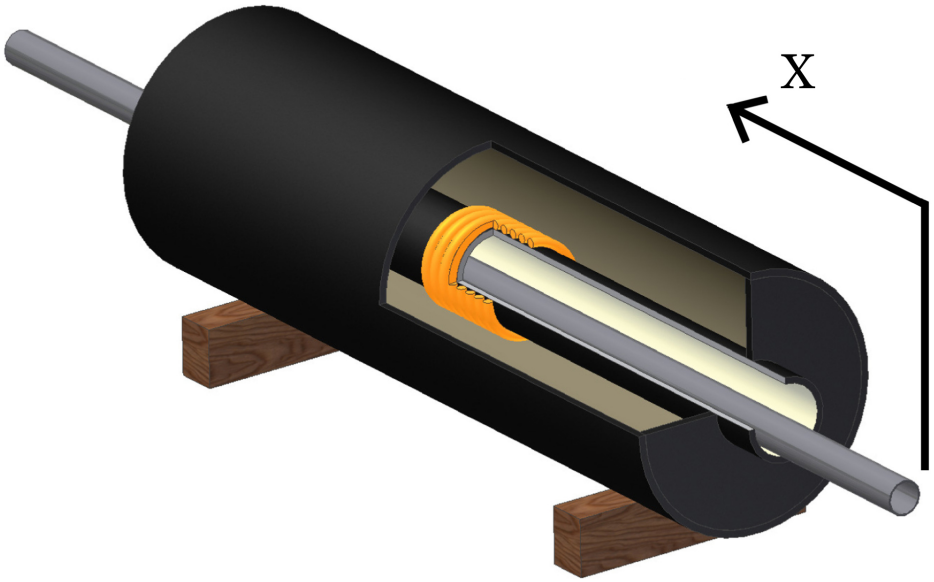

Figure A.1: Normalized furnace temperature profile at 900°C.

Appendix B

Peltier Heating System

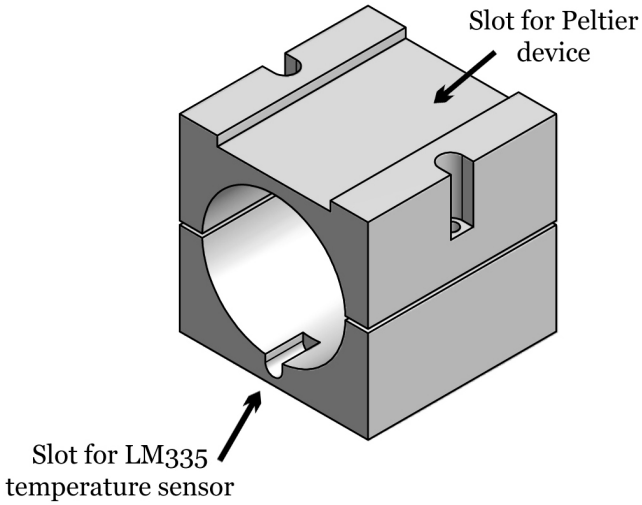

Figure B.1: Aluminium Peltier device housing.

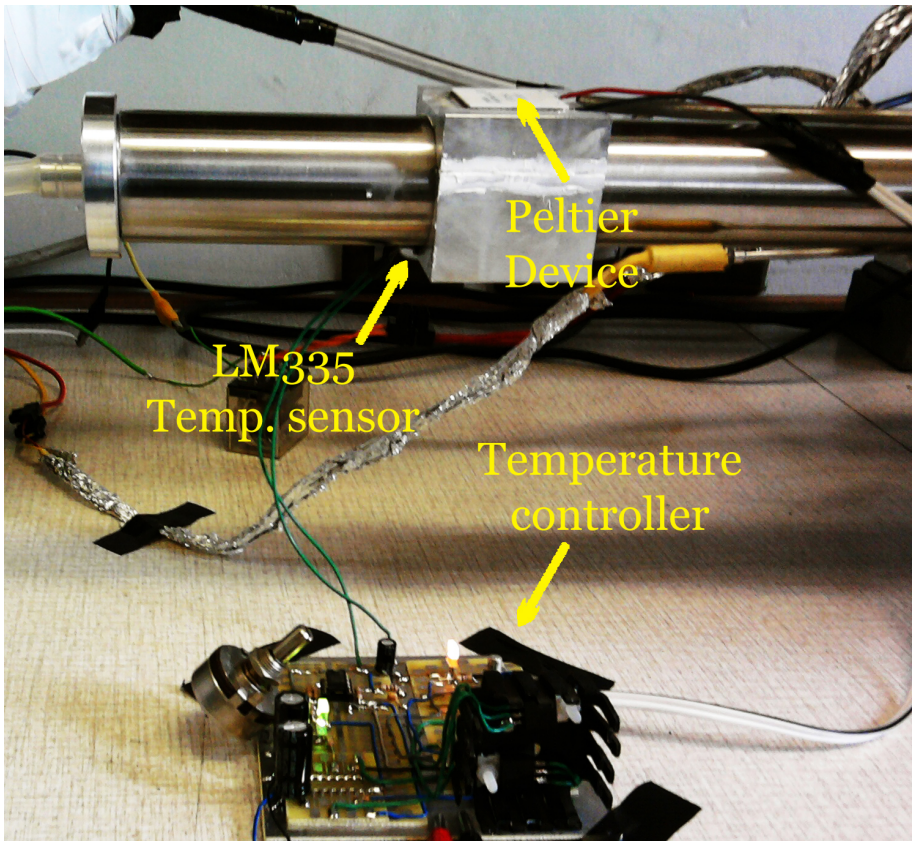

Figure B.2: Photograph of the Peltier heating system

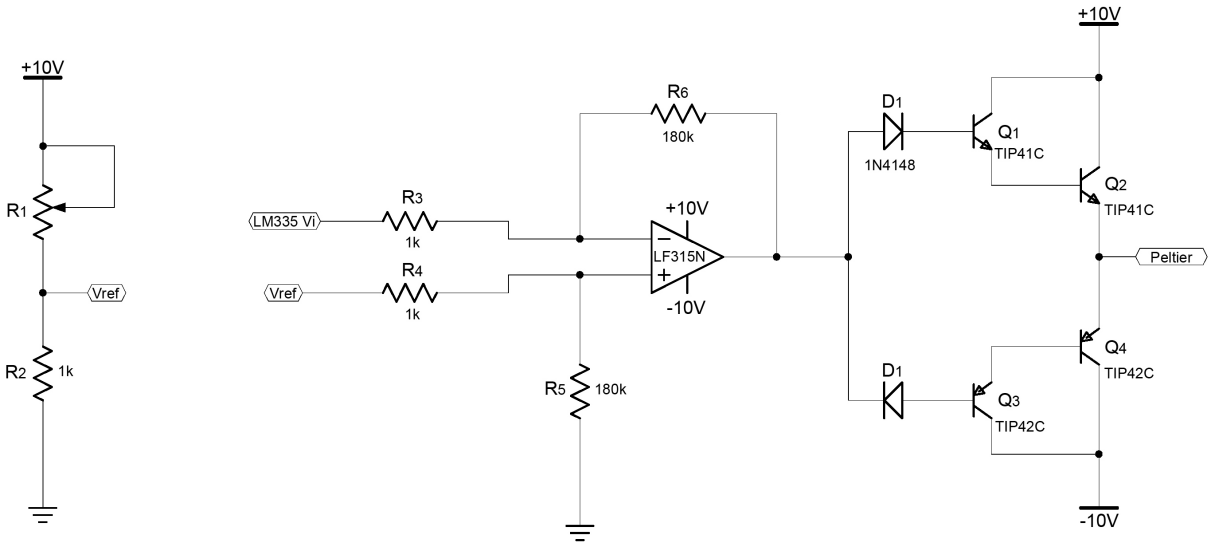

Figure B.3: Peltier system - Temperature controller circuit diagram.

Peltier system - Temperature controller design

$$LM335\,input\,voltage \approx 3.282\,V \;@\,55°C\,(10mV/K)$$

$$\therefore Vref = 3.282\,V$$

$$\therefore R1 = 2.04\,k\Omega$$

$$Av = \frac{R6}{R3} = 180$$

$$\therefore \triangle_{Tvariable} = \pm 1°C\,@\,55°C$$

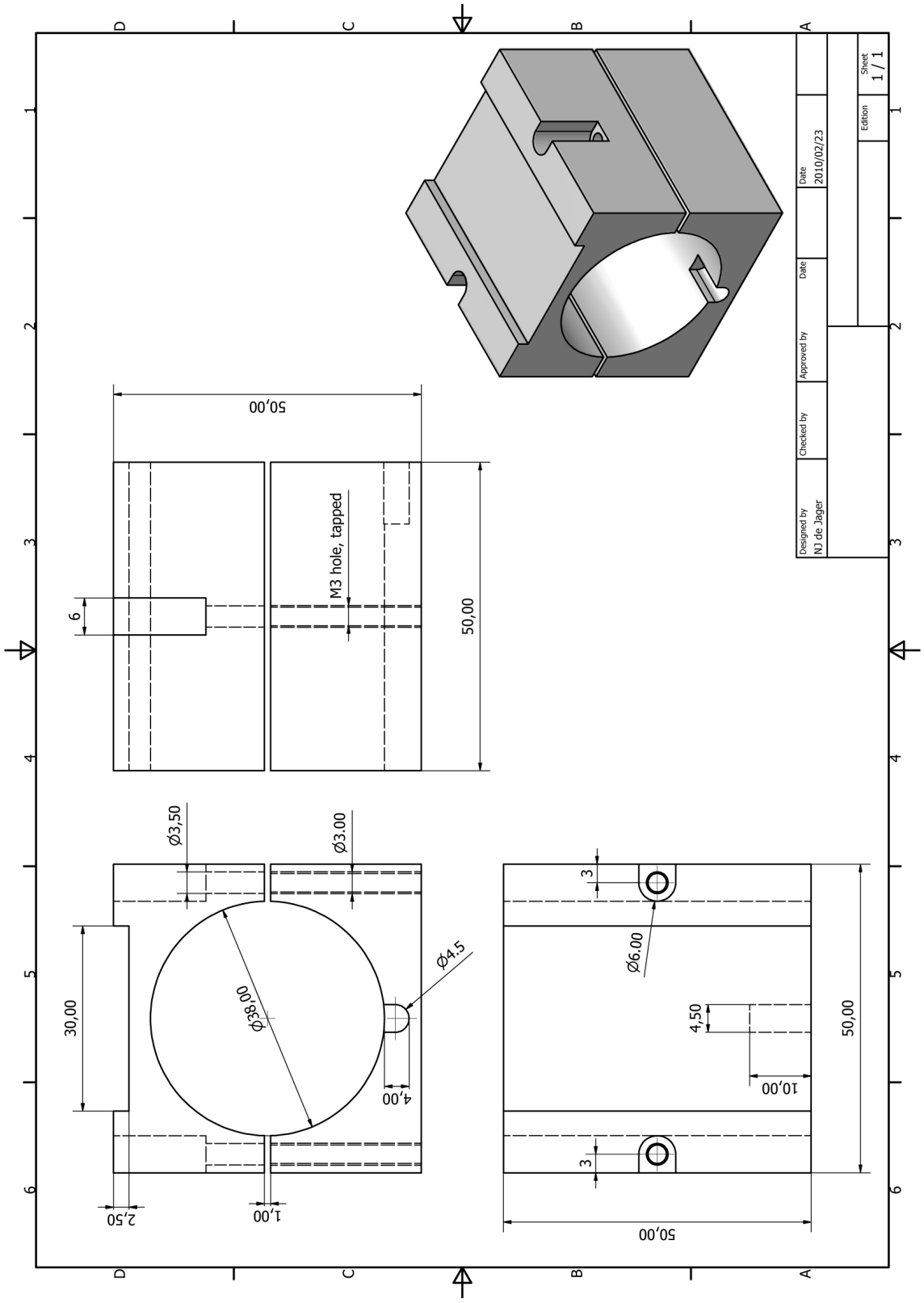

Figure B.4: Isometric CAD drawing of the aluminium peltier housing.

Appendix C

Three-section Stainless-steel tube

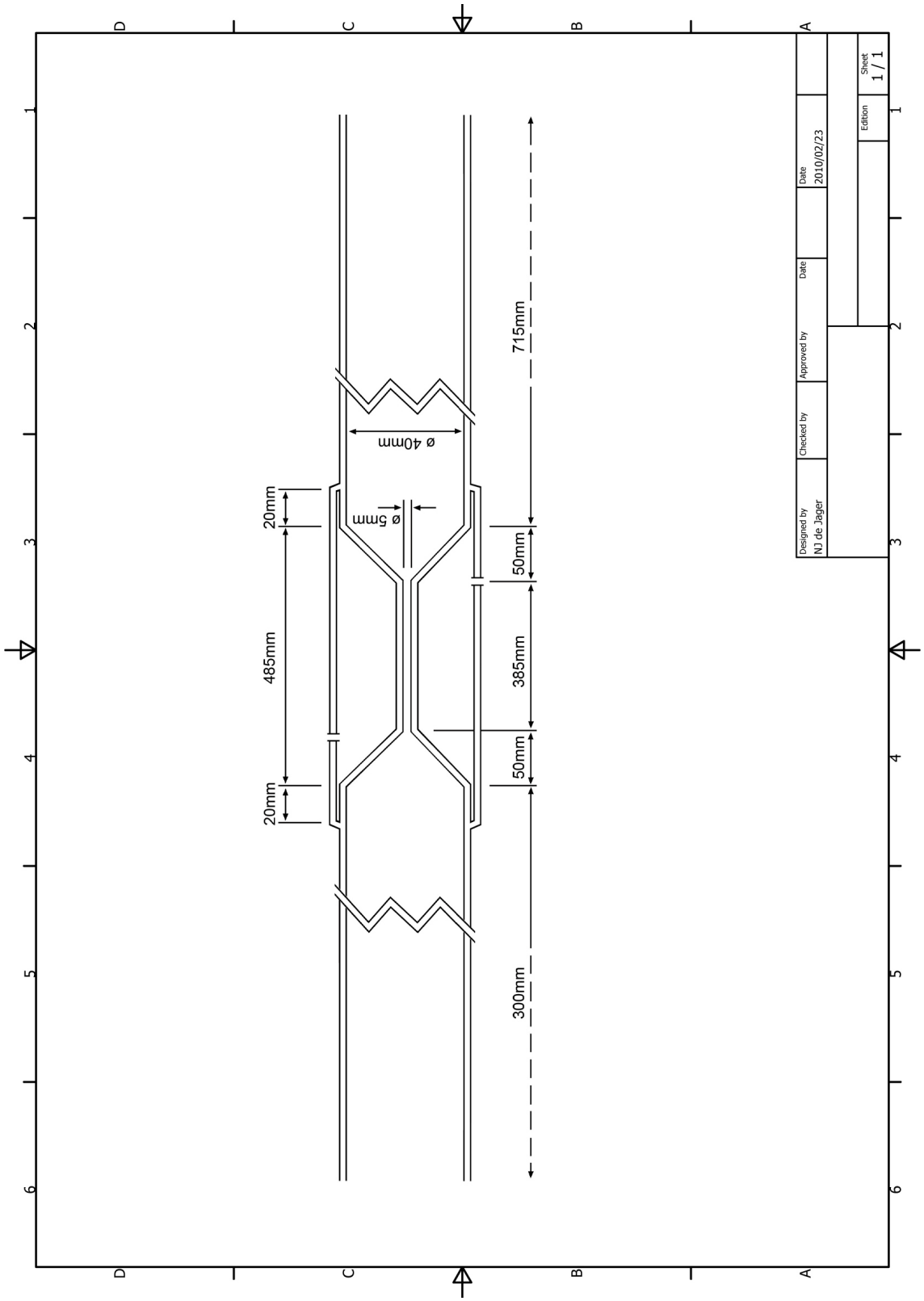

Figure C.1: Three-section stainless-steel furnace tube drawing.

Appendix D

Analogue Temperature Controller Design

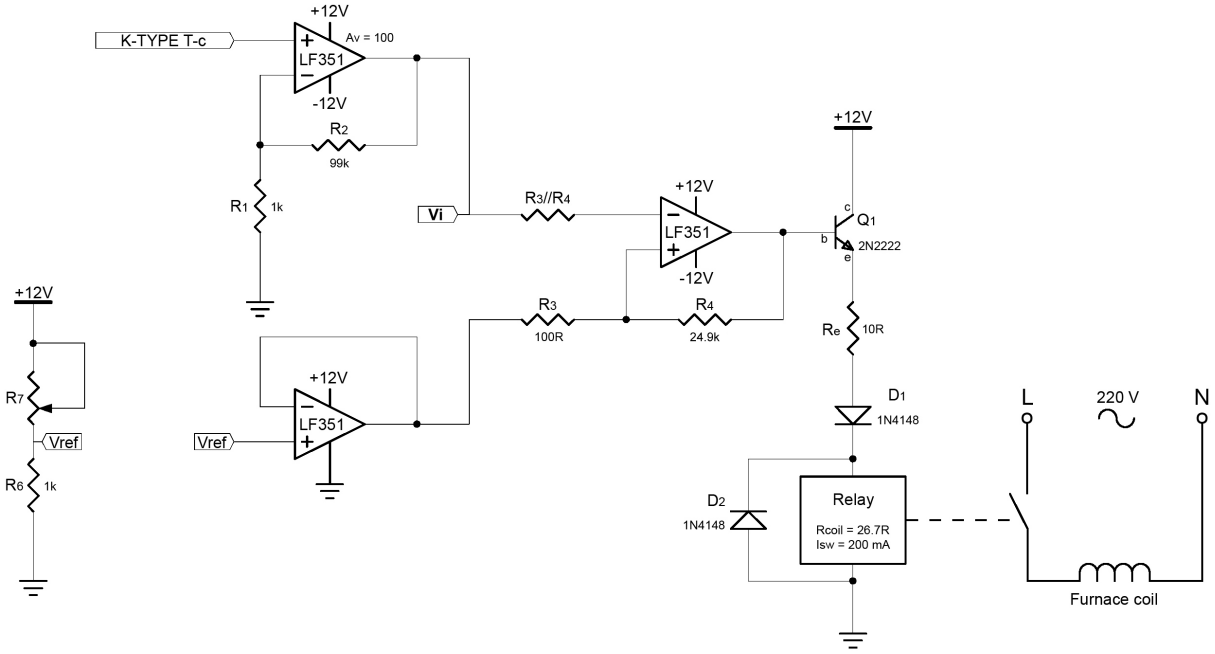

Figure D.1: Analogue Schmitt trigger temperature controller circuit diagram.

K-type thermocouple input

$$V_{T-c} = 41.28\,mV\ @\,1000°C$$

$$Av = 1 + \frac{R_2}{R_1} = 100$$

$$\therefore R_1 = 1\,k\Omega,\ R_2 = 99\,k\Omega$$

$$\therefore V_i = 4.128\,V\ @\,1000°C$$

Schmitt trigger circuit

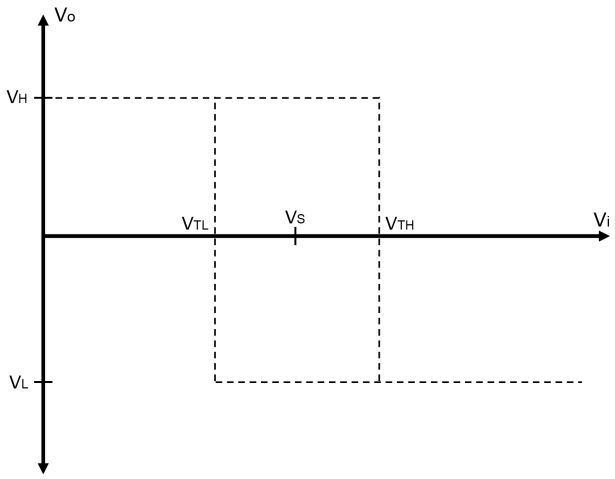

Figure D.2: Schmitt trigger characteristic curve.

$$V_S = V_i = 4.128\,V$$

$$Assume\, V_H = 10.5\,V\; max\; and\, V_L = -10.5\,V\; min$$

$$V_{TH} = V_S + \left(\frac{R_3}{R_3 + R_4}\right) V_H \doteq 4.17\,V \;\; (\triangle_T \approx \pm 10^{\circ}C \,@\, 1000^{\circ}C)$$

$$\therefore R_3 = 100\,\Omega,\; R_4 = 24.9\,k\Omega$$

$$\therefore V_{TL} = V_S + \left(\frac{R_3}{R_3 + R_4}\right) V_L \approx 4.09\,V,\; and$$

$$V_{ref} = \left(\frac{R_3 + R_4}{R_4}\right) V_S = 4.145\,V$$

$$\therefore R_6 = 1\,k\Omega,\; R_7 = 1.89\,k\Omega$$

Relay switch circuit

$$R_{coil} = 26.7\,\Omega$$

$$I_{switch} \simeq 250\,mA$$

$$\therefore R_e = \frac{V_b - V_{be} - V_{D_1} - R_{coil}.I_{switch}}{I_{switch}} \approx 10\,\Omega$$

Appendix E

The Van der Pauw 4-point Measurement Technique

The Van der Pauw variant of the 4-point measuring technique [69], to determine the sheet resistance of a sample, consists of taking two individual measurements, and solving the Van der Pauw equation given by:

$$e^{-\Pi R_{12,34}/R_S} + e^{-\Pi R_{31,42}/R_S} = 1$$

The two required measurements, $R_{12,34}$ and $R_{31,42}$ as is shown in Fig E.1, are referred to as:

i) Resistance along a vertical edge, and
ii) Resistance along a horizontal edge.

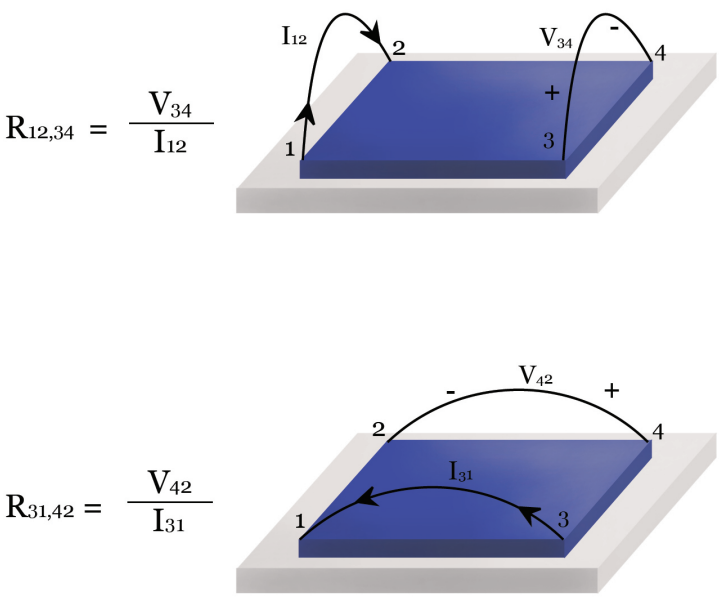

Figure E.1: A graphic illustration of the Van der Pauw 4-point technique.

The Van der Pauw 4-point measurement technique generally provides two major advantages over conventional 2-point measurements, which are:

a) The elimination of contact resistances, and
b) Employment of the entire sheet resistance, by placing four contact points on the edges of the sample.

There are however several considerations that need to be kept in mind when implementing the Van der Pauw technique, which are listed as follows:

i) The measurement requires a symmetrical shaped sample (e.g. square).

ii) No isolated holes may exist in the sheet.

iii) Contacts need to be placed as close to the edges as possible.

iv) Small contacts are required, which reduce the D/L error that is introduced into the measurement, where D = *contact diameter* and L = *distance between contacts*.

The Van der Pauw method can generally be performed more accurately, by taking two sets of measurements and solving the equation:

$$e^{-\Pi R_{Vertical}/R_S} + e^{-\Pi R_{Horizontal}/R_S} = 1$$

where

$$R_{Vertical} = \frac{R_{12,34} + R_{34,12}}{2}$$

$$R_{Horizontal} = \frac{R_{31,42} + R_{42,31}}{2}$$

The presented equation unfortunately does not have a closed solution unless $R_{Vertical} = R_{Horizontal}$, which is quite rarely the case. A small computer program can be implemented with the following C-code, to iteratively solve the value of R_S.

Van der Pauw C-code

```
e = 2.718281828;
Pi = 3.141592654;
R1 = R_Vertical;
R2 = R_Horizontal;
Rs = 0;
sum = 0;

while (sum < 1)
{
    Rs = Rs + 0.01;              // 0.01 step size
    sum = e^(-Pi*R1/Rs) + e^(-Pi*R2/Rs);
    Rs = sum;
}
```

Appendix F

A Constant Current Source and Low-Noise Instrumentation Amplifier to Perform 4-point Measurements

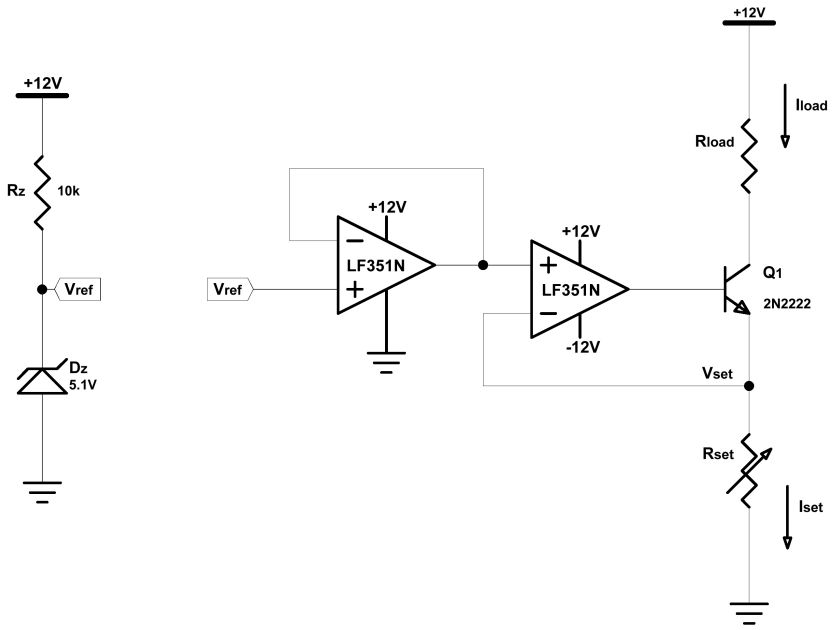

Figure F.1: Constant current source circuit diagram.

Constant current source circuit design

For the constant current source circuit, shown in Fig. F.1, the operational amplifier will drive the gate of the NPN transistor so that

$$V_{ref} = V_{set}$$

$$\therefore \quad V_{set} = V_{Dz} = 5.1\,V$$

Furthermore, the load current I_{load} will be approximately equal to I_{set}, which yield

$$I_{load} \approx I_{set} = \frac{V_{set}}{R_{set}}$$

For a load current $I_{load} = 100\,\mu A$, we calculate the value of R_{set} as

$$R_{set} = \frac{V_{set}}{I_{set}} = 51\,k\Omega$$

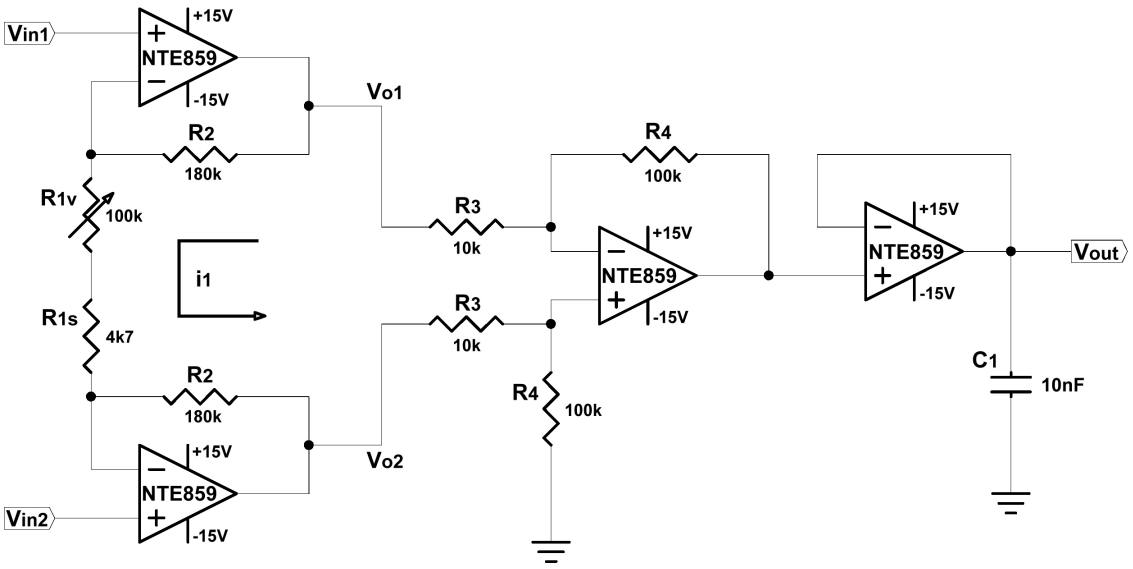

Figure F.2: Instrumentation amplifier circuit diagram.

Instrumentation amplifier circuit design

From the virtual short concept of ideal operational amplifiers

$$i_1 = \frac{V_{in1} - V_{in2}}{R_{1s} + R_{1v}}$$

Thus, we get that

$$V_{o1} = V_{in1} + i_1 R_2$$

$$= \left(1 + \frac{R_2}{R_{1s} + R_{1v}}\right) V_{in1} - \frac{R_2}{R_{1s} + R_{1v}} V_{in2}$$

and

$$V_{o2} = V_{in2} - i_1 R_2$$

$$= \left(1 + \frac{R_2}{R_{1s} + R_{1v}}\right) V_{in2} - \frac{R_2}{R_{1s} + R_{1v}} V_{in1}$$

Now we obtain V_{out}, given by

$$V_{out} = \frac{R_4}{R_3}\left(V_{o2} - V_{o1}\right)$$

$$\therefore \quad V_{out} = \frac{R_4}{R_3}\left(1 + \frac{2R_2}{R_{1s} + R_{1v}}\right)\left(V_{in2} - V_{in1}\right)$$

The total gain is thus presented by

$$A_v = \frac{R_4}{R_3}\left(1 + \frac{2R_2}{R_{1s} + R_{1v}}\right)$$

$$= 10\left(1 + \frac{360 \times 10^3}{4.7 \times 10^3 + R_{1v}}\right)$$

$$(for\ R_1 = 4.7\,k\Omega,\ R_2 = 180\,k\Omega,\ R_3 = 10\,k\Omega\ and\ R_4 = 100\,k\Omega)$$

It is concluded that by adjusting the value of R_{1v}, the operational amplifier's gain can be adjusted to acquire measurements (with $V_{out}\approx$ -13.5 V to +13.5 V) for a wide range of input values.